Stellingen

1. Bestrijding van zwaar aangetaste haarden is de meest effectieve maatregel voor het terugdringen van de infectiedruk van *Phytophthora infestans*.
   (dit proefschrift)

2. Baadjesvorm is een, nog niet eerder beschreven, component van resistentie tegen *Phytophthora infestans*.
   (dit proefschrift)

3. Ondanks haar taak van demystificatie is het de wetenschap nog niet gelukt zichzelf te demystificeren.

4. De belangrijkste wetenschappelijke ontdekkingen van de 20e eeuw zijn de onzekerheidsrelatie van Heisenberg, de stelling van Gödel en de ontdekking van chaos als algemeen voorkomend verschijnsel.

5. Nieuwsgierigheids-gedreven onderzoek is nuttig voor aanbod-gedreven innovaties.

6. Tradition means giving votes to the most obscure of all classes, our ancestors.
   (G.K. Chesterton, 1909: Orthodoxy).

7. Waarover men niet kan spreken, daarover moet men zich anders uitdrukken.
   (vrij naar L. Wittgenstein, 1922: Tractatus Logico-Philosophicus).

8. Deze lijst bevat ten minste één onware stelling.

Stellingen behorend bij het proefschrift van H.P. Spijkerboer:
From lesion to region: epidemiology and management of potato late blight.

Wageningen, 13 September 2004

Voorwoord

Hoera het proefschrift is af! Wat een opluchting! Nou ja, het voorwoord moet nog. Een voorwoord is eerst en vooral de plek om mensen te bedanken. Alhoewel ik de enige auteur ben van dit boekje, was dit proefschrift er zonder anderen niet geweest. Ik wil dan ook graag gebruik maken van de mogelijkheid om iedereen te bedanken die de afgelopen jaren op enigerlei wijze bij heeft gedragen aan het tot stand komen van dit boekje.

Allereerst mijn ouders. Zij hebben dit proefschrift mogelijk gemaakt. Zonder jullie was ik er niet geweest, en dus ook dit proefschrift niet. Daarnaast zijn jullie mij in de afgelopen jaren vaak en op vele manieren tot steun en toeverlaat geweest. Bedankt voor alles wat jullie gedaan hebben.

Mijn zussen, zwagers, nichtjes en neef: Mariët, Anton, Lisa en Merel; en Ienke, Evert, Brian en Joyce. Ik hoop dat we elkaar in de toekomst wat vaker kunnen zien dan de afgelopen jaren het geval was.

Ik wil Wopke, Henk en Rudy bedanken voor de grote inzet waarmee zij, ieder op eigen wijze, hun begeleidingstaken op zich hebben genomen en zo de weten-schappelijke kwaliteit bewaakten.

Ik wil Annelies en Daan bedanken voor de creativiteit en inzet waarmee zij het leeuwendeel van het experimentele werk op zich genomen. Jan Menting heeft in de zomer van 1999 een bijdrage hieraan geleverd.

Naast Wopke, Henk, Rudy, Annelies en Daan hebben nog een aantal andere mensen bijgedragen aan de inhoud van het proefschrift. Ik dank dan ook de andere co-auteurs, nl. Jan Goudriaan, Adrie Jacobs en Jim Powell.

Een aantal mensen hebben dankzij nuttig overleg een specifieke inhoudelijke bijdrage geleverd. De belangrijkste van hen zijn de leden van de gebruikerscommissie. Dank zij het halfjaarlijks overleg met hen heeft dit proefschrift veel aan praktische waarde gewonnen.

Meerdere mensen hebben door nuttige discussies bijdragen geleverd aan de kwaliteit van de verschillende hoofdstukken. Dit waren (o.a.): Donald Aylor, Leontine Colon, Hans Erbrink, Wilbert Flier, Jan Hadders, Hendrik Harssema, Henk Hendriks, Mark Huiskes, Karel Keesman, Geert Kessel, Wim Nugteren, Albert Otten, Huub Schepers, Lo Turkensteen en Marleen Visker.

Dan zijn er ook nog twee mensen die bij de vormgeving van dit proefschrift hebben geholpen: Gon van Laar heeft veel redactioneel werk verricht en Mariët heeft geholpen bij het ontwerp van het omslag.

De collega's van het CPRO en TPE, later Plant Research International en de Haarweg collega's in 'den Nuy', en vooral mijn verschillende kamergenoten, dank ik voor hun collegialiteit.

Oom Jaap, tante Inge, tante Willemien, dank jullie wel voor jullie gastvrijheid en belangstelling.

Mijn vrienden dank ik voor hun support en gezelschap: Dirk Jan, Pim, Clemens, Gerard en Ivelina, Dirk en Rianne, Stephan, Chris.

Muziek is een enorme bron van ontspanning geweest de afgelopen jaren en het is heerlijk om deze passie met anderen te delen. Mijn dank gaat dan ook uit naar mijn mede muziekliefhebbers, met name alle WSKOV-ers. Gloria, gloria! (Antonio Vivaldi).

Ik dank ook mijn mede filosofen van het geloof en wetenschap clubje, Clemens, Mark, Wulf, Maria en Pim voor de interessante discussies.

I would like to thank Don Aylor, Bill Fry and Eduardo Mizubuti for the useful discussions I had with them during my visit to the US in 1998.

I would also like to thank my English-speaking colleagues, especially my roommates, at TPE, CPRO, PRI and Haarweg.

I would like to thank Mirek Martinec for his friendship and for his hospitality during my two visits to his beautiful country, the Czech Republic.

Last, but not least, I would like to thank my friends and travel companions Richard, James, Hywel for our holidays together. I look forward to new ones and hope I'll have a *real* job by that time!

Diedert Spijkerboer

Wageningen, 1 juli 2004

From lesion to region

epidemiology and management of potato late blight

H.P. Spijkerboer

From lesion to region

epidemiology and management of potato late blight

Proefschrift

ter verkrijging van de graad van doctor
op gezag van de rector magnificus
van Wageningen Universiteit,
prof. dr. ir. L. Speelman
in het openbaar te verdedigen
op maandag 13 september 2004
des namiddags te vier uur in de Aula

Abstract

Aerial dispersal of *Phytophthora infestans* spores from distant sources to crops is an essential part of the epidemiology of potato late blight. This makes late blight a regional problem. An interdisciplinary analysis of the regional late blight problem is carried out through model development, experimental parameterisation and analysis and scenario studies that investigate possibilities for effective control of the disease at the regional level.

A new equation was derived to estimate the relative exponential growth rate r (d^{-1}) of a plant disease epidemic from commonly used component parameters for pathogen aggressiveness and host resistance, such as the latency period, infection efficiency, sporulation intensity and lesion growth rate. The use of the equation is demonstrated with field measurements of resistance components against late blight for five potato cultivars. Infection efficiency and lesion growth rate together explained most of the variation in cultivar resistance.

To describe the dispersal of spores at distances up to 10 km downwind from a source of inoculum, the Gaussian plume model was used. A field experiment was set up to calibrate the Gaussian plume model, as applied to the dispersal of spores. A comparison of estimated concentrations with the measurements confirmed that spore clouds originating from a point source take the form of a Gaussian plume: the coefficient of correlation between measured spore concentrations and fitted concentrations was 0.8. The fraction of spores that escaped the canopy and was available for long distance dispersal amounted to 64% ± 17%.

To model deposition and loss of spores from the spore plume at distances between 50 m and 10 km from the source, the source depletion method was used. This is a practical method, but it is simplified in its description of spore loss. The accuracy of the source depletion method was determined by comparing it with the more realistic surface depletion method in a modelling study. It was found that under worst case conditions, the source depletion method may lead to an error of at most a factor 4 in calculated deposition of *Phytophthora infestans* spores.

The infection pressure on receptor crops caused by inoculum from a distant source was calculated with a newly developed model. The sensitivity analysis showed that disease level at the source had by far the greatest impact on infection pressure, followed by distance from the source. Subsequent scenario studies indicated that eradication of sources with high disease levels and spatial separation of cropping systems with different disease tolerances are more effective than use of more resistant cultivars for the receptor crop or a ban on the growing of susceptible cultivars.

The conditions and possibilities for practical implementation of the effective control strategies as well as their consequences for fungicide requirements are discussed.

Contents

CHAPTER 1

General introduction

Control of potato late blight is a lasting problem in plant protection. In the Netherlands, for example, it is the most fungicide-demanding disease (Ekkes *et al.*, 2002). Government policies to reduce input of crop protection chemicals can be very effective. The multi-year crop protection plan has led to effective decreases in inputs of pesticides in many crops. However, the input of fungicides against late blight remains above target levels and has in fact increased (Ekkes *et al.*, 2002). The threat from *Phytophthora infestans*, the causal agent of potato late blight, in the Netherlands has increased, due to the introduction of a second mating type. As a result, sexual reproduction now takes place, leading to increased genetic variation and aggressiveness, and infection of crops from oospores that can overwinter in the soil.

Spread of the disease from sources of overwintering inoculum to crops is an essential part of the epidemiology (Zwankhuizen *et al.*, 1998). In the agricultural landscape, sources of inoculum may be found on waste piles, in organically-grown crops, in sprayed crops and in community gardens. The levels of disease in these sources and their rate of growth will vary because of variability in resistance and pathogenicity and in management, particularly fungicide use. Together with variation in wind direction and other weather factors, this gives a very complex spatio-temporal pattern of disease development.

In this complicated setting, individual farmers make day to day spraying decisions. In these decisions, they can be aided by commercial spray advice systems, like Prophy (Opticrop B.V., Vijfhuizen, the Netherlands) and Plant Plus (Dacom PLANT-Service B.V., Emmen, the Netherlands), that are specifically aimed at the control of late blight. The use of information on sources of inoculum in a region in combination with models to calculate spread of inoculum can make the spray recommendation from these systems more specific, thus avoiding unnecessary sprays. Control measures, such as eradication of heavily diseased sources and the use of more resistant cultivars, can be taken to reduce the risk of infection. To make spray recommendations more specific and give support to control policies, more knowledge is needed about the regional epidemic. Models are especially suitable to generate this knowledge, because they allow to focus on different aspects of a phenomenon separately from other factors. Models have previously been used to study the large-scale population dynamics of whitefly infestations in tomato and eggplant crops (Brewster and Allen, 1997a, b), to determine the risk to fruit trees and native trees due to control of black cherry with the silverleaf fungus (De Jong, 1988), and to study dispersal of tobacco blue mold between states in the US (Aylor, 1986).

For practical applications, simple and mechanistic models are preferable to more complex or empirical models. For a practical application, knowledge must be disseminated to non-modellers. Simple models can more easily be explained to non-

modellers. By using mechanistic descriptions, the assumptions behind the model can be easily explained and thus become open for discussion with a wide audience.

This thesis describes the results of a project aimed at quantification of infection pressure from distant sources of *Phytophthora infestans* and its consequences for the fungicide requirements in potato crops. An interdisciplinary analysis of the regional late blight problem is carried out through model development, through experimental parameterisation and through analysis and scenario studies that investigate possibilities for effective control of the disease at the regional level.

The models that are developed, combined with information about presence and severity of sources can be used in practice to give farmers site-specific spray recommendations. Programmes for detection and registration of sources, which were co-ordinated by Dacom PLANT-Service B.V. and by the Dutch Plant Protection Service (Dacom and PD, 1999), were carried out at the same time as this project.

A model of regional epidemics necessarily should include two aspects: local development of the disease on inoculum sources and dispersal of inoculum from sources to vulnerable crops. Models to describe these processes individually have been available for some time. Local epidemic models of late blight have been developed by Bruhn and Fry (1981), Michaelides (1985) and Van Oijen (1991). A limitation in existing local epidemic models is the way they describe lesion growth. The growth rate of lesions determines when spores are produced and thus determines the speed of the epidemic. A realistic description of lesion growth is therefore needed, but is not given in any of these models. In this thesis, a mechanistic description of lesion growth was developed and incorporated in a new and simpler local epidemic model. This model was parameterised for five potato cultivars (chapter 2).

Models for dispersal have been developed to study spread of air pollutant gasses from factory chimneys. A commonly used model in this field is the Gaussian plume model (Pasquill, 1974), which has previously been used for the study of atmospheric spread of fungal spores (De Jong, 1988).

A special challenge is the coupling of a local epidemic model with a dispersal model. The dispersal model is based on the Gaussian plume model. The Gaussian plume model was developed for gasses, but is used for spores here. Spores can be captured by the crop at the source, and can sediment from the air. The Gaussian plume model requires the release rate of spores as input. The release of spores from the canopy is hampered by leaves and stems. Only a fraction of all spores escapes the canopy, because some spores land on the leaves and stems and keep the local epidemic going. An experiment was carried out to quantify this so-called escape fraction and test if the Gaussian plume model, originally developed for gasses can describe release of spores from a crop and spore concentrations close to the source (chapter 3).

The Gaussian plume model was linked to a simple meteorological model, which allows a calculation of deposition of spores to the ground from the calculated aerial spore concentration. The effect of loss of spores due to deposition was calculated in a simplified way, using the source depletion method (Van der Hoven, 1968). The ability of this simple combined model to describe regional deposition gradients, between 50 m and 10 km downwind from the source is discussed in chapter 4.

The local epidemiological model and the dispersal and deposition model combined provide a model for studying the instantaneous risk of infection posed by distant sources of inoculum. The sensitivity of this model to its component parameters is studied. The model was then used to evaluate the effectiveness of control measures aimed at reducing infection pressure and fungicide requirements (chapter 5).

The final chapter (chapter 6) gives an overview of the results that have been obtained and an outline of the possibilities for further developments in research and practical control.

CHAPTER 2

A new epidemic index applied to potato late blight

Abstract

A new equation was derived to estimate the relative exponential growth rate r (d^{-1}) of a plant disease epidemic from commonly used component parameters for pathogen aggressiveness and host resistance, like the latency period, infection efficiency, sporulation intensity and lesion growth rate. The index applies to leaf pathogens with spreading lesions and is based on well-established ecological theory in combination with a new, mechanistic, model for lesion growth and sporangium production on leaves with a finite size. The index may be used to predict the effect of changes in component parameters on the growth rate of epidemics in the field. The use of the equation is demonstrated with field measurements of resistance components against late blight for five potato cultivars. The index appeared sensitive to changes in all component parameters, except a shape factor for the leaves. Uncertainty in estimated index value was mostly due to uncertainty in the values of only three parameters: infection efficiency, sporulation intensity, and to a lesser extent, lesion growth rate. Infection efficiency and lesion growth rate together explained most of the variation in cultivar resistance. The index offers a new tool for targeting breeding efforts to those parameters that have significant epidemiological impact, and predict that impact.

Key words: Disease index, epidemics, modelling, Phytophthora infestans.

Introduction

The measurement of components of resistance or aggressiveness offers a tool for explaining and predicting the behaviour of plant diseases. They give more detailed information than parameters like the AUDPC (area under the disease progress curve) that describe the overall behaviour and, because they are measured at the lesion scale rather than the field scale, they can be measured year-round in climate cabinets.

The components that need to be studied depend on the behaviour of the disease. This chapter focuses on potato late blight, but the results can be applied to plant diseases with a similar ecology and behaviour. The specific behaviour of the pathogen studied here is that it infects leaves and then causes an expanding lesion. It sporulates on the outer edge of this lesion (Lapwood, 1961). The disease components with which such diseases can be characterised are infection efficiency, latency period, lesion growth rate and sporulation intensity.

To interpret the importance of variation in disease components, a translation to the field scale is required. The importance of variation found in one component depends on the relative importance of this variation as compared with other components. It also depends on the values of the other components. Therefore, it is necessary to find a method to weigh each component in such a way that their relative importance is expressed in such a way that it represents behaviour at the field scale.

One method for assessing the relative importance of components of resistance and aggressiveness is with composite disease indexes. Composite disease indexes have been developed to assess the relative importance of components of resistance and aggressiveness (Day and Shattock, 1997; Flier and Turkensteen, 1999). These indices combine the different parameters in a simple and explicit mathematical expression that produces a single integrated quantitative outcome characterising the host-pathogen combination. Indexes are easy to use, but to ascertain their value, a firm theoretical basis is necessary. For a theoretically sound assessment of the relative importance of parameters, epidemic models (e.g. Bruhn and Fry, 1981; Van Oijen, 1989, 1991) are useful. The disadvantage of using models though, is that they are less transparent and more difficult to apply than indexes based on explicit formulas.

In this chapter an integration of the modelling approach and the disease index approach is presented. An existing model (Van Oijen, 1989; 1991) and standard ecological theory were combined to derive an expression for the relative exponential growth rate parameter r (d^{-1}). This simple expression can be used as a composite disease index, since it incorporates parameters for all the relevant processes at the lesion scale, including the latency period, lesion growth rate, sporulation intensity and

infection efficiency. The index was applied to weigh components of resistance against late blight for one American and four Dutch potato cultivars.

Material and methods

Used symbols

parameter	description
A_b (m^2)	leaflet area
d (-)	fitted function for average distance between two points within an ellipse
D (m)	distance between two points
f	average distance between two points within an ellipse
IE (-)	infection efficiency: chance of infection per sporangium
I (d^{-1})	impact of cultivar variation in a parameter on the index
l_b (m)	length of leaflet
LAI (m^2 m^{-2})	leaf area index
LG (m d^{-1})	lesion growth rate
LP (d)	latency period
p	dummy parameter in equation for index
P (-)	significance level
r (d^{-1})	relative growth rate
R_0 (-)	net reproduction, number of daughter lesions per mother lesion
S (d^{-1})	sensitivity of the index to a relative change in a given parameter
s_b (-)	shape of leaflet, expressed as length / width ratio
SI (# m^{-2})	sporulation intensity: number of sporangia produced per area of the lesion
T (d)	generation time, the average time between production of the mother lesion and production of its daughter lesions
T_d (d)	average time between production of sporangia and time that they are dispersed
T_p (d)	average time between the end of the latency period and the moment that any given sporangium is produced
T_s (d)	time it takes a lesion to grow from the point of infection to a given point on a leaflet
U (d^{-1})	Uncertainty in index r due to uncertainty in a given parameter
w_b (m)	width of leaflet

x (m)	x co-ordinate
y (m)	y co-ordinate
α (-)	confidence level
ε (# landed LAI^{-1} $\#^{-1}$ produced)	inoculum dispersal efficiency, fraction of sporangia that lands on other leaflets, per unit of *LAI*
λ	Poisson parameter
π	mathematical constant ($\pi \approx 3.14$)
Ψ	given point on a leaflet

Derivation of the index

Expression of relative growth rate in terms of R_0 *and* T

The relative growth rate r describes the growth rate of epidemics during the exponential growth phase (Zadoks and Schein, 1979). According to a basic (and approximate) approach, this exponential growth rate depends on two parameters: net life time reproduction, R_0 (-), and generation time, T (d) (Gotelli, 1998). The first quantity, R_0 represents the total number of new (female) offspring that are produced by a single mother during her lifetime. The generation time, T, equals the average age of the mother during production of her offspring. This equation is developed further, taking the lesion as individual.

The relative growth rate r can be calculated from R_0 and T as (Gotelli, 1998):

$$r \approx \frac{\ln(R_0)}{T} \tag{1}$$

Expressions are derived to calculate R_0 and T from component parameters, using some simple and straightforward assumptions.

Calculation of the net reproduction R_0 *from disease components*

The calculation of the net reproduction R_0 follows Van Oijen's (1989, 1991) late blight model. Van Oijen (1989) assumed sporulation only to take place on the newly formed lesion area. This assumption is consistent with the observation that new sporangia are produced on the edge of the lesion (Lapwood, 1961). The further assumption was made that each leaflet gets infected only once. This assumption is valid in the exponential phase of the epidemic, when few leaflets have more than one infection. Using this assumption and Van Oijen's (1989) approach, R_0 can be calculated as:

$$R_0 = A_b \cdot SI \cdot \varepsilon \cdot LAI \cdot IE \tag{2}$$

Basically, this equation says that during the life span of a lesion, sporangia are produced on the entire leaflet area (A_b, m^2) with a constant sporulation intensity (*SI*, # m^{-2}). The produced sporangia are dispersed with an inoculum dispersal efficiency ε (fraction of landed sporangia per unit of leaf area index; sporangia landed per sporangia produced, per unit LAI) on a crop with leaf area index *LAI* (m^2 leaf m^{-2} soil). Each landed sporangium then has a chance *IE* (-) to infect the leaflet it lands on.

Calculation of generation time T *from disease components*
The generation time *T* can be expressed as the sum of three parts:

$$T = LP + T_p + T_d \tag{3}$$

The first part is the latency period (*LP*, d), i.e. the time between infection and the moment that a lesion first produces sporangia. This parameter can be derived from experiments. The second part is the production period (T_p, d), i.e., the average time between production of the first sporangium and production of any other sporangium on the lesion. The third part is the dispersal period T_d (d), i.e., the time between the moment that a sporangium is produced and the moment that it causes a successful infection on another leaflet. T_d is assumed to be negligible.
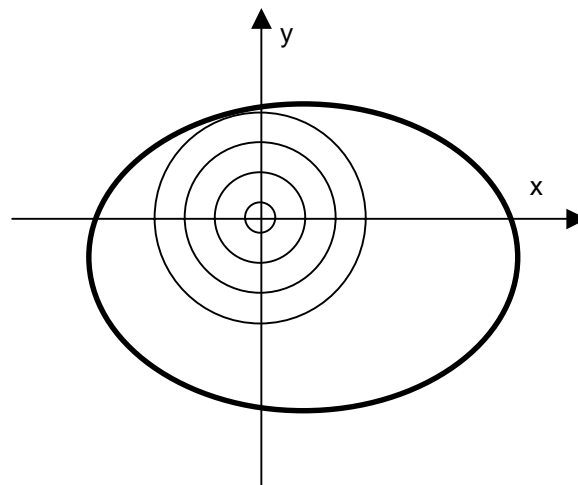
Figure 1: Model of a growing lesion on a leaflet. The large ellipse represents the leaflet. The concentric circles represent the size of the lesion on consecutive days. An (*x*, *y*) co-ordinate system is chosen in such a way, that its centre is at the centre of the lesion.

To calculate the average production period T_p, a mathematical expression was derived from measured leaflet characteristics and the lesion growth rate LG (m d^{-1}). The expression is based on a mechanistic model of lesion growth and sporulation. In this model, lesions are described as circles and leaflets as ellipses. The model describes the growth of circular lesions on the ellipse-shaped leaflets (figure 1).

From the moment of infection until the end of the latency period, the lesion has a radius of 0 m. After that, it grows at a constant lesion growth rate LG until it has covered the entire leaflet.

Sporulation takes place on the outer edge of the growing lesion at a constant sporulation intensity SI (# m^{-2}). A sporangium is produced on a given part of the lesion as soon as the growing lesion reaches that part of the leaflet. The time T_s (d) that it takes the growing lesion to reach the part where a given sporangium is produced can be calculated as:

$$T_\mathrm{s}(x,y) = \frac{D(\Psi, \Psi_\mathrm{c})}{LG} \tag{4}$$

where, D is the distance between the point Ψ where the sporangium is produced and the centre of the lesion, Ψ_c, where infection took place. Assuming that the points Ψ and Ψ_c have locations (x, y) and $(x_\mathrm{c}, y_\mathrm{c})$, respectively, the distance can easily be calculated, using Pythagoras' theorem.

The average production time, i.e., the average time between the end of the latency period and the moment that any given sporangium is produced, equals the average time of T_s for all possible points of infection Ψ_c and points of sporangium production Ψ:

$$T_\mathrm{p} = \overline{\overline{T_\mathrm{s}}} \tag{5}$$

where, the two overbars represent averaging over both Ψ and Ψ_c.

To calculate this double average, it was assumed that both the produced sporangia and the initial sites of infection are distributed uniformly over the entire leaflet area. This means that the average travel distance can be calculated as the average distance between two randomly chosen points on a leaflet ellipse. The average travel distance depends on the size and shape of the leaflet. The shape of the leaflet is characterised by the shape parameter s_b (-):

$$s_\mathrm{b} = \frac{l_\mathrm{b}}{w_\mathrm{b}} \tag{6}$$

where, l_b and w_b are the length and width of the leaflet (m).

It can be proven (see appendix 1) that the average distance is directly proportional to the square root of the leaflet area (A_b, m^2). The average travel distance can now be expressed as:

$$\overline{\overline{D(\Psi, \Psi_c)}} = \sqrt{A_b} \cdot f(s_b) \tag{7}$$

where, $f(s_b)$ is an unknown function that only depends on s_b. $f(s_b)$ characterises the average distance between two points on an ellipse with length/width ratio s_b and an area of 1.

As the function can to the best of our knowledge not be solved analytically, a Monte Carlo integration method (Evans and Swartz, 2000) was used to calculate the average distance for various leaflet shapes. Two random points, (x, y) and (x_c, y_c), were repeatedly drawn on an ellipse with shape s_b, and the average distance between them was determined. For each value of s_b 10^5 repetitions were used and the estimated relative error in $f(s_b)$ was found to be less than 0.2%.

An empirical function $d(s_b)$ was found that closely fits the estimated values of $f(s_b)$ for leaflets with a shape parameter s_b in the range from 1 to 60:

$$d(s_b) = -0.643 + 0.577 \cdot \left(s_b^{0.404} + s_b^{-0.404} \right) \tag{8}$$

The relative difference between $d(s_b)$ and $f(s_b)$ is less than 0.6% for values of s_b between 1 and 6 and less than 2% for values of s_b between 10 and 60.

Using this function for $d(s_b)$ and equations 3, 4, 5, 7 and 8, the generation time T can be calculated:

$$T = LP + \frac{\sqrt{A_b}}{LG} \cdot \left(-0.643 + 0.577(s_b^{0.404} + s_b^{-0.404}) \right) \tag{9}$$

Index parameter r *expressed in terms of disease components*
By combining equations 1, 2 and 9, an expression of r in terms of component parameters is obtained:

$$r = \frac{\ln(A_b \cdot SI \cdot \varepsilon \cdot LAI \cdot IE)}{LP + \dfrac{\sqrt{A_b}}{LG} \cdot \left(-0.643 + 0.577(s_b^{0.404} + s_b^{-0.404}) \right)} \tag{10}$$

This is the expression for the epidemic index that we were looking for.

Parameterisation of the index for five potato cultivars

Approach

Translation of component parameters measured in climate cabinets to field data is a remaining problem in plant pathology. Therefore, the use of climate cabinets was avoided as much as possible. Instead, the disease components were measured under field conditions.

Measurement of resistance components

Certified seed tubers of five potato cultivars (Bintje, Agria, Santé, Karnico, and Katahdin) were pre-sprouted for four weeks and then planted in potting soil in 10 l pots in a greenhouse on 12 April 1999. On April 26, the pots were put outdoors into holes in six raised rows with 15 pots per raised row. Plant spacing was 0.3 m within the row and 0.75 m between rows. Twenty-one pots were used for cv Bintje, 20 pots for cvs Agria, Santé and Karnico and 9 for cultivar Katahdin. The plants were randomised over the plot, but plants of cv Katahdin were not used as the border plants. Border plants were not used for the measurements.

Inoculations were made with inoculum propagated from liquid nitrogen stock (isolate IPO 655-2A, Plant Research International, Wageningen-UR) on June 10. Propagation and preparation of inoculum was carried out according to Colon *et al.* (1995b), to finally obtain an average sporangium concentration of 638 sporangia per 10 µl droplet.

Eight plants of cultivar Bintje and six plants of each of the other four cultivars were inoculated. On each plant, three stems were selected, and on each stem, two mature leaves, at approximately two thirds of the height of the plant. The inoculations were made on the centre of the abaxial side of five of the leaflets of each selected leaf. The inoculated plants were transferred to a humidity chamber to incubate at 95 to 100% RH, 15 °C for 18 h. After that, plants were returned to the field, where they remained for the rest of the experiment.

Measurements for infection efficiency and latency period

To determine the infection efficiency, *IE*, and latency period, *LP*, inoculated leaflets were scored for visible signs of infection on day 3, 4, 5, and 6 after inoculation. Some of the lesions on Karnico and Santé did not grow, indicating a hypersensitive response. Lesions that showed this hypersensitive response were regarded as unsuccessful infections. A check for hypersensitive response was carried out on cultivars Santé and Karnico on day 15.

Measurement of lesion growth and sporulation intensity

On day 5, 15 lesions per cultivar were randomly selected to determine lesion size. Lesion sizes were measured daily, following the method of Lapwood (1961).

Sporulation intensity was measured on cv Bintje. On days 6, 7, 9, 10 and 11, ten infected leaflets of cv Bintje were randomly selected for measurement of the sporangium production. They were cut off from the plants, rinsed with water to remove sporangia and their petioles were inserted into moist florists' oasis. From 16:00 h until 8:00 h the following day, they were put in a dark humidity chamber at 20 °C. After that, sporangia were washed off and counted with a Coulter Counter model Z2 (Coulter Electronics, Luton, UK).

Analysis of infection efficiency

Infection efficiency was calculated from the proportion of successful infections (p) that resulted from inoculation with droplets containing an average of $N = 638$ sporangia. It is assumed that the number of successfully infecting sporangia in a droplet (k) follows (approximately) a Poisson distribution with mean $\lambda = N \cdot IE$. The probability of zero infections resulting from a droplet is then equal to the zero-class probability of the Poisson distribution: $\exp(-N \cdot IE)$. The infection efficiency was determined for each variety by equating $1-\exp(-N \cdot IE)$ to observed p and solving for IE:

$$IE = -\frac{\ln(1-p)}{N} \tag{11}$$

Confidence bounds (95%) for λ, given an observed p, were determined using exact cumulative probability functions for the Poisson distribution (Microsoft Excel), and translated into confidence bounds for IE as $IE = \lambda/N$.

Analysis of latency period

The latency period LP (d) was calculated as the period from inoculation until the average day on which lesions first became visible. Cultivar differences in distribution of the day of appearance of lesions were determined with a χ^2 test.

Analysis of lesion growth rate

Lesion growth rate (LG, m d^{-1}) was calculated with linear regression. Lesion diameters were used in the regression only if the edge of the leaflet had not yet been reached. Growth rates were first determined for each lesion and then averaged per cultivar. Significance of differences between cultivars was determined with an ANOVA and t-tests.

Analysis of sporulation intensity

Sporulation intensity (SI, # m^{-2}) was calculated by regressing sporangium production on lesion area growth increment. The lesion area growth increment was determined from the measured increase in lesion area between the day that leaflets were cut off and the next day, when sporangia were washed off.

Regressions between lesion growth increment and sporulation were carried out with and without intercept. The regression with intercept was made to verify that there was no intercept, as expected under the assumption of proportionality between sporangium production and lesion growth increment. Linear regression with the intercept set to zero was used to calculate the sporulation intensity.

Measurement and analysis of leaflet area and shape

Leaflet width and length were determined on potted plants of four potato cultivars (Bintje, Agria, Santé and Karnico) in the field in 1998. Plants were grown from certified seed tubers in the same way as in the 1999 experiment and put in the field on 23 April.

Leaf area measurements were carried out on June 12 on six plants per cultivar. For each plant, the length and width of five leaflets on each of two mature leaves were measured. Cultivar differences were studied with one-way ANOVA and t-tests. The variety Kathadin was not included.

Choice of parameter values for the index

The index was parameterised with the measured resistance components and calculated for all cultivars. In the calculations, the same sporangium production parameter (SI) was used for all five cultivars in this study, *viz.* the one measured for cv Bintje. As leaflet shape factor for cv Katahdin, the average value measured for the other four varieties was used. A value of $1.3 \cdot 10^{-4}$ was used for the dispersal efficiency ε (Van Oijen, 1989). This value was used for all cultivars, because it describes a physical dispersal process, largely unrelated to the antibiotic resistance parameters IE, SI, LG and LP.

Sensitivity and uncertainty analysis

Analyses were carried out to study (1) how the index behaves mathematically in response to variation in parameter values, (2) how experimental uncertainty in parameter values affects the index, and (3) to study which components explain most of the variation in host resistance.

The mathematical behaviour of the index was calculated with a parameter for sensitivity, S_p (d^{-1}). This parameter describes the absolute change in r (∂r) resulting from a relative change in the parameter value ($1/p_i \cdot \partial p_i$):

$$S(p_i) \;=\; \frac{\partial r}{\dfrac{1}{p_i}\partial p_i} = p_i\,\frac{\partial r}{\partial p_i} \tag{12}$$

This non-standard way of combining absolute and relative sensitivity (often called elasticity) uses the strength of elasticity and avoids a weakness. The strength is that the term $1/p_i \cdot \partial p_i$ in the denominator makes changes in different parameter values comparable by making them independent of their scale of measurement. The weakness which is prevented by not dividing by r in the numerator of equation 12 is that pathological behaviour (extreme positive or negative values), if r is close to zero, is avoided.

The effect of uncertainty (U, d^{-1}) in the index parameter r because of measurement uncertainties in parameter p_i is:

$$U(p_i) \;=\; \Delta p_i \cdot \frac{\partial r}{\partial p_i} \tag{13}$$

where, Δp_i is the uncertainty in p_i. The uncertainty in r was calculated for all parameters in the equation. For Δp_i, half of the two-sided 0.95 confidence interval of p_i was used. The derivatives of r with respect to all parameters p_i were calculated analytically and are given in appendix 2.

A third and final analysis was carried out to determine which component parameters have the greatest impact on cultivar resistance. A list of published estimates of resistance components characterising variability of cultivars was created by combining literature data compiled by Van Oijen (1989) with data presented here. The impact of individual component parameters on overall resistance was quantified by calculating the difference in r for extreme parameter values:

$$I(p_i) = r(p_{i,\,max}) - r(p_{i,\,min}) \tag{14}$$

where, I (d^{-1}) is the impact of the given parameter on the index and $r(p_{i,max})$ and $r(p_{i,min})$ refer to index values calculated with the maximum, respectively, minimum value for p_i in the known range. For the other parameters (p_j) the mid-points of their range were used:

$$p_{j,s} = \frac{p_{j,\,max} + p_{j,\,min}}{2} \tag{15}$$

The impact of the dispersal efficiency ε was not studied, since no information on its variability is available and it is not thought to be influenced by cultivar variability.

Results

Resistance components on different cultivars

Measured values of parameters for different varieties are summarised in table 1. Substantial differences between varieties occur in infection efficiency and lesion growth rate.

Infection efficiency

The overall χ^2 test showed there were significant cultivar effects ($P<0.001$) on the percentage of infected leaves. The infection efficiency is highest on cv Katahdin and lowest on cv Karnico (table 1). The χ^2 tests to compare pairs of cultivars showed that there were significant ($P<0.001$) differences between all pairs of cultivars, except between cvs Bintje and Katahdin.

Table 1: Measured index parameters for five potato cultivars, ± half length of 0.95 confidence interval. *IE* stands for infection efficiency (-): chance of infection per sporangium, *LP* for latency period (days), *LG* for lesion growth rate (m d^{-1}), *SI* for sporulation intensity: (# m^{-2}), A_b for leaflet area (m^2) and s_b for leaflet shape (-). Numbers followed by the same letter are not significantly different at P = 0.001.

Cultivar	*IE*		*LP*	*LG*		A_b	s_b	
Bintje	0.006[a]	± 0.002	3.7[a]	0.0039[a]	± 0.0004	3.0[a] ± 0.2	1.48[a]	± 0.04
Agria	0.003[b]	± 0.001	3.6[b]	0.0034[a]	± 0.0005	3.0[a] ± 0.3	1.42[b,c]	± 0.05
Santé	0.0013[c]	± 0.0004	3.2[c]	0.0011[b]	± 0.0002	2.5[b] ± 0.2	1.38[b]	± 0.03
Karnico	0.0007[d]	± 0.0003	3.2[c]	0.0005[c]	± 0.0002	2.6[b] ± 0.1	1.45[a,c]	± 0.03
Katahdin	0.008[a]	± 0.004	3.5[b]	0.0038[a]	± 0.0004	-[*]	-[*]	

[*] no data available.

Latency period

Lesions appeared on all cultivars on days 3 and 4 after inoculation, not before or after. Significant differences were found between all cultivars according to the χ^2 test, except between cvs Santé and Karnico. On cvs Santé and Karnico, the latency period was shortest, on cv Bintje, it was the longest.

Lesion growth

Lesion growth rates were largest on cv Bintje and lowest on cv Karnico. No significant differences were found between cvs Bintje, Agria and Katahdin according to *t*-tests. Lesion growth rates on Santé and Karnico were significantly different from these cultivars and from each other in *t*-tests at $\alpha = 0.05$.

Leaflet size and shape

The largest leaflets were found on Bintje and Agria. They were significantly larger than those on Santé and Karnico, which were not significantly different from each other. The leaflets on Bintje were the most elongated, where leaflets of Agria and Santé had a slightly rounder shape (table 1).

Sporulation intensity on Bintje

Figure 2 shows that there is a good correlation between sporulation capacity and the growth increment of lesion area ($R^2 = 0.87$). The sporulation intensity is 484 ± 127 sporangia m^{-2} with the confidence level at $\alpha = 0.05$.

A linear regression with intercept showed that the intercept was not significantly different from 0. This finding supports the hypothesis that lesion growth is indeed directly proportional to sporulation.
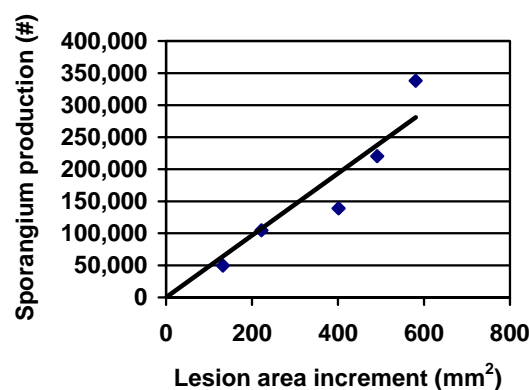
Figure 2: Relationship between sporangium production and lesion area growth on cv Bintje to calculate the sporulation intensity.

Analysis of the index

Index values for different cultivars

Higher values of R_0 and *r* indicate greater susceptibility, whereas a higher value of *T* indicates greater resistance. The five cultivars had the same ranking for each of these three calculated quantities R_0, *T* and *r*, with cv Katahdin being the most susceptible cultivar, followed by cvs Bintje, Agria and Santé (in this order), and cv Karnico being the most resistant (table 2). A remarkable feature is the negative value of *r* for cv Karnico as a result of a smaller than 1 net reproduction, R_0. Given the parameter inputs, an epidemic could not develop on Karnico, except with huge inputs of inoculum from outside.

Sensitivity analysis

Sensitivities are mostly positive, which indicates that an increase in parameter values leads to an increase in *r* (table 3). The sensitivity to *LP*, on the contrary, is negative as a longer latency period increases generation time, reducing *r*, except for cv Karnico, where *r* is negative, resulting in slower 'decay' of an epidemic if *LP* is large. For cv Karnico, the sensitivities to the other two parameters affecting generation time, *LG* and s_b, are also negative.

The sensitivity to different components varies substantially between cultivars. This variation reflects the nonlinearity of the equation for the index: the sensitivity greatly depends on the value of the index and of the measured parameters. For cvs Santé and Karnico, the sensitivities are generally quite low because *r* is small. Overall, in the five investigated varieties, the index is most sensitive to the sporulation intensity and the infection efficiency and least sensitive to the leaflet shape s_b. This means that the same

Table 2: Calculated values of net reproduction (R_0, -), generation time (*T*, d) and relative growth rate index (*r*, d^{-1}), compared with overall leaf resistance data from the Dutch variety list (Anonymous, 2002) for five potato cultivars.

	Bintje	Agria	Santé	Karnico	Katahdin
R_0	5.6	3.4	1.02	0.58	6.8
T	11	12	27	57	10
r	0.16	0.10	0.00090	−0.0096	0.18
overall leaf resistance	3	5.5	5	8	-[*]

[*] no data available.

Table 3: Sensitivities (S, d^{-1}), of the index r to a relative change in component parameters for different potato cultivars. *IE* stands for infection efficiency (-): chance of infection per sporangium, *LP* for latency period (d), *LG* for lesion growth rate (m d^{-1}), *SI* for sporulation intensity: (# m^{-2}), A_b for leaflet area (m^2) and s_b for leaflet shape (-).

Parameter	Bintje	Agria	Santé	Karnico	Katahdin
IE	0.09	0.08	0.04	0.02	0.09
LP	−0.05	−0.03	−0.0001	0.0005	−0.06
LG	0.10	0.07	0.0008	−0.009	0.1
SI	0.09	0.08	0.04	0.02	0.09
A_b	0.04	0.05	0.04	0.02	0.03
s_b	0.01	0.009	0.00009	−0.001	0.02

relative changes in sporulation intensity and infection efficiency would change the value of r most and relative changes in leaflet shape would change it the least. The sensitivity to lesion growth rate and leaflet shape varies most between cultivars.

Uncertainty analysis

The uncertainty analysis (table 4) indicates that experimental error in the measurement of infection efficiency and sporulation intensity has the largest contribution to uncertainty in the estimate of r, followed (at some length) by uncertainty in lesion growth rate. The other parameters have comparatively small contributions to index uncertainty. The results indicate that accurate estimation of the index would benefit most from a more accurate quantification of infection efficiency and sporulation intensity. Note that the uncertainty resulting from inaccurate knowledge of dispersal efficiency could not be quantified, and might be substantial and influential.

Impact analysis

The analysis of the impact of variation in component parameters between varieties on r (table 5) shows that infection efficiency is the major variety-dependent parameter responsible for differences in relative growth rate, followed by lesion growth rate and sporulation intensity. Leaf area index also has a noteworthy effect, especially when it is considered that a high leaf area index not only increases dispersal efficiency, but also makes the microclimate in the crop more suitable for infection. (The latter aspect is not considered in the index calculation). The other parameters do not cause significant changes in r.

Table 4: Uncertainty (U) in index because of experimental error in measured parameters for five potato cultivars. *IE* stands for infection efficiency (-): chance of infection per sporangium, *LP* for latency period (d), *LG* for lesion growth rate (m d^{-1}), *SI* for sporulation intensity: (# m^{-2}), A_b for leaflet area (m^2) and s_b for leaflet shape (-).

Parameter	Bintje	Agria	Santé	Karnico	Katahdin
IE	0.025	0.018	0.011	0.0072	0.050
LP	−0.0074	−0.0044	−1.7·10^{-5}	8.5·10^{-5}	−0.0085
LG	0.011	0.011	0.00014	−0.0036	0.013
SI	0.024	-*	-*	-*	-*
A_b	0.0028	0.0050	0.0029	0.00085	-*
s_b	0.0004	0.00032	2.0·10^{-6}	−2.5·10^{-5}	-*

* no data available.

Table 5: The impact (I, d^{-1}) of known cultivar variation in resistance components on the index r (d^{-1}). Data on cultivar variation in parameter values are based on this study and a list compiled by Van Oijen (1989). Subscripts 'max' and 'min' refer to the maximum and minimum value published, respectively. *IE* stands for infection efficiency (-): chance of infection per sporangium, *LP* for latency period (d), *LG* for lesion growth rate (m d^{-1}), *SI* for sporulation intensity: (# m^{-2}), A_b for leaflet area (m^2), s_b for leaflet shape (-) and *LAI* for leaf area index (m^2 m^{-2}).

Parameter	Variation	$r\,(p_{max}) - r\,(p_{min})$
IE	0.0007 - 0.024	0.23
LP	3.2 - 5	−0.02
LG	0.001 - 0.0039	0.14
SI	4.8·10^8 - 8.5·10^8	0.04
A_b	0.0025 - 0.0029	0.001
s_b	1.38 - 1.45	−0.0007
LAI	3 - 5	0.03

Discussion and conclusions

Measurements of resistance components

The resistance ranking that follows from the estimation of r for four Dutch potato varieties in this chapter (Karnico>Santé>Agria>Bintje) corresponds broadly to the published long term overall field resistance for these same varieties

(Karnico>Agria>Santé>Bintje) (Anonymous, 2002), with the exception of the ranking of Agria and Santé. Our experimental results suggest that Santé should be the more resistant variety, whereas long term experiments have shown that Agria is generally less heavily affected by late blight than Santé. It has been found that the ranking of resistance of Santé and Agria varies between experiments (L.T. Colon and G.J.T. Kessel, personal communication). Thus, the (small) difference could be a 'year' effect. Another explanation may be the use of a different isolate. The isolate that is generally used for the determination of the overall resistance (isolate I82001, Plant Research International, Wageningen; L.T. Colon, pers. communication) is different from the one used here (isolate IPO 655-2A, Plant Research International, Wageningen-UR).

The negative value of r for Karnico implies that each new generation of lesions would be smaller than the previous one. This would suggest that late epidemics cannot really develop on Karnico. This conclusion however depends on the value of the inoculum dispersal efficiency parameter (ε), which is based on a limited amount of experimental data and is therefore not well known (Van Oijen, 1991). More experiments are needed to measure the dispersal efficiency more accurately and, possibly, also in more detail.

Effect of component parameters on the index
A remarkable aspect of this index is the inclusion of size and shape of the leaflet. Leaflet characteristics have not been incorporated in previous indexes, or models. The uncertainty analysis indicated that they have little effect on the index, because little variation in these parameters was measured. The actual variation between cultivars may however be larger than the variation found in the group of four cultivars that was studied here.

The leaf area index also plays a role in the index, because the modelled interception of sporangia increases with the amount of leaf area in the canopy. This suggests that epidemics will develop more slowly at the start of the growing season, when the leaf area index is lower.

Effect of measurement uncertainties on the index
In this chapter, field data were used to parameterise the index. When using data measured in climate cabinets, one should be aware that these data may not well represent the field situation (e.g. Colon *et al.*, 1995a; Dorrance and Inglis, 1997; Singh and Birhman, 1994). The comparatively large uncertainty of estimated r with respect to the parameters *LG, SI* and *IE* indicates that a more accurate measurement of these parameters would add most to a more precise estimate of r. Apart from these parameters, the dispersal efficiency, ε, needs to be measured accurately and the

assumption that it does not vary between cultivars must be tested. The dispersal time, the time between production of a sporangium and the time it causes a new infection might also be estimated.

Role of component parameters in explaining cultivar resistance

The very minor effect of the leaflet shape indicates that variation in this parameter may be neglected. Using a standard value for s_b of 1.4 would simplify the expression for r to:

$$r = \frac{\ln(R0)}{T} = \frac{\ln(A_b \cdot SI \cdot \varepsilon \cdot LAI \cdot IE)}{LP + 0.522 \cdot \dfrac{\sqrt{A_b}}{LG}} \tag{16}$$

The large effect of between-variety variation in *IE* and *LG* on *r* indicates that infection efficiency and lesion growth rate are the most important resistance components. This result is consistent with the results of Van Oijen (1991). Practically, this means that in screening for resistance, selection of resistant cultivars should be based on infection efficiencies and lesion growth rates.

Wider applications of the index

Although this index was applied to potato late blight, there are many other pathogens that behave similarly. The index could be applied to leaf pathogens with radially expanding lesions, at most one per leaflet, that sporulate on the edge and grow on leaves with a roughly elliptical shape. Analyses similar to the ones that have been carried out here can also be applied to study the effects of variation in aggressiveness.

This index can be used to quickly assess the effect of variation in resistance and aggressiveness on the epidemiological behaviour of a range of pathogens and therefore has a wide range of applications in plant disease epidemiology.

Appendix 1: Proof for relation between leaflet size and average distance

The proof of the proportionality between the average distance between two points on a leaflet-ellipse and $\sqrt{A_b}$ is given by proving that the distance between any two points increases with $\sqrt{A_b}$ if the leaflet size is changed. When this is proven for the combination of any two points, it is also proven it for the average of all combinations of points. To obtain the proof, a leaflet B_0 is defined with area $A_{b,0}$ and a given length-width ratio s_0. The leaflet has length $l_{b,0}$ (m) and width $w_{b,0}$ and size $A_{b,0}$:

$$A_{b,0} = \frac{1}{4}\pi \cdot l_{b,0} \cdot w_{b,0} \tag{17}$$

On this leaflet we define two arbitrary points, Ψ_1 and Ψ_2, with locations $(x_1, y_1)_0$ and $(x_2, y_2)_0$, respectively. The distance D_0 between these points is:

$$D(\Psi_1, \Psi_2)_0 = \sqrt{(x_2 - x_1)^2 + (y_2 - y_1)^2} \tag{18}$$
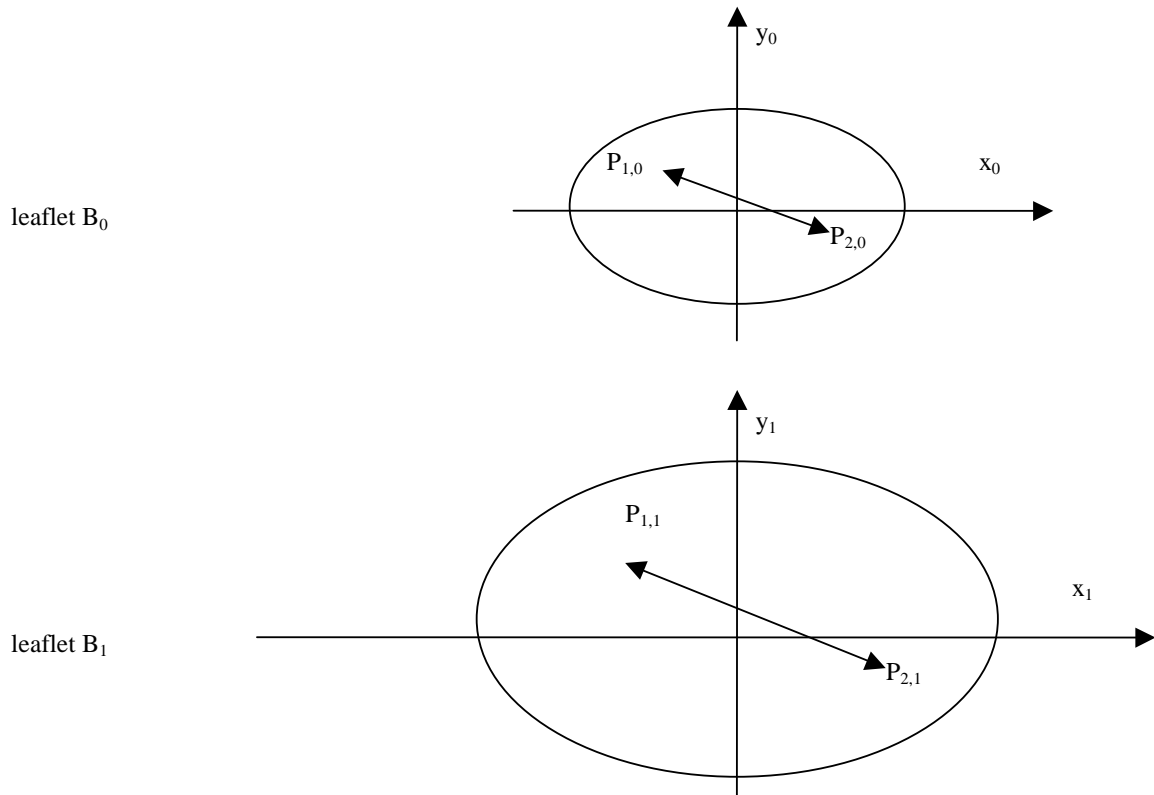
Figure 3: Effect of a change in size on distance between to points on a leaflet ellipse. The arrows indicate the distance between two points on leaflet B_0 and the distance on of the corresponding points on B_1.

The area of this leaflet B_0 is now changed by inflating or deflating it. This is done by stretching of shrinking both the x- and the y- axis by a factor of *n*. The process is shown in figure 3, where we see $\Psi_{1,0}$ and $\Psi_{2,0}$ on leaflet B_0 and the corresponding points $\Psi_{1,1}$ and $\Psi_{2,1}$ on the leaflet B_1. The leaflet thus obtained is B_1. The two points Ψ_1 and Ψ_2 on B_0 get a corresponding location on leaflet B_1. The coordinates of Ψ_1 and Ψ_2 on B_1 correspond to those on B_0 as:

$$(x_{1,1}, y_{1,1}) = (n \cdot x_{1,0}, n \cdot y_{1,0}) \tag{19}$$

$$(x_{2,1}, y_{2,1}) = (n \cdot x_{2,0}, n \cdot y_{2,0}) \tag{20}$$

The distance between these points on B_1 is:

$$
\begin{aligned}
D(\Psi_1, \Psi_2)_1 &= \sqrt{(n \cdot x_{2,0} - n \cdot x_{1,0})^2 + (n \cdot y_{2,0} - n \cdot y_{1,0})^2} \\
&= \sqrt{n^2 \cdot (x_{2,0} - x_{1,0})^2 + n^2 \cdot (y_{2,0} - y_{1,0})^2} \\
&= n\sqrt{(x_{2,0} - x_{1,0})^2 + (y_{2,0} - y_{1,0})^2} = n \cdot D(\Psi_1, \Psi_2)_0
\end{aligned}
\tag{21}
$$

The length and width of the leaflet have also increased by a factor *n*:

$$l_{b,1} = n \cdot l_{b,0} \tag{22}$$

$$w_{b,1} = n \cdot w_{b,0} \tag{23}$$

so the area $A_{b,1}$ is:

$$A_{b,1} = \frac{1}{4}\pi \cdot l_{b,1} \cdot w_{b,1} = \frac{1}{4}\pi \cdot (nl_{b,0}) \cdot (nw_{b,0}) = n^2 \cdot \frac{1}{4}\pi \cdot l_{b,0} \cdot w_{b,0} = n^2 \cdot A_{b,0} \tag{24}$$

We wanted to prove that if two leaflets have the same shape, the ratio of the average distance between two points on those leaflets is equal to the square root of their areas. In terms of leaflets B_0 and B_1, this requires proving that:

$$\frac{D(\Psi_1, \Psi_2)_1}{D(\Psi_1, \Psi_2)_0} = \sqrt{\frac{A_{b,1}}{A_{b,0}}} \tag{25}$$

Filling in the relations we have found (equations 21 and 24), this can be written as:

$$\frac{n \cdot D(\Psi_1, \Psi_2)_0}{D(\Psi_1, \Psi_2)_0} = \sqrt{\frac{n^2 \cdot A_{b,0}}{A_{b,0}}} \tag{26}$$

25

Noting that we are only interested in positive values of *n*, this can be written as:

$$n = n \tag{27}$$

Which, of course, is true for all values of *n* and therefore the proof has been given.

Appendix 2: Partial derivatives of the function for the index

$$\frac{\partial r}{\partial IE} = \frac{1}{IE \cdot T} \tag{28}$$

$$\frac{\partial r}{\partial LP} = \frac{-\ln(R_0)}{T^2} \tag{29}$$

$$\frac{\partial r}{\partial SI} = \frac{1}{SI \cdot T} \tag{30}$$

$$\frac{\partial r}{\partial LAI} = \frac{\dfrac{1}{LAI}}{LP + \dfrac{\sqrt{A_b}}{LG} \cdot \left(-0.643 + 0.577(s_b^{0.404} + s_b^{-0.404})\right)} = \frac{1}{LAI \cdot T} \tag{31}$$

$$\frac{\partial r}{\partial \varepsilon} = \frac{1}{\varepsilon \cdot T} \tag{32}$$

$$\frac{\partial r}{\partial LG} = \frac{\ln(R_0) \cdot (T - LP)/LG}{T^2} \tag{33}$$

$$\frac{\partial r}{\partial A_b} = \frac{T - 1/2 \cdot \ln(R_0) \cdot (T - LP)}{A_b \cdot T^2} \tag{34}$$

$$\frac{\partial r}{\partial s_b} = \frac{\ln(R_0) \cdot \dfrac{\sqrt{A_b}}{LG} \cdot 0.577 \cdot 0.404 \cdot (s_b^{-0.596} - s_b^{-1.404})}{T^2} \tag{35}$$

CHAPTER 3

Ability of the Gaussian plume model to predict and describe spore dispersal over a potato crop

H.P. Spijkerboer, J.E. Beniers, D. Jaspers, H.J. Schouten,
J. Goudriaan, R. Rabbinge and W. van der Werf, 2002

Abstract

The Gaussian plume model is considered a valuable tool in predictions of the atmospheric transport of fungal spores and plant pollen in risk assessments. The validity of the model in this area of application has not been extensively evaluated.

A field experiment was set up to test and – if necessary – adapt the Gaussian plume model, as applied to the dispersal of spores. Spores of the fern *Lycopodium clavatum* were released artificially over a period of 10 min. from a source placed 70 cm above the surface in a potato crop. Spore catches were made with a network of Rotorod and Burkhard samplers, placed up to 100 m downwind from the source and at several heights and cross wind distances from the anticipated plume axis.

The width and height of Gaussian plumes depend on atmospheric mixing, as affected by weather. Mixing parameters in risk assessments are commonly predicted on the basis of weather conditions. A low correlation ($R = 0.4$) was found between measured spore concentrations and predicted spore concentrations, using a widely used prediction method (Gaussian plume model; Pasquill, 1974), based on cloud cover, wind speed, season and time of day.

More precise methods for predicting the width and height of Gaussian plumes require detailed site-specific information (measurements of wind speed and temperature at two heights above the vegetation), and are therefore not readily applicable in risk assessments. An alternative that is often adequate is to use a worst case approach, in which the dispersal parameters are used that give the highest spore concentration at the location of interest. Predictability could be improved by measuring atmospheric stability during and just after weather conditions conducive to release of the pollen or spores of interest.

The model was calibrated with a weighted least squares method. Calibrating the model led to a more than hundredfold decrease in the sum of weighted squares. A comparison of estimated concentrations with the measurements confirmed that spore clouds originating from a point source take the form of a Gaussian plume: the coefficient of correlation between measured spore concentrations and fitted concentrations was 0.8.

The fraction of spores that escaped the canopy and was available for long distance dispersal amounted to 64% ± 17%. An 83% correlation was found between this so-called escape fraction and wind speed.

Key words: Aerobiology, crop protection, plant disease epidemiology, prediction, risk assessment, calibration, escape.

Introduction

Aerial transport by means of spores is an important dispersal mechanism for many plant fungal pathogens, especially over longer distances. Modelling studies have indicated that tobacco blue mold (*Peronospora tabacina*) epidemics can start from sources of inoculum several hundred km's away (Aylor *et al.*, 1982). There is some evidence that *Phytophthora infestans*, the causal agent of potato late blight, can spread over distances of 11 km (Van der Zaag, 1956).

The research described here was conducted to assess the risk of potato late blight infection from distant sources of *Phytophthora infestans.* Spores of the fungus *Phytophthora infestans*, the causal agent of potato late blight, are wind borne (Hirst, 1953) and spread readily between nearby potato refuse piles, potato production fields and allotment gardens (Zwankhuizen *et al.*, 1998). Quantification of the risk posed to potato fields by distant sources is a relevant component of decision support systems for potato late blight control which are currently used by farmers (e.g. Prophy, Opticrop B.V., Vijfhuizen, the Netherlands; Plant Plus, Dacom PLANT-Service B.V., Emmen, the Netherlands).

The risk of infection can be quantified as the number of infections on a susceptible crop caused by spores that come from a distant source. This risk can be calculated from the rate of release from the source, the atmospheric dispersal from the source to the crop, the atmospheric deposition and the chance of infection per spore.

The Gaussian plume model (GPM) is a simple atmospheric dispersal model, requiring only the input of release and routinely measured weather data (KNMI, 1979). De Jong (1988) used the Gaussian plume model (Pasquill, 1974) to study the risk of infection by fungal plant pathogens from distant sources. It has also been used to model the spread of pollen (Di-Giovanni *et al.*, 1989).

The Gaussian plume model has been tested for dispersal of pollutant gasses (Hinrichsen, 1984; Rao *et al.*, 1979) and is widely used for this purpose (Lyons and Scott, 1990). Although the Gaussian plume model has been applied in plant pathology, it has not been tested with respect to the spread of spores, and no spore concentration measurements have been conducted beyond distances of 30 m from a source (Aylor, 1990 and references therein; Eversmeyer and Kramer, 1992). The premise of the acceptability of this model for describing the spread of spores and other small particles requires further substantiation.

The work described in this chapter had a double purpose:
(1) to evaluate whether the Gaussian plume model provides an acceptable description of spore dispersal up to a distance of 100 m from a source; and

(2) to quantify model parameters, such as the escape fraction.

Material and methods

Used symbols

parameter	description
π (-)	mathematical constant ($\pi \approx 3.14$)
$\Delta\theta$ (°)	estimated minus observed wind direction
σ_y (m)	standard deviation of spore concentration in cross wind direction
σ_z (m)	standard deviation of spore concentration in vertical direction
a (-)	parameter in function for σ_z
b (-)	parameter in function for σ_z
C (m^{-3})	spore concentration
d (m)	displacement height ($d = 0.55$m)
f_e (-)	escape fraction
h (m)	crop height ($h = 0.7$m)
H (m)	height at which spores are released
K (-)	correction in σ_z and σ_y for effects of surface roughness
p (-)	parameter in function for σ_y
q (-)	parameter in function for σ_y
Q (s^{-1})	source strength
R (-)	reflection coefficient
T (-)	numerical value for the stability class
u (m s^{-1})	mean horizontal wind speed at 10 m height
x (m)	downwind distance from the source
y (m)	horizontal distance from the plume centre
z (m)	height above the surface
z_0 (m)	roughness length ($z_0 = 0.029$m)

Approach

In 35 measurement sessions, spores of the fern *Lycopodium clavatum* were released at the top of the canopy in a 200×200 m^2 potato field near Wageningen in the summer of 1997.

The ability of the Gaussian plume model to *describe* spore plumes was tested by fitting the model to the data by iterative parameter estimation, and assessing the

goodness of fit. This fitting exercise determines whether the Gaussian plume model has the appropriate shape to describe the plumes.

The ability of the Gaussian plume model to *predict* the spore plumes was tested by calculating expected spore concentrations on the basis of independent data, and again assessing goodness of fit. The predictions are made on the basis of a widely used classification of expected atmospheric stability (KNMI, 1972), using readily available information on wind speed, cloud cover, time of day and day of the year. The input data needed for the model were obtained during the measurement sessions.

The Gaussian plume model itself was parameterised to describe the effect of the potato canopy on the shape of the spore plume.

To be able to fit the Gaussian plume model to data, the discrete classification scheme for atmospheric stability was converted into a continuous system with parameters describing atmospheric stability that varied on a continuous scale. More details are given below.

The spore dispersal experiment

A spore dispersal experiment was carried out in a 200 m × 200 m potato field in Wageningen, the Netherlands. Spore concentrations were measured above the potato crop at up to 100 m from a point source of *Lycopodium clavatum* spores to collect input data for the Gaussian plume model. A total of 35 measurement sessions were carried out.

The potato field was separated from a road by some trees on the southern and eastern side. Small plots with 20 to 100 cm high agricultural crops surrounded the plot on the other two sides.

Spores of the fern *Lycopodium clavatum* (Fluka Chemie AG, Buchs, Switzerland) were released at crop height ($h = 0.7$ m) from an Erlenmeyer bottle by blowing air into the bottle through a hole in the side over a period of 600 s. This was roughly the period it took to empty the bottle.

To determine the number of spores that were released, the weight of the bottle with spores was measured before and after each session. The number of spores released was calculated from the weight loss using the average number of $1.36 \cdot 10^8$ spores per gram (own data, unpublished).

Spore concentrations downwind from the source were determined with spore samplers mounted on masts at a network of locations at distances between 20 and 100 m downwind from the source and in the crosswind direction at distances between 0 and 40 m from the expected plume axis. All masts with samplers were placed between potato plants. The samplers and source were placed at least 30 m from the edge of the potato vegetation. The location of the masts was determined before the start of each

session, depending on wind direction. Two different instrument set-ups were used (figure 1). In the first set-up all masts with spore traps were located on one or two lines perpendicular to the wind direction (figure 1a). One of these lines was 50m downwind from the source. In some cases instruments were also placed on the other line 100m downwind.

A different set-up was used in later sessions, because digging the holes for the masts proved to be very time consuming. For the second set-up, a grid of holes (figure 1b) was dug. Masts were placed in some of these holes, depending on wind direction, in such a way that they stood along a crosswind line as much as possible.

One to four spore traps were mounted on each mast. The lowest spore trap was always placed at 2 m above the surface. Other traps were placed at intervals of 2 m above the first trap, up to 8 m high.

Ten Rotorod model 20 spore traps (Sampling Technologies, Inc, Minnetonka, MN, USA) were used in each session. In most sessions, two Burkhard volumetric spore traps (Burkhard Manufacturing Ltd. Rickmansworth, Hertfordshire, England) were also used. The placement of the spore traps relative to that of the spore source was determined before the start of each session. The wind direction was measured by aiming a compass at a wind vane placed in the field at a height of 6 m above the surface.

The fraction of cloud cover (eighths), that is required as input for the Gaussian plume model, was determined before the start of each session.

The wind speed (u, m s^{-1}) at 10 m above the surface was not measured at the experimental site, but obtained from a weather station about 3 km to the south-west of the potato field.

The Gaussian plume model

The Gaussian plume model (Pasquill, 1974) describes dispersal over distances up to 10 km from a source. It predicts the concentration (C, # m^{-3}) of gasses or particles downwind from a source that can be regarded as a point source. Spore concentrations at a given point depend on the distance from the source, the wind direction, the number of released spores, the wind speed and the amount of mixing in the atmosphere as affected by weather conditions and the effects of the vegetation on the wind flow.
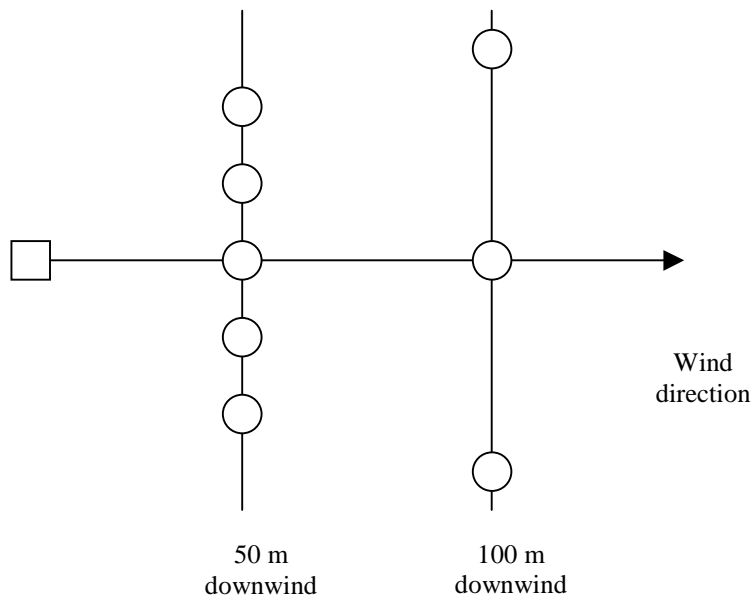
A: Instrument set up for sessions 1 through 5
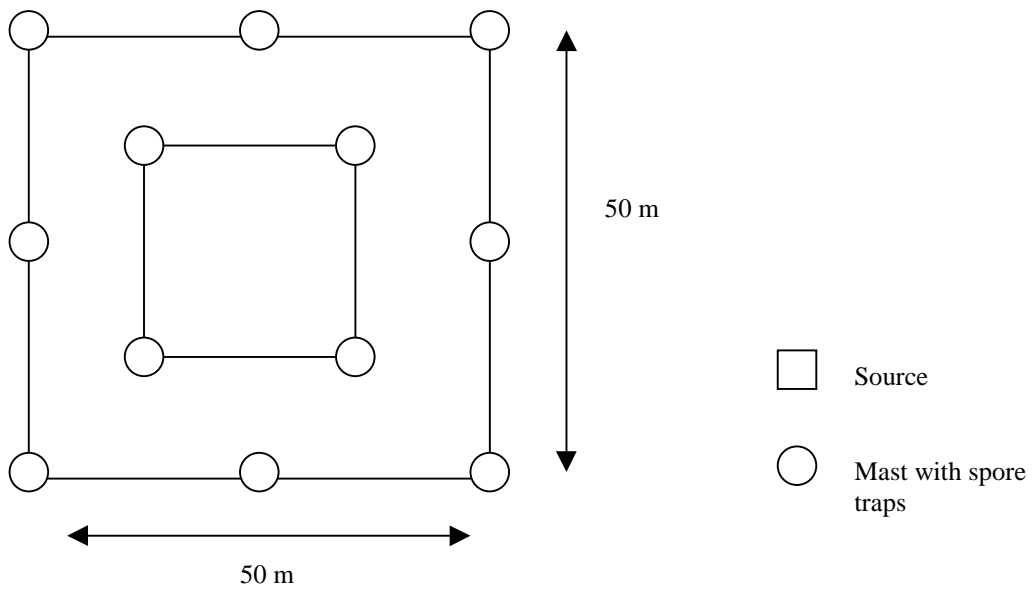
B: Instrument set up for sessions 6 through 15

Figure 1: Location of spore traps and spore source as used in measurement sessions. open square: source; open circle: possible locations for masts with spore traps (not all locations were used in each session).

With the Gaussian plume model, the spore concentration C at any location (x, y, z) downwind from a source is calculated as (Pasquill, 1974):

$$C(x, y, z) = \underbrace{\frac{Q}{2\pi u}}_{1} \quad \underbrace{\frac{\exp(-y^2 / 2\sigma_y^2)}{\sigma_y}}_{2} \cdot \frac{1}{\sigma_z} \left\{ \underbrace{\exp\left[-\frac{(H - z)^2}{2\sigma_z^2}\right]}_{3a} + \underbrace{R \cdot \exp\left[-\frac{(H + z)^2}{2\sigma_z^2}\right]}_{3b} \right\} \tag{1}$$

In this equation, x, y and z (m) are the co-ordinates that define the location of the spore traps. The co-ordinate system is Cartesian and depends on the location of the source and on the wind direction. The source is located in the origin of the system at release height H (m) above the surface. Its co-ordinate are $(0, 0, H)$. The positive x-axis, also called the plume axis, lies in the direction of the mean wind. The z co-ordinate is the height above the surface (m). The y-axis lies in the crosswind direction.

The number of released spores and the wind speed are described in factor 1 of equation 1. The source strength Q (s^{-1}) is the rate of spore release. The parameter u (m s^{-1}) is the mean wind speed at 10 m above the surface.

Factors 2 and 3 describe the height and width of the plume. Factor 2 describes the crosswind shape of the plume as a Gaussian curve with standard deviation σ_y (m) with its peak on the x-axis. The factors 3a and 3b describe the shape of the plume in the vertical direction. Factor 3a describes a Gaussian curve with standard deviation σ_z (m) and a peak at height H. Factor 3b describes the effect of the ground surface, assuming that a fraction of R of the plume is reflected at the earth's surface. This reflection is modelled as a source at height $-H$, below the earth's surface. A default value of 1 for R (complete reflection) was assumed.

The standard deviations σ_y and σ_z determine the height and width of the plume. They depend on the downwind distance from the source (x, m) and on the amount of mixing (turbulence) in the atmosphere.

Predictions with the Gaussian plume model

The Gaussian plume model was used to predict spore concentrations, with input data from our own measurement sessions and from a nearby weather station (table 1).

The Gaussian plume model co-ordinates of the spore traps were derived from the measured wind direction and the location of the spore traps relative to the source.

The source strength Q was calculated as the ratio of the number of released spores and the length of the release period (600 s).

The parameters σ_y and σ_z were calculated with empirical functions. Formulas that were also used by De Jong (1988) were used to calculate σ_y and σ_z:

$$\sigma_z = K(z_0) \cdot a \cdot x^b \tag{2}$$

$$\sigma_y = K(z_0) \cdot 10^p \cdot x^q \tag{3}$$

In these formulas, *a*, *b*, *p* and *q* are dimensionless empirical constants and $K(z_0)$ is calculated as:

$$K(z_0) = (10 \cdot z_0)^{0.53 \cdot x^{-0.22}} \tag{4}$$

in which, z_0 (m) is the roughness length. The amount of mixing in the atmosphere determines the values of *a*, *b*, *p* and *q*. The roughness length z_0 is a characteristic of the surface cover. The value of σ_y depends on the averaging period. The above formula for σ_y is specific for averaging periods of 10 min. The averaging period has no effect on σ_z.

Table 1: Summary of the model used for prediction of spore concentrations.

$$C = \frac{Q}{2\pi u} \cdot \frac{\exp(-y^2/2\sigma_y^2)}{\sigma_y} \cdot \frac{1}{\sigma_z} \left\{ \exp\left[-\frac{((H-d)-(z-d))^2}{2\sigma_z^2} \right] + \exp\left[-\frac{((H-d)+(z-d))^2}{2\sigma_z^2} \right] \right\} \tag{5}$$

$$\underbrace{}_{1} \quad \underbrace{}_{2} \quad \underbrace{}_{3a} \quad \underbrace{}_{3b}$$

measurements: *u, H, y, z, θ* (θ determines co-ordinate system)

$$Q = \frac{\text{number of released spores}}{\text{release period}}$$

measurements: number of released spores, release period

$$d = 0.78 \cdot h \qquad \text{(Legg } et\ al., 1981)$$

measurements: *h*

$$\sigma_z = K(z_0) \cdot a \cdot x^b$$
$$\sigma_y = K(z_0) \cdot 10^p \cdot x^q$$

measurements: *x*

$$K(z_0) = (10 \cdot z_0)^{0.53 \cdot x^{-0.22}} \qquad \text{(equation 4; De Jong (1988))}$$

measurements: *x*

$$z_0 = 0.041 \cdot h \qquad \text{(Legg } et\ al., 1981)$$

measurements: *h*

a, b, p, q : values depend on stability class

(tables 1, 2 based on De Jong (1988))

stability class: table from KNMI (1972)

measurements: season, time of day, *u*, cloud cover

The parameters *a*, *b*, *p* and *q* describe the effect of the weather conditions on the amount of mixing. The effect of weather conditions on the amount of mixing is empirically classified into six categories, or stability classes. For each stability class, the parameters *a*, *b*, *p* and *q* have different values. There are six stability classes; A through F. Class A is the stability class that describes the most unstable atmosphere and F the most stable one. In an unstable atmosphere, there is more mixing and plumes are wider and higher than in a stable atmosphere.

Values of *a*, *b*, *p* and *q* for the different stability classes that were taken from De Jong (1988). They are given in tables 2 and 3. The stability class can be predicted on the basis of the percentage cloud cover and the wind speed at 10 m above the surface. Tables in KNMI (1972) were used to choose the stability class, depending on the time of day, the season, the wind speed *u* at 10 m above the surface and the percentage cloud cover.

The roughness length z_0 describes the effect of the surface cover on the amount of mixing. It is a surface characteristic that describes the effect of the roughness of vegetation elements on the wind flow. It is derived from the logarithmic wind profile (Stull, 1988) that describes a logarithmic increase of wind speed with height. The roughness length represents the height at which the wind speed equals 0. The value of

Table 2: Values of stability parameters *a* and *b* in function for σ_z.

Stability class	*a*	*b*
A	0.28	0.9
B	0.23	0.85
C	0.22	0.80
D	0.20	0.76
E	0.15	0.73
F	0.12	0.67

Table 3: Values of stability parameters *p* and *q* in function for σ_y.

Stability class	*p*	10^p	*q*
A	−0.27819	0.527	0.865
B	−0.43063	0.371	0.866
C	−0.67985	0.209	0.897
D	−0.89279	0.128	0.905
E	−1.00877	0.098	0.902
F	−1.18709	0.065	0.902

z_0 must be derived from wind speed measurements for each type of vegetation. A formula that is specific for potato crops (Legg *et al.*, 1981) was used to calculate z_0 from the crop height. Using this formula for a crop height of 0.7 m (own measurements) gives a roughness length of 0.029 m.

The Gaussian plume model was adjusted to make it compatible with the wind speed profile described by Legg *et al.* (1981). The equation that Legg *et al.* use for the logarithmic wind profile includes an extra parameter, the displacement height *d* (m). This parameter has the effect that it lifts the whole wind profile from the ground over a distance *d*. To make the Gaussian plume model consistent with this shifted wind profile, the height at which the plume is reflected was lifted over a distance *d*. The plume is now reflected at height *d* and the virtual source is located at height *d*–(*H*–*d*), i.e. at 2*d*–*H*, instead of at height –*H*. A formula given by Legg *et al.* (1981) was used to calculate *d* from the height of the potato crop and obtained a value of 0.55 m. Spore concentrations were predicted with an adapted version of the Gaussian plume model (equation 1) that incorporates the effects of the displacement height:

$$C = \underbrace{\frac{Q}{2\pi u}}_{1} \cdot \underbrace{\frac{\exp\left(-y^2/2\sigma_y^2\right)}{\sigma_y}}_{2} \cdot \frac{1}{\sigma_z}\left\{\underbrace{\exp\left[-\frac{(H-z)^2}{2\sigma_z^2}\right]}_{3a} + \underbrace{\exp\left[-\frac{(H+z-2d)^2}{2\sigma_z^2}\right]}_{3b}\right\} \qquad (5)$$

Simulations with the Gaussian plume model

To get an impression of the effect of stability class on predicted downwind concentrations, some simulations were carried out with the Gaussian plume model. 10 minute-average surface concentrations downwind of a source with a release rate of 10^6 particles per second and a wind speed of 5 m s^{-1} were calculated for the different stability classes.

Calibration of the Gaussian plume model

To determine whether goodness of fit could be improved, the Gaussian plume model was calibrated, using the observed spore concentrations (table 4). Parameter estimation targeted the following aspects:
- standard deviations σ_z and σ_y
- escape fraction
- wind direction

The model was calibrated for σ_z and σ_y to determine if the plume height and width are predicted accurately. The values of σ_z and σ_y were not estimated directly, but indirectly, through the stability class. The discrete stability classes (A through F) were turned into a continuous system, using a stability number *T* (-). Linear relations

between the stability number *T* and the parameters *a, b, p* and *q* were derived and the standard deviations σ_z and σ_y were calculated from these parameters *a, b, p* and *q* with equations 2 and 3.

Table 4: Summary of the model used for calibration of spore concentrations.

$$C = f_e \cdot \frac{Q}{2\pi u} \cdot \frac{1}{\sigma_y \sigma_z} \cdot \exp\left(-\frac{y^2}{2\sigma_y^2}\right) \cdot \left\{ \exp\left[-\frac{((H-d)-(z-d))^2}{2\sigma_z^2}\right] + R \cdot \exp\left[-\frac{((H-d)+(z-d))^2}{2\sigma_z^2}\right] \right\} \quad (9)$$

$$\underset{1}{\longleftrightarrow} \quad \underset{2}{\longleftrightarrow} \quad \underset{3a}{\longleftrightarrow} \quad \underset{3b}{\longleftrightarrow}$$

measurements: *H*, *y*, *z*, θ (θ determines co-ordinate system)

calibration: f_e, Δθ

$d = 0.78 * h$ (Legg *et al.*, 1981)	
measurements: *h*	

$\sigma_z = K(z_0) \cdot a \cdot x^b$	(2)
$\sigma_y = K(z_0) \cdot 10^p \cdot x^q$	(3)
(based on De Jong (1988))	
measurements: *x*	

$K(z_0) = (10 \cdot z_0)^{0.53 \cdot x^{-0.22}}$	(4)
(De Jong (1988))	
measurements: *x*	

$z_0 = 0.041 \cdot h$ (Legg *et al.*, 1981)	
measurements: *h*	

$a = 0.306 - 0.0302T$	(6a)
$b = 0.940 - 0.044T$	(6b)
$p = -0.097 - 0.185T$	(6c)
$q = 0.890$	(6d)

calibration: *T*

The stability number *T* has a value of 1 for stability class A, 2 for class B, etc. The following linear functions were derived to describe the relationship between the stability number *T* and the parameters *a, b, p* and *q*:

$$a = 0.306 - 0.0302T \tag{6a}$$
$$b = 0.940 - 0.044T \tag{6b}$$
$$p = -0.097 - 0.185T \tag{6c}$$
$$q = 0.890 \tag{6d}$$

These functions give good approximations of the actual values of *a, b, p* and *q* for the different stability classes (tables 2 and 3). The R^2 values are larger than 95% for *a, b* and *p*. The values of *q* published in KNMI (1972) are less than three percent different from the average value used here.

The predicted stability numbers were compared with the estimated stability numbers *T* to compare the actual height and width of the plume with the predicted height and width of the plume. If the estimated value of *T* is higher than predicted, the atmosphere is more stable than expected, the values of σ_z and σ_y will be lower and plumes are lower and narrower and vice versa. To determine whether the estimated value of *T* was significantly larger or smaller than expected on the basis of weather data, a Wilcoxon test was done.

The escape fraction (f_e, -) was also calibrated. f_e is expected to be smaller than 1 due to loss of spores by deposition, which takes place especially during the first meters.

The location of the plume was calibrated with the parameter $\Delta\theta$, the change from the measured wind direction to the estimated wind direction. The wind direction determines the co-ordinate system of the Gaussian plume model. Only small deviations are anticipated.

To estimate the values of the parameters *T*, f_e and $\Delta\theta$, a weighted least squares parameter estimation method was used. The Gaussian plume model that was adapted to a potato crop (equation 5) was fitted to the data:

$$C = f_e \cdot \underbrace{\frac{Q}{2\pi u}}_{1} \cdot \underbrace{\frac{1}{\sigma_y \sigma_z} \cdot \exp\left(-\frac{y^2}{2\sigma_y^2}\right)}_{2} \cdot \left\{ \exp\left[-\underbrace{\frac{((H-d)-(z-d))^2}{2\sigma_z^2}}_{3a}\right] + \exp\left[-\underbrace{\frac{((H-d)+(z-d))^2}{2\sigma_z^2}}_{3b}\right] \right\} \tag{7}$$

Parameter values were estimated by minimising the sum of weighted least squares:

$$\sum_i \frac{\left(C_{cal,i} - C_{meas,i}\right)^2}{C_{cal,i}} \tag{8}$$

where, the subscript 'cal' refers to calculated values and 'meas' to measured values. This method is recommended for parameter estimation of Gaussian curves (Ross, 1990).

Calculated concentrations (C_{cal}) were used as weights, not measured concentrations (C_{meas}), because in many cases the measured spore concentration was 0 spores m^{-3} and a division by zero would have occurred.

For each session, the calibrations were carried out several times with different, randomly chosen initial values for T, f_e and $\Delta\theta$.

To obtain reliable estimates of parameters of Gaussian curves, measurements at both sides of the peak of the Gaussian distribution are needed (Ross, 1990). Variability in wind direction may cause the plume axis not to pass through the line of measurement devices. In that case, measurements are only made on one side of the peak, not both sides. As a result, both the location and the height of the peak must be derived from an extrapolation, instead of an interpolation. This makes the estimates of the parameters that represent the location of the peak and the plume width ($\Delta\theta$ and T, respectively) too unreliable. It was, therefore, decided to use only the fifteen best sessions and discarded those measurement sessions where less than half of the plume was measured.

Analysis of model parameters

The correlation structure of the model was determined with a partial correlation analysis for each session to evaluate possibilities for a parameter reduction.
The correlation between the calibrated parameters and the weather variables of windspeed and cloudiness was also determined.

Results

Figure 2 gives an impression of the three-dimensional concentration distribution predicted by the Gaussian plume model for stability class C. Concentrations are highest near the source. Gradients are large near the source but become less steep with downwind distance. This reflects the fact that plume become wider with downwind distance. The figure shows only the concentrations for positive y-values. However, the concentrations are symmetrical around the $y=0$ plane:

$C(x,-y,z) = C(x, y, z)$
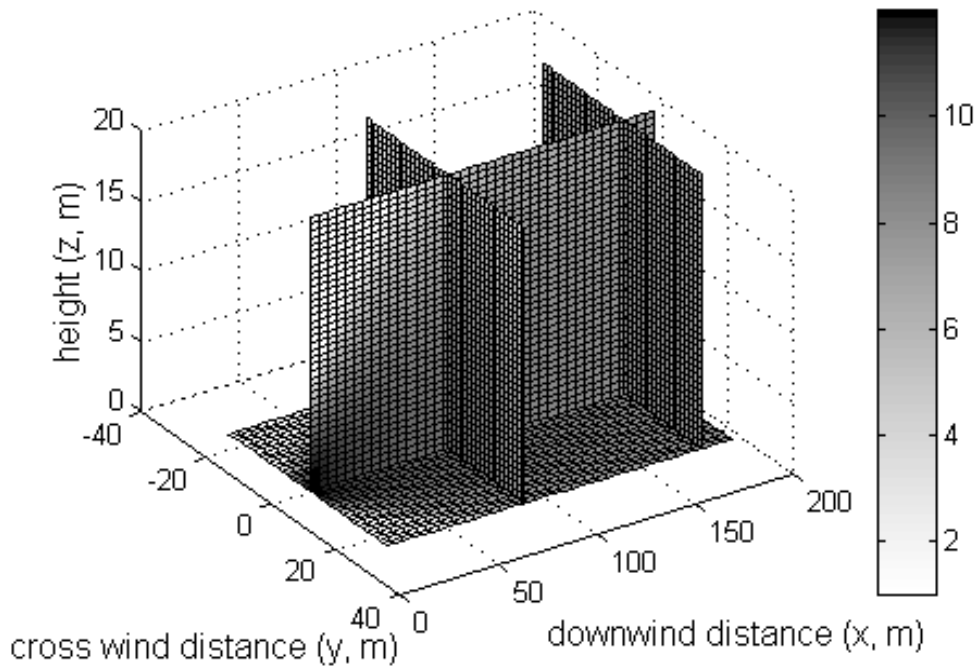
Figure 2: Slice plot of concentrations predicted with the Gaussian plume model. Colourshading indicates values of log(concentration) for stability class C. Release is 10^6 particles per second, wind speed is 5 m s^{-1}. Axis ranging from 0 to 200: downwind distance x (m); axis ranging from –40 to + 40: crosswind distance y (m); Vertical axis: height z (m).

Figure 3 shows contour plots of expected downwind concentrations for all stability classes. There is a significant increase in crosswind concentration gradients from class A to class F, reflecting the fact that for the more stable classes, plumes are narrower. In the downwind direction, gradients decrease from class A to class F. Peak concentrations increase from class A to class F. Note the small contour of 1,000,000 particles per m^3 near $x = 20$ m for class F, which is not present in the other graphs.

Figures 4a and 4b show a comparison of predicted concentrations (3D surface) and measured concentrations at 2 m height and 4 m height respectively for session 1. The predicted plume seems to be flatter than the measurements indicate. Peak concentrations are lower than predicted. Also, the predicted and measured plume do not overlap: concentrations are still high where they should have gone down to zero on both sides of the plume.

After parameter estimation, the modelled concentrations are similar to the measured concentrations (figures 4c and 4d).
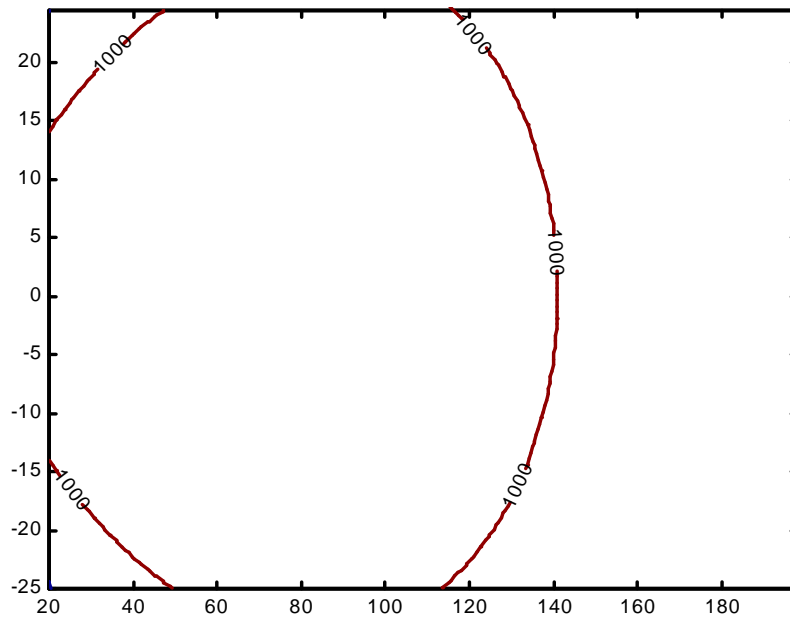
A: surface concentrations for stability class A
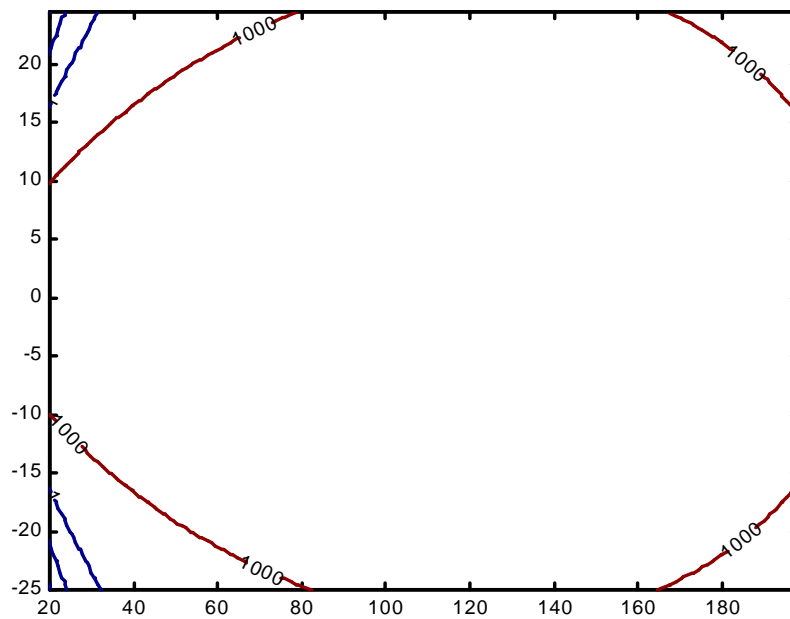
B: surface concentrations for stability class B

Figure 3: Surface concentrations (# m^{-3}) calculated with a Gaussian plume model for different stability classes. Contour intervals are a factor 1000. Release is 10^6 particles per second, wind speed is 5 m s^{-1}.
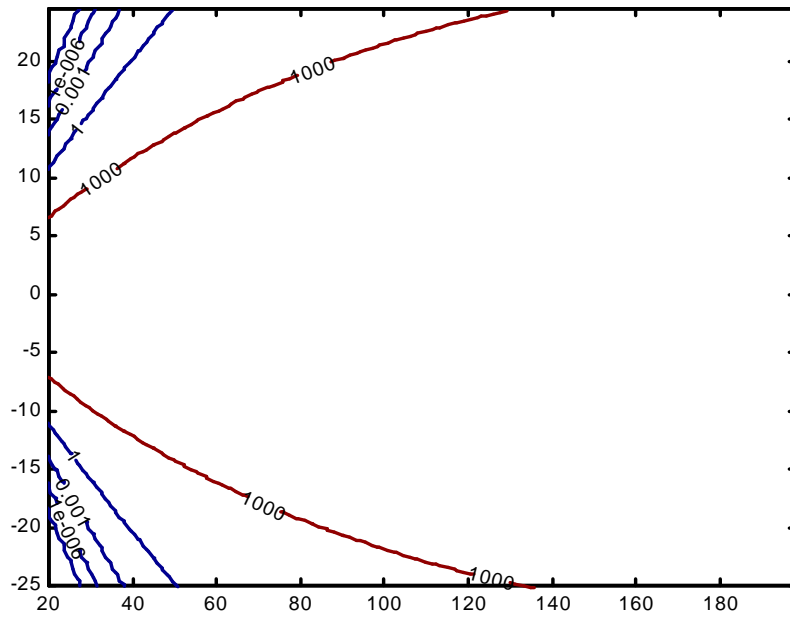
C: surface concentrations for stability class C
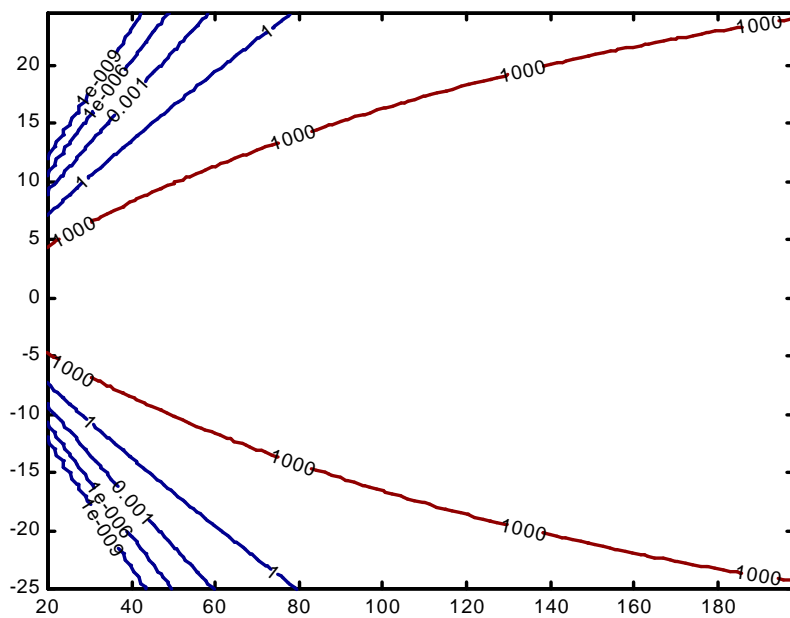
D: surface concentrations for stability class D

Figure 3 (continued)
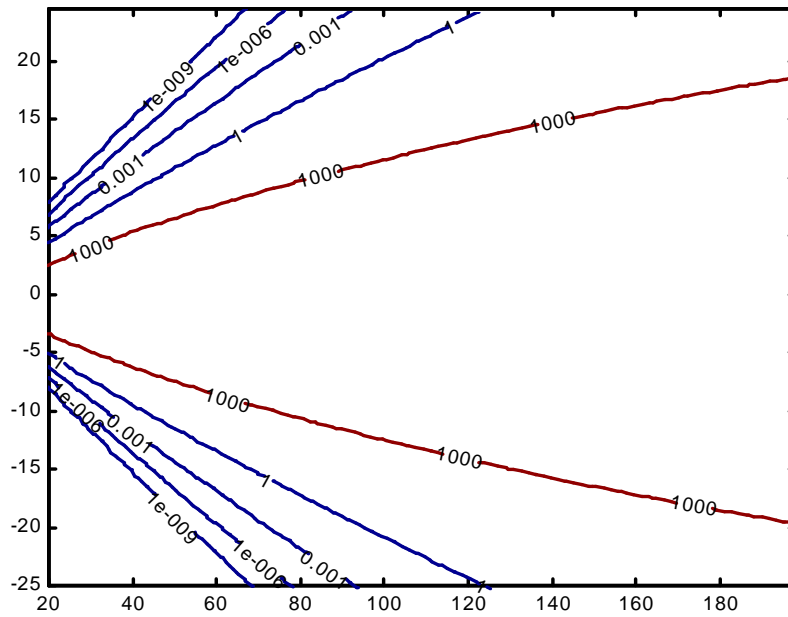
E: surface concentrations for stability class E
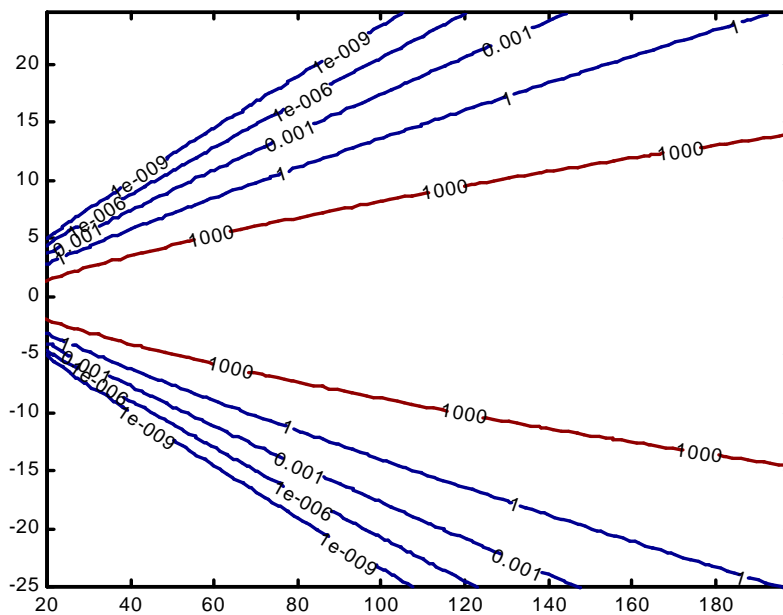
F: surface concentrations for stability class F

Figure 3 (continued)
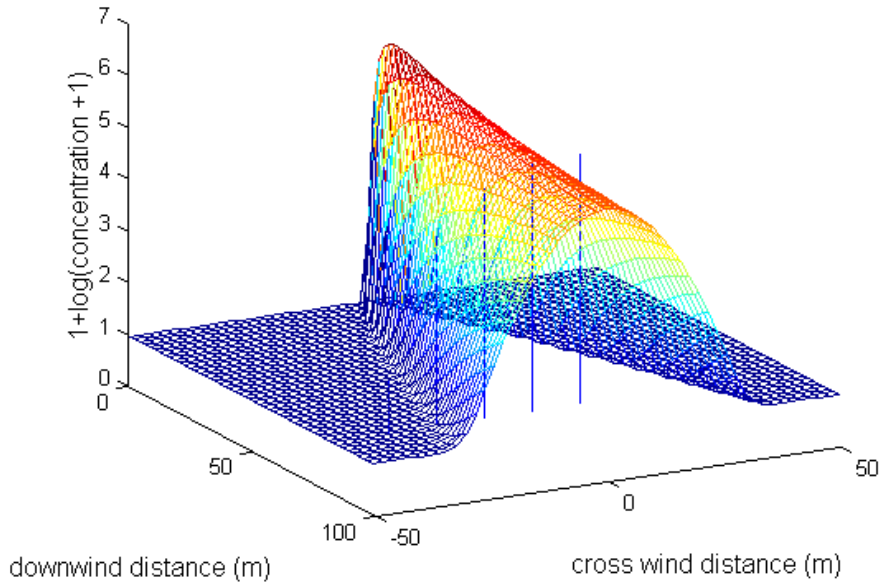
A: predicted concentrations at 2 m height
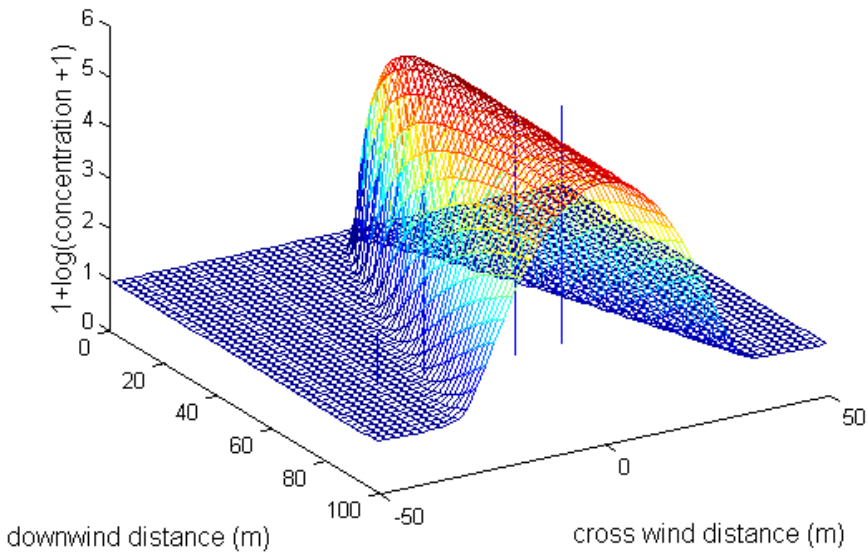
B: predicted concentrations at 4 m height

Figure 4: Modelled concentrations (C, # m^{-3}) compared with measured concentrations (n=15). 3D-surfaces: modelled concentrations; vertical lines: measured concentrations; vertical axis: $(1 + {}^{10}\log (C+1))$; axis ranging from –50 to + 50: crosswind distance y (m); axis ranging from 0 to 100: downwind distance x (m).
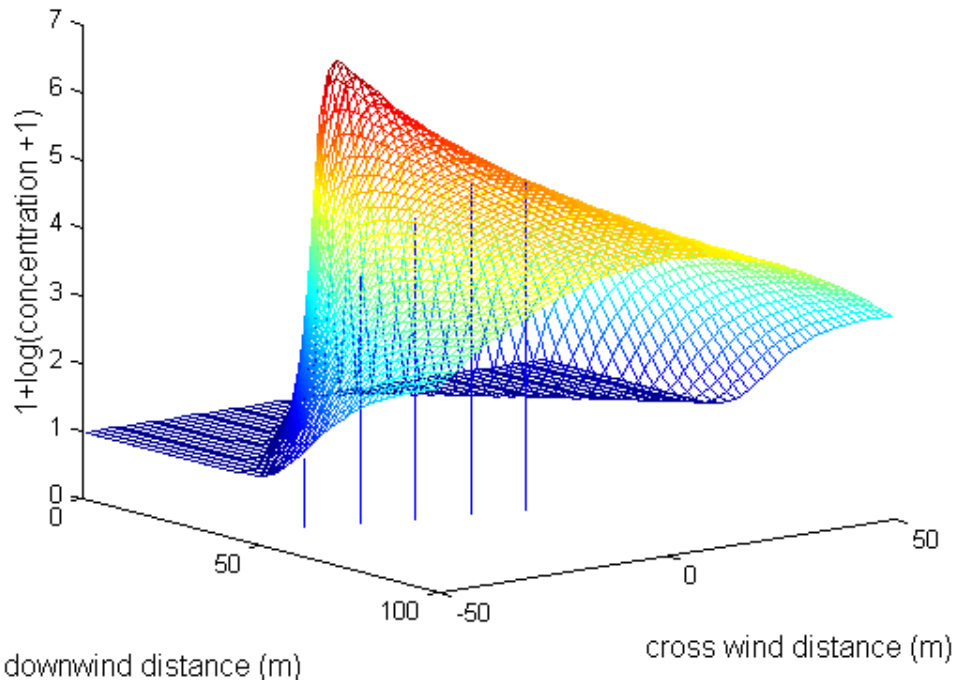
C: Estimated concentrations at 2 m height
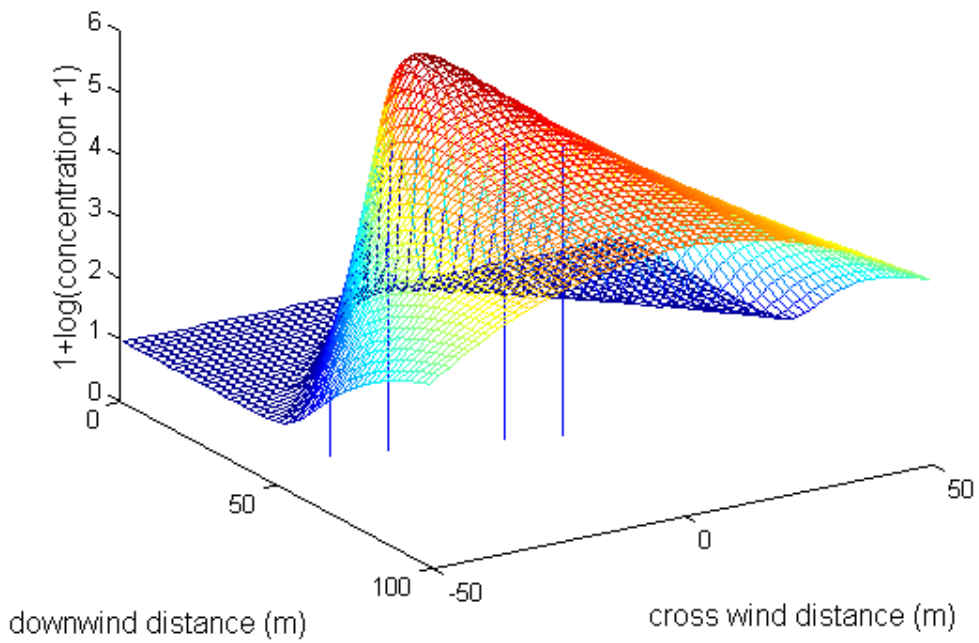
D: Estimated concentrations at 4 m height

Figure 4 (continued)

An overall comparison of model predictions with measurements for all sessions (figure 5) shows that no clear relation between the two can be seen. The sum of weighted squares for the model predictions ranged between $4 \cdot 10^3$ and $3 \cdot 10^{242}$ (table 5). The correlation coefficient (r) between measured and predicted concentration is 40%.

Figure 6 shows a similar plot for measured concentrations and concentrations calculated with the calibrated model. The sum of weighted squares ranged between $5 \cdot 10^1$ and $3 \cdot 10^4$ (table 5). The correlation coefficient (r) between measured and calculated concentrations was 80%. This indicates that the calibrated Gaussian plume model can properly describe the measured concentrations in most cases.
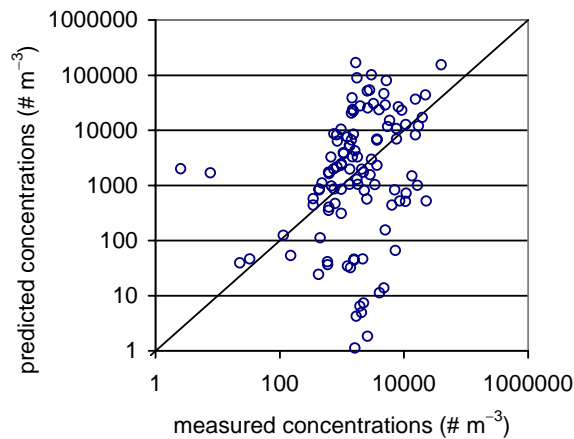
Figure 5: Predicted concentrations compared with measured concentrations (n=15). solid line: calculated concentration = measured concentration; open circles: calculated concentration.
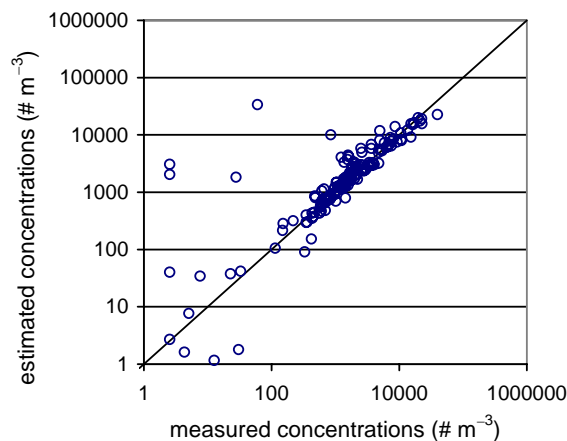
Figure 6: Calibrated concentrations compared with measured concentrations (n=15). solid line: calculated concentration = measured concentration; open circles: calculated concentration.

Estimated values of T tended to be lower than predicted values (table 5). They were significantly smaller than predicted values according to the Wilcoxon test ($P<0.05$). The lower values of T cause plumes to be higher and wider, because of the increase in σ_y and σ_z.

Escape fractions were lower than the predicted value of 1. The escape fraction (f_e) was $0.64 \pm 0.17(P<0.05)$, which means that a significant number of spores is deposited and is not available for long distance dispersal.

The estimated values of $\Delta\theta$ (°) ranged between -11 and $+17$ ° (table 5).

Table 5. Results of measurements and model calibration.

	Observations			Predictions				Calibrations			
Session	Start time (CET)	cloudi-ness (eigth's)	Wind-speed (m/s)	Stability class	T (-)	θ (°)	*Sum of weighted squares*	f_e (-)	T (-)	$\Delta\theta$ (°)	*Sum of weighted squares*
1	16:36	8	5.5	D	4	292	2.7E+10	0.87	1.48	16.8	2.2E+02
2	15:25	3	3.1	B	2	207	6.4E+04	0.19	1.60	10.5	2.6E+02
3	14:40	7	1.8	D	4	354	1.9E+08	0.14	0.40	8.3	6.9E+02
4	15:33	6	1.9	D	4	354	6.6E+08	0.24	0.97	−7.8	6.7E+02
5	16:11	8	2.3	D	4	47	2.8E+07	0.36	1.33	−8.3	7.7E+02
6	15:47	5	6.0	C	3	270	4.5E+03	0.72	2.28	−3.8	4.2E+01
7	14:57	7	3.5	D	4	228	2.1E+11	0.47	1.27	−0.9	4.1E+02
8	12:20	8	2.8	D	4	175	2.9E+55	0.69	0.10	−10.5	4.7E+03
9	14:40	4	5.4	C	3	240	9.1E+19	0.88	0.98	−2.2	1.8E+02
10	11:09	7	5.5	D	4	260	2.8E+242	1.13	0.47	−5.8	3.1E+04
11	13:17	6	7.5	C/D	4	260	2.5E+10	0.99	1.83	−5.5	9.9E+03
12	16:03	7	2.6	D	4	27	1.6E+107	0.40	0.41	1.5	1.3E+04
13	11:51	1	6.1	B	2	78	4.3E+29	1.18	−0.45	−3.9	9.6E+03
14	14:24	2	6.0	C	3	73.5	5.5E+05	0.61	1.07	−2.2	5.2E+01
15	14:37	8	5.4	D	4	269.5	1.8E+06	0.69	2.76	−3.8	6.8E+02

Table 6. Correlations (ρ) between estimated parameters and weather variables.

	f_e (-)	$\Delta\theta$ (°)	T_{est} (-)
Cloudiness (eighths)	−0.20	−0.03	0.23
u (m/s)	0.83	−0.06	0.29

Table 6 shows correlations between calibrated parameters and the weather variables of cloudiness and wind speed. The correlations are mostly small, except for the correlation between escape fraction and wind speed ($\rho = 0.83$).

Table 7. Correlation matrices for the 15 sessions as calculated with the 3-parameter estimation.

Session		f_e (-)	$\Delta\theta$ (°)	T (-)	Session		f_e (-)	$\Delta\theta$ (°)	T (-)
1	f_e (-)	1.00	0.64	−0.96	9	f_e (-)	1.00	−0.88	−0.91
	$\Delta\theta$ (°)	0.64	1.00	−0.61		$\Delta\theta$ (°)	−0.88	1.00	0.97
	T (-)	−0.96	−0.61	1.00		T (-)	−0.91	0.97	1.00
2	f_e (-)	1.00	−0.20	−0.89	10	f_e (-)	1.00	0.98	−0.98
	$\Delta\theta$ (°)	−0.20	1.00	0.29		$\Delta\theta$ (°)	0.98	1.00	−0.97
	T (-)	−0.89	0.29	1.00		T (-)	−0.98	−0.97	1.00
3	f_e (-)	1.00	0.67	−0.94	11	f_e (-)	1.00	0.61	−0.70
	$\Delta\theta$ (°)	0.67	1.00	−0.65		$\Delta\theta$ (°)	0.61	1.00	−0.58
	T (-)	−0.94	−0.65	1.00		T (-)	−0.70	−0.58	1.00
4	f_e (-)	1.00	−0.38	−0.90	12	f_e (-)	1.00	0.76	−0.70
	$\Delta\theta$ (°)	−0.38	1.00	0.36		$\Delta\theta$ (°)	0.76	1.00	−0.84
	T (-)	−0.90	0.36	1.00		T (-)	−0.70	−0.84	1.00
5	f_e (-)	1.00	0.38	−0.88	13	f_e (-)	1.00	−0.20	−0.83
	$\Delta\theta$ (°)	0.38	1.00	−0.32		$\Delta\theta$ (°)	−0.20	1.00	0.08
	T (-)	−0.88	−0.32	1.00		T (-)	−0.83	0.08	1.00
6	f_e (-)	1.00	−0.26	−0.79	14	f_e (-)	1.00	−0.11	−0.85
	$\Delta\theta$ (°)	−0.26	1.00	0.18		$\Delta\theta$ (°)	−0.11	1.00	0.08
	T (-)	−0.79	0.18	1.00		T (-)	−0.85	0.08	1.00
7	f_e (-)	1.00	0.37	−0.92	15	f_e (-)	1.00	−0.26	−0.80
	$\Delta\theta$ (°)	0.37	1.00	−0.37		$\Delta\theta$ (°)	−0.26	1.00	0.49
	T (-)	−0.92	−0.37	1.00		T (-)	−0.80	0.49	1.00
8	f_e (-)	1.00	−0.19	−0.78					
	$\Delta\theta$ (°)	−0.19	1.00	0.25					
	T (-)	−0.78	0.25	1.00					

The partial correlation analysis (table 7) showed a high correlation between f_e and T. It was found however, that fixing one of these values would lead to a large change in weighted squares as is shown in figure 7. This figure shows that the gradient of the sum of weighted squares is quite high near the estimated values of f_e and T. So not estimating f_e or T would lead to a large increase of the sum of weighted squares. It was therefore decided not to reduce the number of estimated parameters.
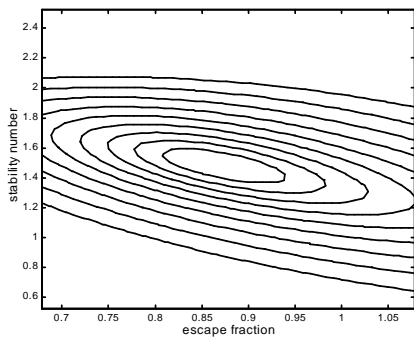
A: session 1
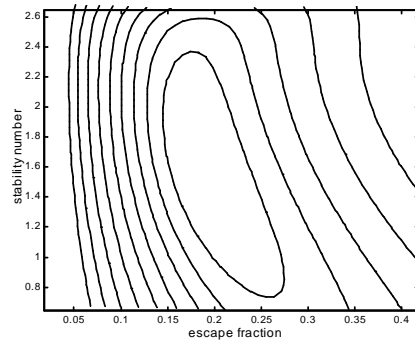
B: session 2
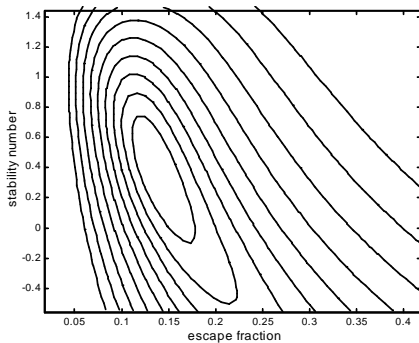
C: session 3
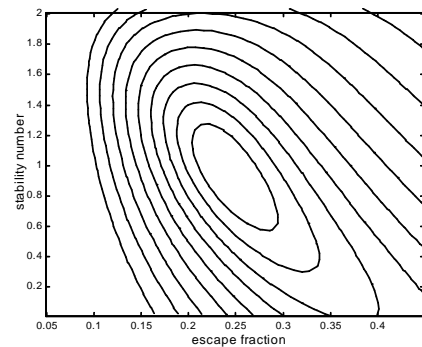
D: session 4

Figure 7a-7o: Contourplots of weighted squares against T and f_e for the 15 sessions. The estimated values of T and f_e (T_{est} and $f_{e, est}$) are located in the centre of the plot. The range of value for T and f is: $(f_{e, est} - 0.2, f_{e, est} + 0.2)$, $(T_{est} - 1, T_{est} + 1)$. A maximum of ten contours has been drawn in each plot with logarithmically chosen intervals of a factor of $\sqrt{2}$ starting at the minimum in the centre of the plot.
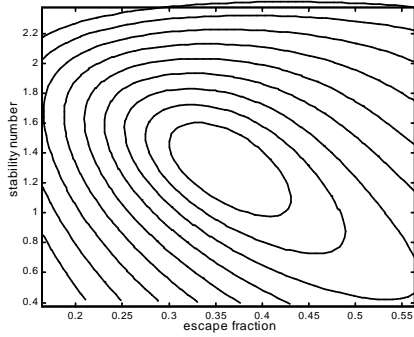
E: session 5
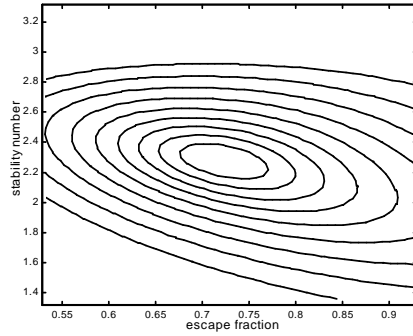
F: session 6
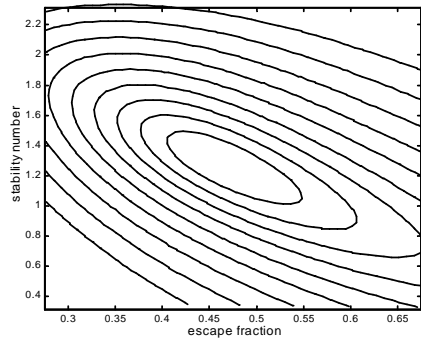
G: session 7
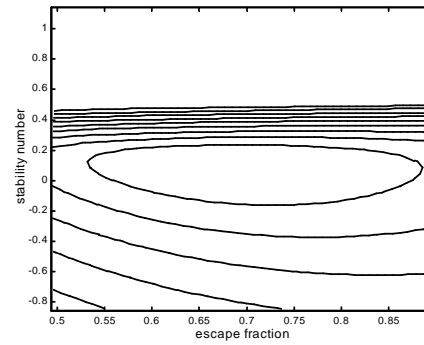
H: session 8
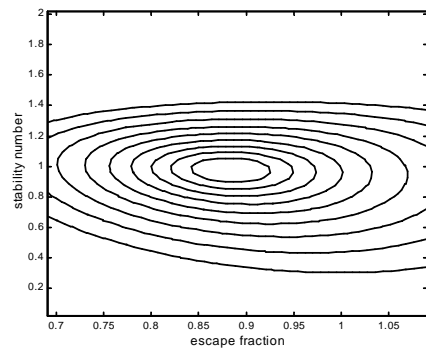
I: session 9
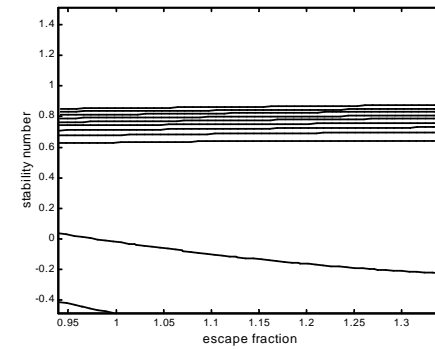
J: session 10

Figure 7 (continued)
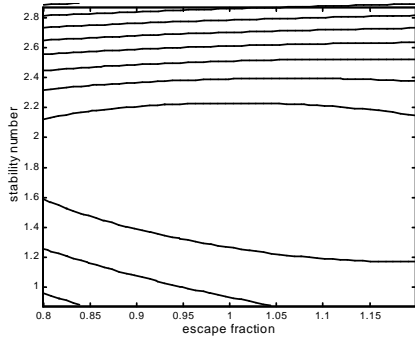
K: session 11
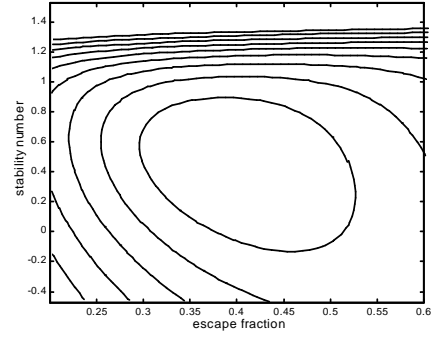
L: session 12
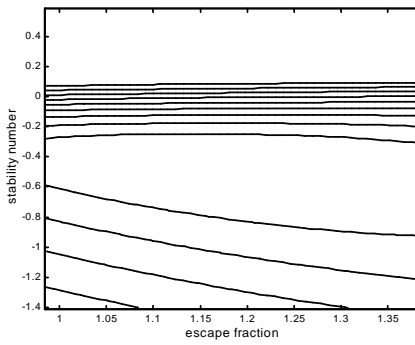
M: session 13
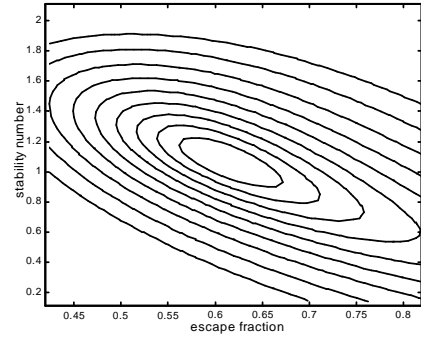
N: session 14
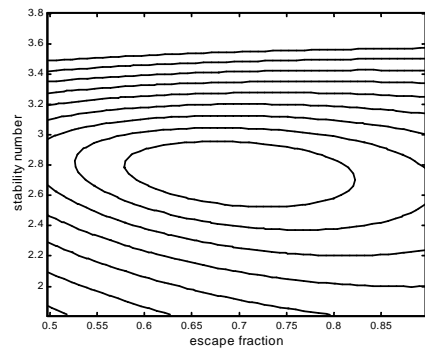
O: session 15

Figure 7 (continued)

Discussion and conclusions

The increase in concentration gradients in the cross-wind direction from class A to class F is caused by the decreasing values of σ_y. The lower values of σ_y cause the exponential term (2) in equation 5 to go to zero very quickly, whereas at the centre of the plume where the exponential term has the value of 1, the low value of σ_y in the denominator of term (2) give a higher function value. This reflects the physical effect that when stability increases, there is less mixing so all particles stay near the centre of the plume.

The decreasing concentration gradient from class A to F in the downwind direction is also caused by the decreased amount of mixing, which causes the particles to stay near the centre of the plume, so that the concentration there remains high. This effect is reflected in equation 5 by the σ_y and σ_z in the denominator of terms (2) and (3) which increase less with distance from class A to class F as can be seen in equations 2 and 3 and tables 2 and 3.

The low correlation between predicted and measured spore concentrations was not caused by the fact that particles were used instead of gasses. The difference between particles and gasses is that particles settle and are deposited due to the force of gravity and gasses are not. This should only affect the vertical shape of the plume, not the plume width. Because it was found that plumes were both higher and wider, it is not likely that the different behaviour of particles as compared with gasses was the cause of the difference between measured and predicted spore concentrations. This is supported by the fact that the Gaussian plume model can describe spore concentrations accurately after parameter estimation.

Hanna *et al*. (1993) compared observed and predicted plume widths for a number of models, including the Gaussian plume model. These comparisons were carried out for several experiments in which gasses were released. They found that the Gaussian plume model underpredicted the plume width, as did the other models. The degree of underprediction of the other models was not significantly different from the Gaussian plume model. This is consistent with our findings that estimated values of *T* were lower than predicted ones, since lower values of *T* lead to wider plumes.

Actual plumes were probably wider than predicted plumes, because the stability classes were not correctly predicted using the tables from KNMI (1972). These tables classify atmospheric stability on the basis of information on cloud cover, wind speed, season and time of day. In many cases the atmosphere was more unstable than expected from the stability class. Results of Erbrink and Van Jaarsveld (1992) support this view. From a modelling study, they concluded that the frequency of occurrence of

class D is overestimated using the conventional classification tables (KNMI, 1972). In eight of our sessions, class D was derived from the observed weather data. This makes it likely that uncertainty in the determination of atmospheric stability was an important cause of the wider and higher plumes. It has been suggested to us that the wider plumes could be caused by shifts in the wind direction caused by large eddies. Large eddies could move the plume as a whole. On a 10 min. scale, the large eddies would be observed as a gradual change in wind direction. A result of the changing wind direction, plumes would spread out over a wider area. This would lead to larger values of σ_y. However, the Gaussian plume model parameterisation is based on dispersal experiments with a duration of 10 mins (e.g., Barad, 1958). This effect will therefore already be incorporated in the model. Using an alternative method to classify atmospheric stability could improve model predictions. These alternative methods are not as widely applicable though.

Mohan and Siddiqui (1998) and Sedefrian and Bennett (1980) compared different classification schemes and found big differences in frequency of occurrence of different stability classes. Mohan and Siddiqui (1998) concluded that methods based on Monin Obukhov length and Richardson number gave the best results. However, these methods require measurement of wind and temperature at different heights in the field where the dispersal takes place. The method used here can be used in both clima-tological studies and for predictions, because the input data can be obtained from weather forecasts or from routine weather observations carried out at many weather stations world-wide. The disadvantage of the method used here is that it may be less accurate in climates that are very different from that in the Netherlands. However, similar methods to derive the stability class have been developed by national weather services in other countries. An alternative method to improve predictability is to measure atmospheric conditions conducive to release. Several spores and pollen only are released under certain weather conditions (for spores see, e.g., Hirst, 1953). Measurement of atmospheric stability during and just after release could be used to determine the stability class, which would improve model performance.

When using the Gaussian plume model, one must make allowance for the uncertainty in plume height and width and the effect this has on accuracy of calculations. In cases where the maximum risk is required, the stability class that gives the highest predicted concentration at the point of interest is best used. To calculate actual risks when tables indicate stability class D during the day, the increased uncertainty in height and width of the plume must be incorporated in the calculations.

The big decrease in weighted squares found by calibration of the model and the 0.80 correlation between measurements and calculations after calibration show that calibrating the model greatly improves the fit and the plumes do have a Gaussian

shape.

The high correlation between f_e and T suggests that the number of calibrated parameters could be reduced by fixing either f_e or T. To check this assumption, contour plots were made. The weighted squares residuals were plotted against f_e and T near the calibrated values of these parameters for each session. These plots (figure 7) show that generally the value of the weighted squares minimising function increases strongly from the minimum at the estimated values of f_e and T. This means that fixing either of these parameters would lead to a big increase in the value of the minimising function. It was therefore decided not to reduce the number of calibrated parameters. The found correlation is probably only a local characteristic near the estimated values of T and f_e, related to the nonlinearity of the Gaussian plume model.

The escape fraction was found to be 64%. Aylor and Ferrandino (1989) determined the escape fraction of spores released inside a 0.8 to 0.9 m high wheat canopy at two heights (0.4-0.5 m and 0.7-0.8 m). The escape fraction found by Aylor and Ferrandino (1989), at a distance of 2 m downwind from the sources, was more than 16 to 44% for the lower source and more than 41 to 50% for the upper source. Their value for the low source is lower than ours, because spores have a bigger chance of being trapped when they are released inside the canopy. The escape fraction found here is typical for particle release near the top of the canopy and is consistent with the value found by Aylor and Ferrandino (1989) for the high source. The positive correlation found between escape fraction and windspeed is consistent with experimental results of Aylor and Taylor (1983) and with model results of De Jong *et al.* (1991).

This chapter looked at the ability of the Gaussian plume model to describe spore concentrations released near a source in the top of a canopy. Results in this paper indicate that 64% of the spores are available for long distance dispersal. The results also indicate that the Gaussian plume model is as suitable for modelling dispersal of spores and other small particles as it is for modelling gas dispersal and, therefore, it has a wide range of ecological applications.

CHAPTER 4

Domain of applicability of the Gaussian plume model for particle dispersal and deposition studies

Abstract

A model study was carried out to estimate the errors that are involved when calculating particle deposition with a Gaussian plume model adapted for deposition with the commonly used 'source depletion method'. The Gaussian plume model with source depletion method provides a simple and fast model for calculating particle dispersal and deposition. It is a simplified model, however, because it ignores the effect of settling of particles in the air and the effect of deposition on the distribution of particles with height. As a result, it is less accurate than alternative, more complex and time-consuming models. Depending on the accuracy of the source depletion method and the accuracy required for a given study, the Gaussian plume model, combined with the source depletion method, may or may not be a useful tool to calculate particle dispersal and deposition.

We determined the accuracy of the Gaussian plume model with source depletion by comparing it with a more realistic (surface depletion) model. The studies were carried out with two versions of an advection-diffusion model: a source depletion version without settling and a surface depletion version with settling. The models were parameterised to describe the aerodynamic behaviour of a range of pollen and spores and to give a worst-case estimate of the error of the source depletion model, as compared with the surface depletion model.

The accuracy of the source depletion model depends on the settling velocity of the particle. We found that the accuracy of the source depletion method decreases with increasing settling velocity of a particle. For particles with a settling velocity of 0.05 m s^{-1} or more, the maximum error was over a factor 1000, suggesting that the Gaussian plume model with source depletion is not suitable for modelling the dispersal of these particles. Maximum errors in the predicted deposition rate ranged from a factor 1.4 for particles with a settling velocity of 0.001 m s^{-1} to a factor 9 for a settling velocity of 0.025 m s^{-1}. Results are compared with published data of settling velocities (Gregory, 1973) of pollen and spores. This information can help to decide whether the Gaussian plume model, combined with the source depletion method provides an accurate enough tool for a given study.

Key words: Aerobiology, modelling, source depletion, surface depletion.

Introduction

The Gaussian plume model (Pasquill, 1974) is an easy to use, mathematically explicit, static model that describes concentrations of gasses dispersing over distances of 0 m to ~10 km downwind from a source. Because the model is easy to use and has been experimentally calibrated and validated, it is widely used in environmental impact studies with air pollutants. It has also been used to model dispersal of fungal spores (De Jong, 1988; Mizubuti, unpublished).

With the Gaussian plume model (GPM), spore concentrations C (# m^{-3}) at location (x, y, z) downwind from a point source can be calculated. As input, the Gaussian plume model requires the rate of release of particles, or source strength, Q (s^{-1}).

Experiments have indicated that the Gaussian plume model is able to describe spore concentrations at distances from 20 to 100 m downwind from a point source if an escape fraction (f_e, -) is incorporated to describe loss of spores near the source (Spijkerboer *et al.*, 2002; chapter 3):

$$Q_{esc} = f_e \cdot Q \tag{1}$$

where, Q_{esc} (s^{-1}) is the rate of escape of particles from the canopy.

Spores continue to be lost from the plume due to deposition. Since the Gaussian plume model was developed for gasses, it describes neither the loss of particles to deposition, nor the effects of this loss on the particle concentration. With a so-called source depletion adaptation (Van der Hoven, 1968) the Gaussian plume model can also be used to model dispersal and deposition of particles like fungal spores or plant pollen further downwind. The source depletion method describes the effect of loss of particles on the spore concentration in the plume as a fractional decrease in particle concentration:

$$C(x, y, z) = L(x) \cdot C^0(x, y, z) \tag{2}$$

where, C^0 is the concentration calculated for in the non-depleted plume as is calculated with the Gaussian plume model and $L(x)$ (-) is the function that describes the fraction of spores still present at downwind distance x.

This method of calculating the effect of loss of particles from the plume implies that the loss, which in reality occurs at the surface, and hence lowers concentrations especially at low altitude in the plume, is accounted for homogeneously as a constant proportion of loss over the entire height of the plume. The effect of settling on the vertical distribution of particles is also ignored. This means that the source depletion method does not describe the effects of settling and deposition on the vertical

concentration profile of the particle plume. This results in errors in the estimation of deposition (McCartney and Fitt, 1985). An over-estimation of deposition can be expected close to the source and an under-estimation at greater distances from the source. Moreover, the model with source depletion is expected to produce a faster decrease in spore density in the plume with distance than is realistic, due to the 'artificial mixing' (Horst, 1977) that results from neglecting the vertical profile of spores.

The surface depletion method, on the other hand, is a mechanistically realistic and in all likelihood more accurate method to describe particle transport (Horst, 1977). This method describes the loss of particles to deposition as a flux at the ground surface. The disadvantage of this method is that it describes the dynamics rather than the results of deposition. It is therefore computationally intensive, and because it is dynamic, it cannot be used in combination with the static Gaussian plume model.

The decision of whether or not to use the source depletion method depends on the accuracy of the source depletion method and on the accuracy required for the study in which it is used.

Draxler and Elliot (1977) and Horst (1977) investigated the accuracy of the source depletion method by comparing it with a surface depletion method when it is applied to dispersal of a gas. The surface depletion model of Horst is a Gaussian plume model to which a loss term at the surface is added. Horst modelled loss to deposition at the surface as diffusion from a source with negative source strength at the surface. Draxler and Elliot modelled deposition to the surface with an advection diffusion equation. They modelled loss at the surface as a flux.

Both Horst (1977) and Draxler and Elliot (1977) neglected gravitational settling in the air, because their models were meant to describe loss of gasses from the plume due to surface deposition. Gasses can be removed from the plume through chemical processes at the surface, but they do not settle in the air, as particles do. To model dispersal of particles, the effect of gravity on particles suspended in the air must be incorporated in the model.

A mechanistic way to model dispersal of gasses and particles is with an advection diffusion equation. McCartney and Fitt (1985) give an advection diffusion equation that can describe the dispersal of fungal spores. Their equation contains a term that describes settling of spores:

$$u \frac{\partial C}{\partial x} = K_y \frac{\partial^2 C}{\partial y^2} + K_z \frac{\partial^2 C}{\partial z^2} + v_s \frac{\partial C}{\partial z} \tag{3}$$

where, K_y and K_z (m^2 s^{-1}) are eddy diffusivities that are assumed to be constant. The term on the left-hand side of this equation describes advection of particles with the

mean wind. The first two terms on the right hand side describe turbulent diffusion in the y and z direction and the last term describes settling. In this equation, a stationary situation has been assumed (no changes with respect to time).

The advantage of the advection diffusion equation is that it can be used together with both the source depletion method and the surface depletion method to describe the effects of deposition. This allows a comparison of both methods.

The aim of this study is to study the accuracy of the source depletion method when used together with the Gaussian plume model as a tool to describe the dispersal and deposition of particles. Deposition rates calculated with a source depleted version of the advection diffusion equation are compared with deposition rates obtained with the surface depletion version in a modelling study. The parameterisation of the model was chosen in such a way that the difference between the two versions can be interpreted as a measure for the accuracy of deposition rates calculated with the GPM model used together with the source depletion method.

The accuracy of the source depletion method will depend on two aerodynamic properties of the particle: the settling velocity and the deposition velocity. We calculated the accuracy of the source depletion method for a range of settling and deposition velocities to represent fungal spores as well as plant pollen. Results for the different parameterisations are related to published settling velocities of pollen and spores (Gregory, 1973). This provides information on the accuracy of the source depletion method for specific pollen or spores. This information can then be used to decide whether the Gaussian plume model with source depletion method to describe loss provides an accurate enough tool for a given dispersal study.

Material and methods

Used symbols

parameter	description
C (# m^{-3})	source-depleted concentration
C^0 (# m^{-3})	non-depleted concentration
$\tilde{C}$ (# m^{-3})	surface-depleted concentration
d (# m^{-1})	number of particles deposited per m travel downwind
$d(x)$ (# m^{-2} s^{-1})	deposition at distance x
f_e (-)	escape fraction
H (m)	height at which particles are released
h (m)	height of the boundary layer

K (m^2 s^{-1})	diffusion coefficient
K_y, K_z (m^2 s^{-1})	diffusion coefficient for diffusion in the y- and z-direction respectively
$L(x)$ (-)	fraction of released particles still present in the plume at downwind distance x
n (#)	number of particles in a column of air)
Q (# s^{-1})	source strength or rate of release of particles
Q_{esc} (# s^{-1})	rate of escape of particles that are released from inside a canopy
u (m s^{-1})	windspeed
x (m)	downwind distance
y (m)	crosswind distance
z (m)	vertical distance
z_{ref} (m)	reference height
Δx (m)	numerical grid size in downwind direction
Δz (m)	numerical grid size in vertical direction
φ (# m^{-2} s^{-1})	rate of particle transfer through a certain plane
π	mathematical constant ($\pi \approx 3.14$)
v_s (m s^{-1})	settling velocity
v_d (m s^{-1})	deposition velocity

Approach

For our modelling study, we describe dispersal from a line source that extends infinitely in the *y* direction. The result of using this approach is that concentrations do not vary in the *y* direction. Note that the Gaussian plume model (GPM) describes release from a point source and hence does include concentration gradients in the crosswind (*y*-) direction. When using the line source approach, the term that describes eddy diffusion in the *y* direction in equation 3 becomes zero and can be removed. This simplifies the spore dispersal model to:

$$u \frac{\partial C}{\partial x} = K_z \frac{\partial^2 C}{\partial z^2} + v_s \frac{\partial C}{\partial z} \tag{4}$$

A source depletion version (without settling term) and a surface depletion version of equation 4 were used to study the accuracy of the source depletion version as compared with the surface depletion version. There are two main differences between the two versions: (1) the source depletion version does not include the settling term, whereas the surface depletion version does and (2) the source depletion version has a zero-flux

boundary condition, while the surface depletion version has a deposition flux boundary condition to describe removal of spores.

The two versions were run and compared several times with different parameterisations for the particle characteristics. Measures for the accuracy of the source depletion version, as compared with the surface depletion version, were derived to determine the applicability of the source depletion method for different pollen and spores.

The source depletion model

The source depletion model is a combination of the advection diffusion equation for a gas-like substance, with the source depletion method applied to the solution of this equation.

Typical for this source depletion model is that there is no settling ($v_s = 0$ m s^{-1}) in the advection diffusion equation, which leads to an effective removal of the settling term from equation 4:

$$u \frac{\partial C}{\partial x} = K_z \frac{\partial^2 C}{\partial z^2}$$

(5)

Another characteristic that is typical for the source depletion model is that the advection diffusion equation is solved with a zero flux boundary condition at the surface. This zero flux is imposed, because the spore loss that would be described by this flux is calculated with method. The source depletion method is applied to the solution of the advection diffusion equation (equation 5); it is not a part of the solution of this equation. The flux to the surface (φ, # m^{-2} s^{-1}) at $z = z_{ref}$ (reference height) is, therefore, set to zero. In this chapter we choose z_{ref} to be 0 m, which gives:

$$\varphi(x, y, z) = 0 \overset{set}{=} K_z \frac{\partial C}{\partial z} \; at \; z = z_{ref} = 0 \, m$$

(6)

With additional boundary conditions (see below), a solution of equation 5 can be found, which gives the non-depleted concentration (C^0, # m^{-3}). The source depleted concentration (C, # m^{-3}) can be derived from C^0 and the deposition rate through application of the source depletion method (see below).

The surface depletion model

The surface depletion model is the 'gold standard' against which the source depletion model is tested for its accuracy. The surface depletion model is the version of the advection diffusion equation where the settling term is kept in (equation 4). Instead of the zero flux surface boundary condition used in the source depletion model, a

deposition flux is imposed as surface boundary condition here. This deposition flux at the surface is proportional with the concentration at reference height:

$$\varphi(x, y, z) = -\upsilon_d \, \tilde{C}(x, y, z) \overset{set}{=} -K_z \frac{\partial \tilde{C}}{\partial z} - \upsilon_s \, \tilde{C}(x, y, z) \; at \; z = z_{ref} = 0 \, m \tag{7}$$

where, υ_d is the deposition velocity (m s^{-1}) and $\tilde{C}$ is the surface-depleted concentration (# m^{-3}). We have put minus signs before the settling and deposition flux, because the settling velocity and deposition velocity have been given positive sign values, while the fluxes are downward, hence negative. The minus sign in the diffusivity flux occurs, because a positive concentration gradient ($\partial C/\partial z$ positive, i.e., increasing concentrations with height) lead to a downward, hence negative flux.

Additional boundary conditions for the models
The advection diffusion equations for both the source depletion model and the surface depletion model were solved for values of x ranging from 0 m to 10 km. This is the range over which the Gaussian plume model is normally used. To solve these equations, two more boundary conditions must be given: one in the x-direction, and one more in the z-direction.

Each model was solved for two different boundary conditions at $x = 0$ m. These boundary conditions were chosen to describe the source and yield maximal differences between the two models within a realistic range. One boundary condition is a Gaussian plume with its peak at the ground surface and a standard deviation of 3.0 m. The other is a homogeneous distribution of spores with height, extending over the entire height (h, m) of the planetary boundary layer.

Gaussian plume boundary condition at x = 0 m
The Gaussian plume with its peak at the surface and a standard deviation (σ_z, m) of 3.0 m is obtained with the Gaussian plume model for stability class D at 50 m downwind when there is a gas source at a height of 0 m.

The release height was chosen to be 0 m, because spores and pollen are often released near the surface. The source is, therefore, regarded to be at ground level, giving a Gaussian plume with its peak at the ground surface.

A plume at 50 m downwind from the source, not the source itself, was chosen as boundary condition for $x = 0$ m, because the Gaussian plume model cannot describe dispersal close to the source. The source depletion method is used from the escape distance onwards, which is here chosen to be 50 m downwind from the source. Loss of particles from the plume before this escape distance is modelled with the escape

fraction f_e (-). Experimental studies (Spijkerboer *et al.*, 2002; chapter 3) have shown that the Gaussian plume model can adequately describe spore plumes at 50 m downwind.

The concentration was calculated for stability class D to describe a worst-case situation. The accuracy of the source depletion method is lowest when the atmosphere is most stable, which means that there is little mixing (Horst, 1977). The least amount of mixing takes place when the atmosphere is most stable. The most stable stability class during the day is class D. Therefore, class D was used to calculate the boundary condition. At 50 m downwind from the source the standard deviation of the plume for stability class D is 3.0 m. The value of 3.0 m was used for the standard deviation σ_z, of the Gaussian plume boundary condition at $x = 0$ m in the model.

Homogeneous distibution with height boundary condition at x = 0 m

The second boundary condition was used, because of our choice of a flat K_z gradient. In the Gaussian plume model, K_z increases with height, while we used the value near the surface. This means that our model underestimates the effect of mixing downwind from the source. If K_z increases with height particles would get higher up in the atmosphere than with a flat K_z gradient. The second boundary condition at $x = 0$ m is a vertically homogeneous distribution of particles over the entire height of the boundary layer. This boundary condition puts particles high up in the atmosphere and indeed even more so than they would get in a model with a K_z gradient that increases with height. This boundary condition thus compensates for the flat K_z gradient that keeps particles nearer to the ground.

Boundary condition for z direction

The additional boundary condition in the *z* direction was chosen as a zero flux at $z = h$

$$\varphi(x, h) = 0 \tag{8}$$

where, *h* (m) is the height of the planetary boundary layer. The planetary boundary layer is the layer where most of the turbulent mixing occurs (Stull, 1988). This boundary condition describes the effect that mixing only takes place in the boundary layer and there is hardly any exchange with the layer above.

For the source depletion model with the Gaussian boundary condition at $x = 0$ m, a different boundary condition was chosen:

$$\lim_{z \to \infty} C(x, z) = 0 \tag{9}$$

This is the boundary condition that the GPM model also satisfies.

With these additional boundary conditions, the advection diffusion equations for the source and the surface depletion model can be solved.

Parameterisation of the models

Parameter values of the windspeed and the diffusion coefficient were chosen to create a worst-case scenario that gives a maximal error of the source depletion method in a daytime dispersal scenario. The accuracy of the source depletion method is lowest when the atmosphere is most stable, which means that there is little mixing (Horst, 1977). Little mixing means a low value of K_z. During the day, the most stable atmospheric situation is a neutral situation.

An expression to calculate K_z from the wind speed and surface characteristics was parameterised to yield a low value of K_z. For neutral conditions K_z can be calculated from (Stull, 1988):

$$K_z = k \cdot u_* \cdot z \tag{10}$$

where, k is von Karman's constant (0.4) and u_* is the friction velocity (m s^{-1}). The value of u_* can be calculated from the height, the roughness length (z_0) and the wind speed (Stull, 1988):

$$u_* = \frac{k \cdot u(z)}{\ln\left(\dfrac{z}{z_0}\right)} \tag{11}$$

These two equations can be combined to calculate K_z from wind speed and z_0:

$$K_z = \frac{k^2 \cdot u(z) \cdot z}{\ln\left(\dfrac{z}{z_0}\right)} \tag{12}$$

To get a low value for K_z, low values of u and z_0 must be taken. For z, a value of 10 m was used. This is the standard height at which wind speed should be measured for the Gaussian plume model. The roughness length depends on the type of surface. For farmland, z_0 varies from 0.02 to 0.1 m. In urban or mountainous areas, its value is higher. In the model we calculated K_z for $z_0 = 0.02$ m. For the wind speed we used a value of 1.3 m s^{-1}. This is the 0.05 percentile of the hourly windspeed data measured at 10 m height at weather station 'Haarweg' in Wageningen, the Netherlands in daytime, during the months June, July and August in 1997. These values for z, u, and z_0 yield a value for K_z of 0.33 m^2 s^{-1}.

The boundary layer height was chosen to be 1000 m.

If it is unknown, the settling velocity (v_s, m s^{-1}) of a particle can roughly be estimated with the following formula (Gregory, 1973):

$$v_s = 25 \cdot 10^6 \cdot l \cdot w \tag{13}$$

where, l and w are the length and width of the particle (m) and a density of 1000 kg m^{-3} is assumed. Gregory (1973, p. 22) published a list of observed settling velocities of spores and pollen. The observed settling velocity of spores ranged from 0.0001 m s^{-1} 0.028 m s^{-1} and the settling velocity of pollen ranged from 0.016 to 0.39 m s^{-1}. We have assumed that the deposition velocity is three times the settling velocity (Gregory, 1973), which means that deposition velocities range from 0.0002 to 0.056 m s^{-1} for fungal spores and from 0.032 to 0.8 m s^{-1} for plant pollen. In our calculations we modelled particles with settling velocities of 0.001, 0.0025, 0.005, 0.01, 0.025 and 0.05 m s^{-1}, respectively.

Solution of the source depletion model

For the non-depleted concentration distribution (C^0), analytical solutions were found that satisfy equation 5 and the boundary conditions. For the Gaussian plume boundary condition at $x = 0$ m, the solution is:

$$C^0(x,z) = \frac{Q}{u\,\sigma_z\sqrt{2\pi}} \exp\left[-\frac{z^2}{2\sigma_z^2(x)}\right]$$
$$\sigma_z(x) = \sqrt{\sigma_z^{\,2}(0) + \frac{2K_z}{u} \cdot x} \tag{14}$$

For the vertically homogeneous boundary condition at $x = 0$ m, the solution is that C^0 is constant with downwind distance.

The source depleted concentration (C, # m^{-3}) is found by adding a loss function (L, -) to the solution of the non-depleted concentration. This loss function only depends on x, since the source depletion method does not alter the vertical shape of the plume:

$$C = L(x) \cdot C^0 \tag{15}$$

At $x = 0$ m, C is equal to C^0, so $L(0)$ must equal 1. The loss function is derived from C^0 and the deposition rate. The deposition rate is calculated as:

$$d(x) = -\frac{v_d \cdot C(x, z_{ref})}{u} = -\frac{v_d \cdot L(x) \cdot C^0(x, z_{ref})}{u} \tag{16}$$

where, v_d is the deposition velocity (m s^{-1}). Deposition leads to a downwind decrease of the total number of spores in the plume:

$$\frac{\partial \int\limits_{0}^{H} C(x,z)dz}{\partial x} = d(x) = -\frac{v_d \cdot C(x, z_{ref})}{u} \tag{17}$$

The total number of spores in the plume only changes as result of a change in L, not due to changes in C^0, so we can restate equation 15 as:

$$\int\limits_{0}^{H} C^0(0,z)dz \cdot \frac{\partial L}{\partial x} = d(x) = -\frac{v_d \cdot L(x) \cdot C^0(x, z_{ref})}{u} \tag{18}$$

For the Gaussian plume boundary condition at $x = 0$ m and with $z_{ref} = 0$ m, the solution to this equation is:

$$L(x) = \exp\left(-\frac{v_d}{\sqrt{2\pi} \cdot K_z} \sqrt{\sigma_z{}^2(0) + \frac{2K_z}{u} \cdot x}\right) \tag{19}$$

For the homogeneous boundary condition, the solution is:

$$L(x) = \exp\left(-\frac{v_d \cdot x}{u \cdot h}\right) \tag{20}$$

Numerical solution of the surface depletion model
The surface depletion model was solved numerically, using a centred grid for the diffusion and settling terms and a forward grid for the advection term. This scheme is basically a so-called explicit forward time, centred space method (Vreugdenhil, 1989), except that time is replaced by the downwind (x) direction. This is found to be an accurate scheme for solving the advection diffusion equations (Yang *et al.*, 1998)

For the numerical solution of the surface depletion model (equation 4 plus boundary conditions), we chose a discretisation that satisfies the stability condition of the numerical scheme we used. The criterion for numerical stability for this scheme is (Vreugdenhil, 1989):

$$\left(\frac{v_s \cdot \Delta x}{u \cdot \Delta z}\right)^2 < \frac{2K_z \cdot \Delta x}{u \cdot \Delta z^2} < 1 \tag{21}$$

where, Δx (m) is the gridsize in the downwind direction and Δz is the gridsize in the vertical direction. For Δx, we used a value of 1 m and $\Delta z = 2.9$ m, which satisfies the stability condition (equation 21). With this discretisation, the surface depletion model can be solved numerically for appropriate parameter values for u, v_s and v_d.

Calculated outputs

The maximum factors of overestimation and underestimation of deposition rates are used as quantitative measures for the accuracy of the surface depletion model. These factors are the ratios of surface concentrations calculated with the source depletion model and the surface depletion model. The maximum value is determined between $x = 0$ m and $x = 10\ 000$ m downwind. This distance range was chosen because the Gaussian plume model is valid for distances up to about 10 km from the source. The factor of maximum overestimation (F_o, -) is calculated as:

$$F_o = \text{MAX}\left(\frac{C(x,y,z_{\text{ref}})}{\tilde{C}(x,y,z_{\text{ref}})}\right) \tag{22}$$

The factor of maximum underestimation (F_u, -) is calculated as:

$$F_u = \text{MAX}\left(\frac{\tilde{C}(x,y,z_{\text{ref}})}{C(x,y,z_{\text{ref}})}\right) \tag{23}$$

Results

For the settling velocity of 0.001 m s^{-1} and a Gaussian distribution boundary condition at $x = 0$ m (figure 1a) deposition rates quickly decrease with downwind distance. There is only a small difference between the source depletion model and the surface depletion model for this settling velocity. The difference between the models increases with downwind distance. Deposition gradients become steeper when the settling velocity becomes higher (figures 1b-f), as does the difference between the source depletion and the surface depletion model.

   For the homogeneous boundary condition at $x = 0$ m (figures 2a-f), deposition gradients are flatter. Here, the source depletion model predicts flatter gradients than the surface depletion model. The reason for this is that the loss of spores due to deposition has only a small effect on the total content of particles in the column, since the column is so high. For the surface depletion method, deposition reduces the particle concentration near the ground, which leads to smaller deposition rates. At distances further downwind, the gradient flattens out, because settling of particles, and turbulent diffusion, replenish concentrations near the ground. For particles with a settling velocity of 0.025 m s^{-1} or more, the deposition gradient becomes completely
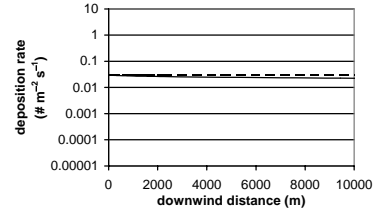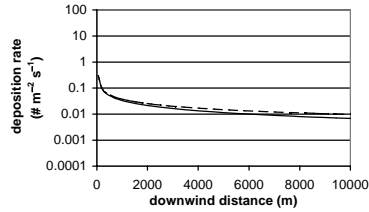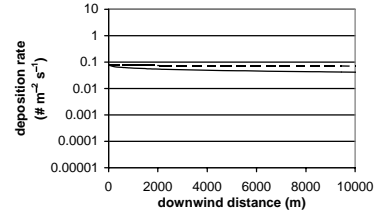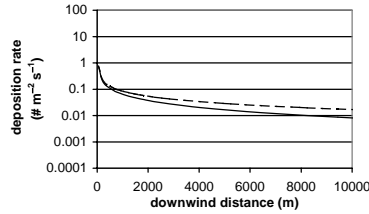
A : $\nu_s = 0.001$ m s^{-1}

B: $\nu_s = 0.0025$ m s^{-1}

C: $\nu_s = 0.005$ m s^{-1}
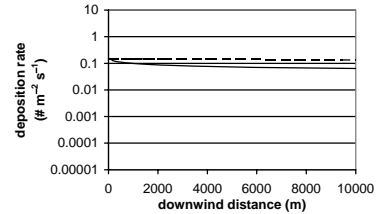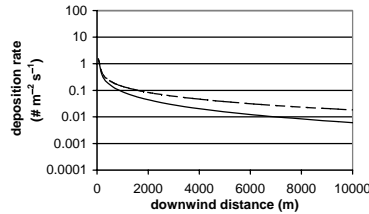
D: $\nu_s = 0.01$ m s^{-1}
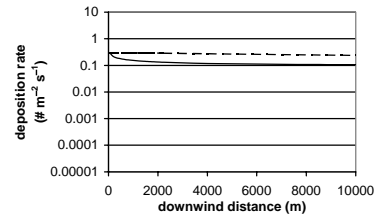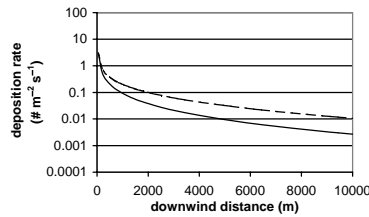
E: $\nu_s = 0.025$ m s^{-1}
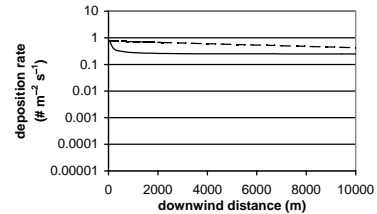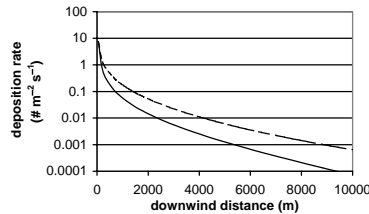
F: $\nu_s = 0.05$ m s^{-1}
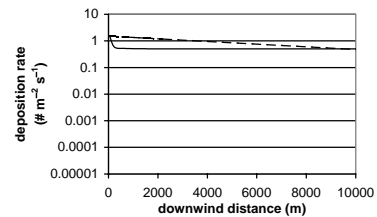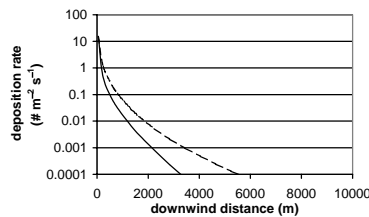
Figure 1

Gaussian distribution

Figure 2

homogeneous distribution

Figure 1, 2: Comparison of deposition gradients calculated with the source depletion and the surface depletion model for different values of the settling velocity and different boundary conditions at $x = 0$ m. Deposition velocities are three times the settling velocity. solid line: surface depletion model; dashed line: source depletion model.
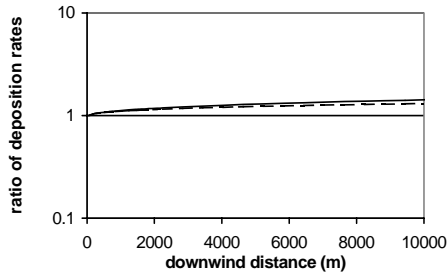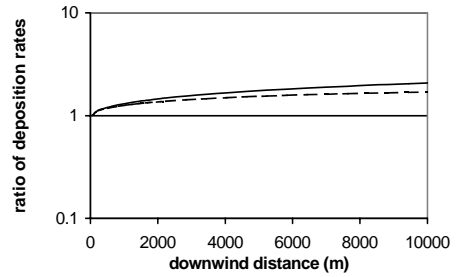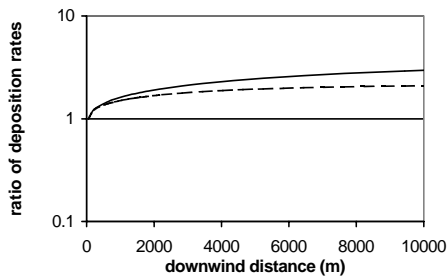
A: $\nu_s = 0.001$ m s^{-1}

B: $\nu_s = 0.0025$ m s^{-1}

C: $\nu_s = 0.005$ m s^{-1}
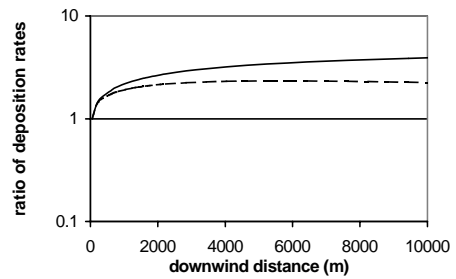
D: $\nu_s = 0.01$ m s^{-1}
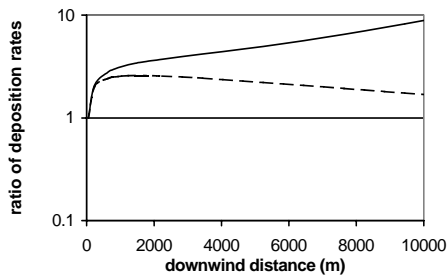
E: $\nu_s = 0.025$ m s^{-1}
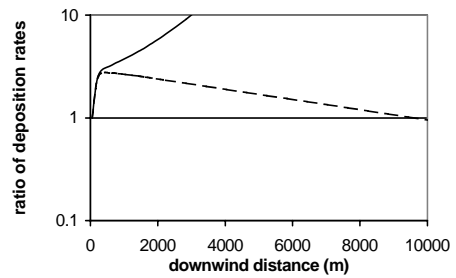
F: $\nu_s = 0.05$ m s^{-1}

Figure 3: Ratio of deposition rates calculated with the source depletion and the surface depletion model for different boundary conditions at $x = 0$ m. solid line: Gaussian distribution boundary condition; dashed line: homogeneous distribution boundary condition.

flat. For these particles, settling is probably more important than diffusion. When that happens, the whole column of particles will move down and will gradually empty out due to deposition. When this happens, there will be an equilibrium between settling of particles and loss due to deposition. This equilibrium leads to the constant deposition rates. The equilibrium occurs sooner when settling and deposition velocities are higher.

For a settling velocity of 0.05 m s^{-1}, the source depletion method starts to underpredict deposition rates further downwind (figures 2f and 3f).

Both the Gaussian and the homogeneous boundary condition at $x = 0$ m cause errors in the source depletion method. The errors are larger for the Gaussian boundary condition (figure 3). For the Gaussian boundary condition, the error of the source depletion method increases with downwind distance (figures 3a-f), whereas with the homogeneous boundary condition, the error quickly becomes larger and then remains constant, or even decreases again.

The error of the source depletion method increases with settling velocity (figure 4). The overprediction error, which is larger than the underprediction error, sharply increases between $v_s = 0.025$ m s^{-1} ($F_o = 8.9$) and $v_s = 0.05$ m s^{-1} ($F_o = 2700$). Underprediction does not occur at settling velocities of 0.025 m s^{-1} and lower. For these settling velocities, the source depletion model overpredicts deposition everywhere downwind. For a settling velocity of 0.05 m s^{-1} and for the homogeneous boundary condition, the downwind error pattern changes and overprediction changes to underprediction further downwind.

A: maximum overprediction   B: maximum underprediction
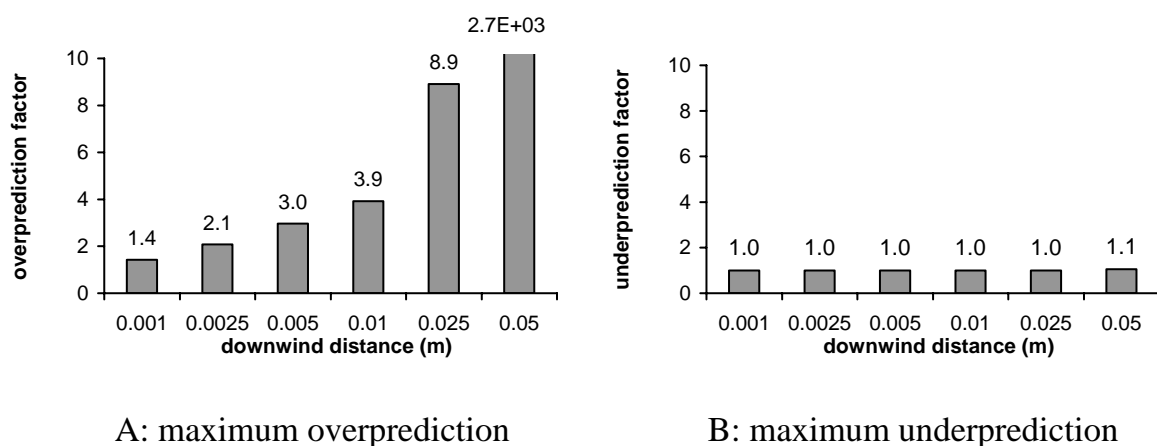
Figure 4: Maximum overprediction and underprediction of deposition rates by the source depletion model as compared with the surface depletion model.

Discussion and conclusions

As predicted, the source depletion model mimics the behaviour of the surface depletion model when the settling velocity is low. Apparently, settling and deposition have only little effect on the distribution of particles over the height of the plume for lighter particles that have lower settling and deposition velocities.

Downwind deposition gradients are steeper when the settling and deposition velocity are higher because of the increased loss of spores. High deposition velocities give higher deposition rates, which lead to increased loss of spores from the plume. The loss of spores causes decrease of the particle concentration at the surface and hence a decrease in deposition. Both the source depletion model and the surface depletion model accurately represent this phenomenon.

The change of overprediction of deposition close to the source to underprediction further downwind, observed for the settling velocity of 0.05 m s^{-1} (figure 3f) was also found by Horst (1977).

As expected, errors caused by the source depletion method increase with increasing settling and deposition velocity. The sharp increase in errors between a settling velocity of 0.025 and 0.05 m s^{-1} suggests that particles with a settling velocity of 0.05 m s^{-1} or higher cannot be modelled accurately with a Gaussian plume model.

For particles with a settling velocity smaller than or equal to 0.025 m s^{-1}, the source depletion method describes deposition gradients reasonably well, better so when the settling velocity is smaller. The Gaussian plume model with source depletion method may be a useful tool for modelling the dispersal of particles with these settling velocities, depending on the required accuracy of the study.

Two simple versions of the advection-diffusion equation were used for this modelling study. The differences between the equation used here and that of McCartney and Fitt (1985) are that the equation used here does not contain the source and sink terms, that the wind speed (u, m s^{-1}) and eddy diffusivity (K_z, m^2 s^{-1}) have been assumed constant and that the line source approach was used here.

The calculations presented here are based on the assumption that particles are released and dispersed during the day and not at night. The accuracy of the source depletion method is lower for particles released and dispersed during the night, when there is little mixing (Horst, 1977). Several types of pollen are released at night. Gregory (1973) found that the observed settling velocity of pollen ranged from 0.016 to 0.39 m s^{-1}. This indicates that the dispersal of only some pollen can be modelled with a Gaussian plume model. For particles released under more unstable conditions, the source depletion method will perform better. We modelled neutral atmospheric

conditions, which for a daytime situation means there is relatively little mixing. When conditions are more unstable, there will be more mixing and the source depletion method will perform better.

Fungal spores have settling velocity in the range of 0.0001 m s^{-1} to 0.028 m s^{-1} (Gregory, 1973) and are often released during the day (Hirst, 1953). This means that the Gaussian plume model with source depletion term potentially is a suitable model to describe dispersal and deposition of many fungal spores. Figure 4 can help to decide whether or not to use the Gaussian plume model with source depletion term in a given modelling context.

CHAPTER 5

Effectiveness of control strategies against infection pressure from distant sources of *Phytophthora infestans*

Abstract

The initiation and rate of progress of potato late blight epidemics in farmers fields not only depends on inoculum produced locally in the field, but also on inoculum produced on external sources. A model was developed to calculate infection pressure on a receptor crop caused by inoculum from a distant source. A sensitivity analysis was carried out to determine the relative importance of various parameters in the model. Subsequent scenario studies with the model were done to study the effectiveness of four control strategies: eradication of heavily infected inoculum sources, use of a more resistant cultivar for the receptor crop, a ban on the growing of susceptible cultivars, and spatial separation of cropping systems with different levels of disease tolerance.

The sensitivity analysis showed that disease level at the source had by far the greatest impact on infection pressure, followed by distance from the source. Other parameters, like net reproduction, infectious period, escape fraction and wind speed were of less importance. Scenario studies indicate that eradication of sources with high disease levels and spatial separation of cropping systems with different disease tolerances are more effective than use of a more resistant cultivar for the receptor crop or a ban on the growing of susceptible cultivars.

*Key words: Policy evaluation, modelling, potato late blight, crop protection,
plant disease epidemiology, risk assessment.*

Introduction

The high input of fungicides against potato late blight is a persistent problem in crop protection. In the Netherlands, for example, a government initiative to reduce overall use of chemical crop protection ('Meerjarenplan gewasbescherming') has been successful in many areas, but not in reducing the use of fungicides against late blight (Ekkes *et al.*, 2002).

Infection of the crop can come from diseased tubers, oospores in the soil and incoming inoculum from sources outside the crop. Incoming inoculum is widely regarded as an important cause of infections. It has been estimated (W.G. Flier, pers. communication) that at least 90% of all potato crops are disease-free at the start of the growing season. This means that requirement for fungicides would strongly depend on the infection pressure from inoculum sources outside the crop. The importance of sources of inoculum outside a farmer's own crop is now widely recognised. As a result, presence of the disease in regions is monitored and used in decision support systems in many countries. In The Netherlands, a policy has now been implemented, that requires farmers to kill the haulm of their crop when the disease severity gets too high. More radical policies, such as a ban on the growing of susceptible cultivars and spatially separating cropping systems with different disease tolerance have been suggested. The effectiveness of these policies is uncertain, however.

No studies on the effectiveness of control strategies against infection pressure from distant sources have yet been carried out. Especially for the more radical strategies, it is very important to assess their possible benefits prior to their implementation.

A first assessment of the effectiveness of control policies can best be done with a model study. No model of late blight infection pressure has been published so far, however. The model required for an effectiveness study should describe relevant processes, including the effects of proposed and existing control strategies.

Aylor (1998) developed a model to calculate relative risks of infection from a heavily diseased distant source of *Venturia inequalis* to a less infected orchard. De Jong (1988) modelled risks of infection posed to orchards by a distant source of *Chondrostereum purpureum* spores on biocontrolled black cherry trees inside a forest.

Models to calculate spread of inoculum from distant sources have been developed by Aylor (1986, 1996, 1998) and De Jong (1988) and De Jong *et al.* (1998, 1990a, b). Aylor (1986) defined five steps in the spore dispersal process: (1) spore production, (2) escape of spores from the canopy, (3) turbulent transport and dilution, (4) survival and (5) deposition. To calculate infection pressure, infection must be added to this chain. It is also common to see release of spores from the hyphae and escape of released spores

from the canopy as two separate steps.

Existing models for local late blight epidemics (Bruhn and Fry, 1981; Michaelides, 1985; Van Oijen, 1991, 1992) contain descriptions of spore production and infection. Spore release has been measured by Aylor *et al.* (2001) and escape has been measured by Aylor *et al.* (2001) and Spijkerboer *et al.* (2002; chapter 3). For turbulent transport and dilution at the regional scale, with distances up to about 10 km, such an investigation could be done with the Gaussian plume model (Pasquill, 1974), which was previously used by de Jong (1990b) to model infection risks downwind from inoculum sources. Aylor (1986) used a deposition velocity model to calculate deposition. Mizubuti *et al.* (2000) determined the effect of solar radiation on survival of spores.

This chapter presents the results of a model study of infection pressure at distances up to 10 km downwind from inoculum sources of *Phytophthora infestans*. The study consisted of model development, sensitivity analysis and scenario studies. Submodels for component processes were integrated to obtain a model for calculating infection pressure. The behaviour of the model was studied under different model parameterisations. After this sensitivity analysis, the model was used to estimate the effectiveness of control strategies for reducing infection pressure.

The scenario studies supply scientific arguments for selection of practical control strategies against late blight. These strategies could be incorporated in decision support systems or be part of late blight control policies aimed at reducing fungicide use.

Material and methods

Used symbols

parameter   description

v_d (m s^{-1})   deposition velocity

v_s (m s^{-1})   settling velocity

π (-)   mathematical constant ($\pi \approx 3.14$)

Π (# m^{-1})   infection pressure

σ_y (m)   standard deviation of spore concentration in cross wind direction

σ_z (m)   standard deviation of spore concentration in vertical direction

a (-)   parameter in function for σ_z

b (-)   parameter in function for σ_z

C (# m^{-3})   spore concentration

d (m)   displacement height

f_e (-)	escape fraction
h (m)	crop height
H (m)	height at which spores are released
IP (d)	duration of the infectious period
K (-)	correction in σ_z and σ_y for effects of surface roughness
L (#)	disease level
p (-)	parameter in function for σ_y
q (-)	parameter in function for σ_y
Q (# s^{-1})	source strength
$R_{0,\,loc}$ (-)	(local) net reproduction
$R_{0,\,reg}$ (-)	regional net reproduction
T (s d^{-1})	duration of spore release period
u (m s^{-1})	mean horizontal wind speed at 10 m height
U (# s^{-1})	rate of release of effective spores (spores that will cause a lesion)
x (m)	downwind distance from source
x_{esc} (m)	escape distance
y (m)	horizontal distance from the plume centre
z (m)	height above the surface
z_{ref} (m)	reference height for deposition calculation
z_0 (m)	roughness length

Approach

Potential infection pressure is defined as the expected number of lesions on a given area, assuming that it is covered by a potato canopy, under temperature and humidity conditions that are optimal for development and dispersal of late blight. These worst-case scenario conditions would typically occur when a wet night, conducive for spore production, is followed by a quick decrease in relative humidity in the morning. As a result, all spores are released over a short time period (one hour) and then dispersed downwind, where they can land on a potato canopy. After the dispersal event, conditions would become wet again, providing suitable conditions for deposited spores to infect the plants they have landed on.

For this worst-case event, a calculation is made of the infection pressure on a 'receptor crop' which is located downwind from a source of spores of *Phytophthora infestans*. The disease level at the source is described in terms of number of diseased leaflets, the standard way to describe the disease level in a practical source registration system in the Netherlands (Dacom and Agrevo, 1992). In this system, the disease level is described with an index number ranging from 0 to 10, depending on the number of diseased leaflets (figure 1).

An infection pressure model was derived. It uses a simple calculation for the regional daily net reproduction, the number of daughter lesions that may potentially be caused outside the source per mother lesion in the source on a given day. It also includes a model for spore dispersal and deposition to calculate where the regional daughter lesions will occur.

A sensitivity analysis targeted the effect of model parameters on potential infection pressure. Scenarios were defined to describe different control strategies. Scenario studies carried out with the model quantify the effect of these control strategies on potential infection pressure and on fungicide requirements.

The Gaussian plume model

The standard Gaussian plume model (GPM) was as proposed by Pasquill (1974) was used, but adjusted for displacement height as suggested by Spijkerboer *et al.* (2002) (chapter 3):

$$C(x, y, z) = \frac{Q}{u} \frac{\exp(-y^2 / 2\sigma_y^2)}{2\pi\sigma_y\sigma_z} \cdot \left\{ \exp\left[-\frac{(H-z)^2}{2\sigma_z^2} \right] + \exp\left[-\frac{(H+z-2d)^2}{2\sigma_z^2} \right] \right\}$$

(1)

in which, C is the spore concentration (# m^{-3}), x (m) is the distance from the source along the mean wind direction (plume axis), y (m) is the distance from the plume axis
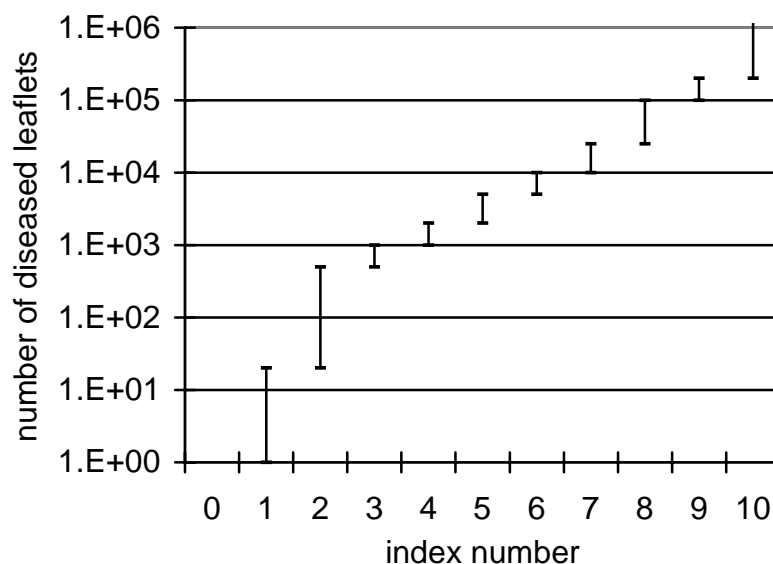
Figure 1: Disease level index used in commercial late blight source registration system. Values vary from 0 (no diseased leaflets) to 10 (more than 200,000 diseased leaflets). Based on: Dacom and Agrevo (1992).

and z is height (m). The displacement height (d, m), together with the roughness length (z_0, m) are used to describe the effect of the crop on the vertical wind speed gradient. They are based on the logarithmic wind profile model, which is a standard meteorological model (Stull, 1988). In this profile, the wind speed is 0 m s^{-1} at a height of $d+z_0$ m above the earth's surface. Values for z_0 and d can be derived from measured wind profiles. Q is the source strength (# s^{-1}), u the mean wind speed (m s^{-1}) at 10 m height and H the height of the spore source. The parameters σ_y and σ_z characterise the Gaussian shape of the plume. They are a function of downwind distance (x). Functions for σ_y and σ_z are taken from KNMI (1979):

$$\sigma_y = 10^p \cdot x^q \cdot \left(\frac{T}{600}\right)^{0.2}$$

(2)

$$\sigma_z = C(z_0) \cdot a \cdot x^b$$

(3)

where, T is the time during which release takes place (s), z_0 is the roughness length (m) and $C(z_0)$ is calculated as:

$$C(z_0) = (10 \cdot z_0)^{0.53 \cdot x^{-0.22}}$$

(4)

Deposition and loss of spores from the plume

Because spores are heavier than air, they will not remain suspended in the air, but will be deposited from the plume, thus creating a pattern of deposited spores downwind from the source. Deposition of spores D (# m^{-2} s^{-1}) is calculated with a deposition model, assuming that deposition is proportional to the concentration at a reference height z_{ref}.:

$$D = v_d \cdot C(z_{ref})$$

(5)

where, v_d (m s^{-1}) is the deposition velocity, a proportionality constant that can be derived from measurements.

As a result of deposition, spores will be lost from the plume. The GPM model must be adjusted to describe this loss. Loss near the source was described differently from loss further downwind. Loss near the source is described with an escape fraction (f_e, -). The escape fraction is the fraction of spores that is still airborne at a given escape distance x_{esc} (m) downwind from the source. Spores that are deposited before they reached the escape distance x_{esc} have not escaped. They constitute a fraction of $1-f_e$ of the total number of spores that were released.

To calculate loss of spores downwind from the escape distance onwards, the source depletion method (Van der Hoven, 1968) was used. The source depletion method describes loss of spores as a downwind decrease in source strength Q. This makes Q dependent on downwind distance x. The loss of spores over a given downwind distance equals the deposition that takes place over this distance. The change in source strength, which describes the loss of spores in the source depletion method can therefore be calculated from the spore deposition rate. Assuming that the spore concentration does not change significantly over a short downwind distance Δx (m), the change in source strength can be calculated as the total deposition rate of spores integrated over the entire width of the spore plume and over the small downwind distance Δx:

$$Q(x + \Delta x) - Q(x) = -\Delta x \cdot \int_{y=-\infty}^{\infty} v_d \cdot C(x, y, z_{\text{ref}}) \cdot dy \qquad (6)$$

The integration over the plume width can be carried out analytically:

$$\int_{y=-\infty}^{\infty} C(x, y, z_{\text{ref}}) \cdot dy = \int_{y=-\infty}^{\infty} \frac{Q}{u} \frac{\exp(-y^2/2\sigma_y^2)}{2\pi\sigma_y\sigma_z} \cdot \left\{ \exp\left[-\frac{(H - z_{\text{ref}})^2}{2\sigma_z^2}\right] + \exp\left[-\frac{(H + z_{\text{ref}} - 2d)^2}{2\sigma_z^2}\right] \right\} dy$$

$$= \frac{Q}{u} \frac{1}{\sqrt{2\pi}\sigma_z} \cdot \left\{ \exp\left[-\frac{(H - z_{\text{ref}})^2}{2\sigma_z^2}\right] + \exp\left[-\frac{(H + z_{\text{ref}} - 2d)^2}{2\sigma_z^2}\right] \right\} \qquad (7)$$

Using this procedure, the source strength Q at $x + \Delta x$ can be calculated from the source strength at x:

$$Q(x + \Delta x) = Q(x) - \Delta x \cdot v_d \cdot \frac{Q}{u} \frac{1}{\sqrt{2\pi}\sigma_z} \cdot \left\{ \exp\left[-\frac{(H - z)^2}{2\sigma_z^2}\right] + \exp\left[-\frac{(H + z - 2d)^2}{2\sigma_z^2}\right] \right\} \qquad (8)$$

This procedure is used from x_{esc} onwards, since loss of spores to deposition before x_{esc} is modelled with the escape fraction. Starting at $x=x_{\text{esc}}$ and with a known value of Q, this procedure can be used to calculate at any given downwind distance x. This allows for a calculation of the spore deposition pattern downwind from a source with known source strength Q.

Expansion of the model to calculate infection pressure

To calculate the potential infection pressure downwind from sources with a given disease level, additional models are needed to relate the source strength (Q) to the disease level, and to relate spore deposition to infection pressure.

To achieve this, the following assumptions were made:
-   All spores have the same chance of causing an infection

- Each late blight lesion will locally cause a total number of $R_{0,\,loc}$ daughter lesions during its infectious period. Locally is defined as within a circle with radius x_{esc} around the source.
- These locally produced new lesions are caused by the fraction $1-f_e$ of the spores, i.e., the spores that have not escaped.

Based on these assumptions, the number of daughter lesions that will be caused regionally, i.e. beyond the escape distance x_{esc} can be calculated. The GPM model adjusted for deposition can then be used to calculate the infection pressure pattern, i.e. the distribution of lesions downwind from a source containing a given number of mother lesions.

Daily infection pressure patterns downwind from a source with L mother lesions are calculated, assuming that the daughter lesions will be produced over a period of IP days, IP being the length of the infectious period (d).

Next, U is defined as the rate of release of effective spores (# s^{-1}), i.e., spores that will cause a lesion, on a given day. Assuming that all spores that are produced on a given day are also released on that day, U can be calculated as:

$$U = \frac{\left(R_{0,loc} + R_{0,reg}\right) \cdot L}{IP \cdot T} \tag{9}$$

where, $R_{0,\,loc}$ (-) is the local net reproduction, based on lesions caused by spores landing within a distance x_{esc} from the source and $R_{0,\,reg}$ is the regional net reproduction, caused by spores landing beyond x_{esc}. L (#) is the number of lesions in the inoculum source, IP (days) is the infectious period of those lesions and T (s day^{-1}) is the period over which spores are released each day. In this equation, only $R_{0,\,reg}$ is unknown. This parameter was derived from the escape fraction and $R_{0,\,loc}$, assuming that all spores have the same effectiveness. If all spores have the same effectiveness, the production of lesions must be proportional to the fraction of spores that cause them:

$$\frac{R_{0,reg}}{R_{0,loc}} = \frac{f_e}{1 - f_e} \tag{10}$$

From this equation an expression for $R_{0,\,reg}$ can be derived:

$$R_{0,reg} = R_{0,loc} \cdot \frac{f_e}{1 - f_e} \tag{11}$$

Filling in this expression in equation 9, the following expression for U can be derived:

83

$$U = \frac{R_{0,\text{loc}} \cdot L}{(1 - f_{\text{e}}) \cdot IP \cdot T} \tag{12}$$

With these assumptions, $Q(x_{\text{esc}})$, the rate of escape of effective spores, can now be calculated:

$$Q(x_{\text{esc}}) = f_{\text{e}} \cdot U = f_{\text{e}} \cdot \frac{R_{0,\text{loc}} \cdot L}{(1 - f_{\text{e}}) \cdot IP \cdot T} \tag{13}$$

With this expression for Q as input, the Gaussian plume model together with the spore loss and deposition model (equations 1, 5 and 8) can be used to calculate where the lesion-causing spores land. Under the conditions of potential infection pressure, as defined here, each effective spore will cause a lesion, so this model provides the desired method to calculate potential infection pressure.

Parameterisation and sensitivity analysis
A sensitivity analysis was done to determine the most important parameters in the model, i.e. those parameters that have most impact on model output. The selected model output was infection pressure (Π, # m^{-1}), expressed as the potential number of infections per m of downwind distance along a crosswind line (Π, # m^{-1}). This infection pressure can be calculated as the integral of the deposition rate of effective spores, integrated cross-wind:

$$\Pi(x) = \int_{-\infty}^{\infty} D \cdot dy \tag{14}$$

where, D (# m^{-1}) is the rate of deposition of effective spores, which can be calculated by filling in equations 1-4, 8 and 10 into equation 5.

To calculate the sensitivity of the model to the different parameters, the model was run with a standard parameterisation and with altered parameterisations. In each alternate run, one parameter was changed from its standard value. For each parameter (λ_i) an upper and lower limit was determined to describe a realistic range of values. A sensitivity factor (S_i, -) was then calculated for each parameter:

$$S_i = \sqrt{\frac{\Pi(\lambda_{i,\text{max}})}{\Pi(\lambda_{i,\text{min}})}} \tag{15}$$

where, the subscripts max and min refer to the upper and lower limit of parameter λ_i in its realistic range.

The parameter values that were used in the sensitivity analysis are given in table 1. Variation in disease level was based on the disease scale used in practice (Dacom and

Agrevo, 1992). Variation in downwind distance x is based on the range over which the GPM model is applicable. The range of values of R_0 was suggested by Turkensteen and Kessel (pers. communication). The variation in infectious period is based on chapter 2; 7 days is the value found for cv Bintje, the most commonly grown cultivar in the Netherlands, 10 days the value for cv Santé and 3.5 days an estimate for a very aggressive isolate on a very susceptible cultivar.

The stability class was used to determine the values of a, b, p and q in the Gaussian plume model. Values for a, b, p and q for the different stability classes were taken from KNMI (1979). Stability classes range from A (highly unstable) to F (highly stable). During the potato growing season, classes E and F do not occur during the day, when spores are released. Therefore, the sensitivity analysis was limited to the extreme classes A and D. For deposition velocity, a standard value of three times the settling velocity was used (McCartney *et al.*, 1985). The settling velocity of *Phytophthora infestans* spores is about 0.01 m s^{-1} for (Gregory, 1973). For the lower limit, the deposition velocity was assumed to be equal to the settling velocity. As upper limit, a value based on a formula from Aylor (1986) was used:

$$v_{\mathrm{d}} = (1 + LAI) \cdot v_{\mathrm{s}} \tag{16}$$

where, LAI (-) is the leaf area index, for which the high value of 5 was taken, leading to a value of 0.06 m s^{-1} for v_{d}.

Table 1: Values of parameters used in sensitivity analysis.

Parameter	Standard	Lower limit	Upper limit
L (#)	1000	10	100,000
x (m)	100	1,000	10,000
f_{e} (m)	0.64	0.20	0.81
R_0	10	3	30
IP (days)	7	3.5	24
v_{d} (m s^{-1})	0.03	0.01	0.06
u (m s^{-1})	3	1	10
stability class	D	A	D
x_{esc} (m)	50	20	100
z_0 (m)	0.03	0.03	0.1
z_{ref} (m)	2	1	4
d (m)	0.55	0	0.55
H (m)	0.7	0	0.7

The standard value for the escape fraction (0.64) was taken from Spijkerboer *et al.* (2002) (chapter 3). The upper limit for f_e was based on the 0.95 confidence interval. The lower limit was based on measurements of Aylor and Ferrandino (1989), for release from a source low inside the canopy.

For x_{esc} and z_{ref} the locations where spore traps were mostly located in the experiments of Spijkerboer *et al.* (2002) (chapter 3) was taken, with a factor 2 variation for the upper and lower limits.

The standard values of z_0 and d are based on formulae proposed by Legg *et al.* (1981) and a measured height of a fully developed crop of 0.7 m (Spijkerboer *et al.*, 2002) (chapter 3). Changing z_0 to 0.1 and d to 0 would simplify the GPM model. The height from which spores are released can be no higher than the crop height (0.7 m) and no lower than the surface (0 m).

Scenario studies for effectiveness of control strategies

The effectiveness of four control strategies was compared:
- eradication of sources;
- use of more resistant cultivars by individual farmers;
- banning the growing of susceptible cultivars;
- spatial separation of cropping systems with different disease tolerance.

Scenarios were defined for each strategy (table 2). The model was then run for each of these scenarios and results were compared.

The effectiveness of the strategies was compared through their effect on infection pressure on protected and unprotected potato crops. For the infection pressure calculations, the model that was used in the sensitivity analyses was slightly adapted. The adaptations involved the inclusion of the effect of host resistance and of fungicides. Host resistance was described through its effect on net reproduction, generation time and infection efficiency. The effect of fungicides was described in terms of fungicide efficacy, the reduction in expected number of infections (ε, -). The infection pressure on a crop protected with fungicides (Π_f) relates to that of an unprotected crop (Π_0) as:

$$\Pi_f = (1 - \varepsilon) \cdot \Pi_0 \tag{17}$$

In the scenario studies fungicide efficacies of 0 (no fungicide protection), 70, 90 and 99% were used. These values describe the range found in practice (H.T.A.M. Schepers, pers. communication). The infection pressure was calculated for each of these fungicide efficacies in all scenarios.

The standard scenario calculates infection pressure from a large source located 100 m upwind from the receptor crop and grown with cv Bintje. According to calculations in chapter 2, Bintje has a local net reproduction $R_{0,\text{loc}}$ of 5.6 and an infectious period *IP* of 7 days (*IP* calculated as generation time – latency period). The disease level of the source is 200,000 diseased leaflets, corresponding with a disease index value of 10 (figure 1) in the scale that is used for disease registration in the Netherlands (Dacom and Agrevo, 1992).

The source eradication strategy is based on eliminating all sources which have reached a set maximum. For this scenario, the disease level at the source was reduced to the maximum level allowed under current Dutch policies. This is 2000 diseased leaflets (htttp://www.hpa.nl/main/Akkerbouw/index.htm). Apart from the disease level at the source, the parameterisation was the same as in the standard scenario.

The scenario for use of a more resistant cultivar calculates the infection pressure on the crop of a farmer who has chosen to grow a more resistant cultivar. This does not influence the rate of deposition of spores onto his crop, but it does reduce the number of infections caused by these spores. In the scenario, the effect of this strategy was expressed as the effect of the reduction in infection efficiency on R_0. Because R_0 is proportional to infection efficiency, a reduction in infection efficiency (*IE*, -) leads to a proportional reduction in R_0:

$$R_{0,\text{res}} = R_{0,\text{std}} \cdot \frac{IE_{\text{res}}}{IE_{\text{std}}} \tag{18}$$

where, subscript 'res' stands for the resistant cultivar scenario and 'std' for the standard scenario. Note that the other parameters in R_0 as well as *IP* are not changed, because they are determined by the resistance characteristics of the source crop. For this scenario, cv Santé was used to represent the resistant cultivar. Values of *IE* are

Table 2: Scenario-specific parameterisations for study of effectiveness of control strategies. *L* is the disease level (#), R_0 the net reproduction (-), *IP* the infectious period (d) and *x* the downwind distance (m).

Strategy	*L* (#)	R_0 (-)	*IP* (d)	*x* (m)
standard	200,000	5.6	7	100
source eradication	2,000	5.6	7	100
use of resistant cultivars at receptor crop	200,000	1.2	7	100
ban on the growing of susceptible cultivars	200,000	1.02	24	100
spatial separation of cropping systems systems	200,000	5.6	7	10,000

taken from chapter 2 and are 0.006 for cv Bintje (cultivar in the standard scenario) and 0.0013 for Santé.

A ban on the growing of susceptible cultivars will decrease both the number of spores produced at the source crop, as well as the number of infections caused by a given amount of spores. The effect of this strategy is represented by a change in R_0 and *IP*. Again, cv Santé was used to represent the more resistant cultivar in this scenario. Santé has an R_0 of 1.02 and an *IP* of 24 days (chapter 2).

The idea behind spatial separation of cropping systems is that farmers in low disease tolerance systems will not accept their crops to have disease levels observed in some other systems. When special areas are designated for such cropping systems, they are spatially separated from crops grown under systems where disease tolerance is higher. In the designated region, all farmers will take measures to prevent that disease levels become higher than the tolerance level. Higher disease levels, which might be tolerated in other cropping systems will not occur, thus reducing the potential infection pressure in their area. The effectiveness of spatial separation of systems depends on the difference in tolerated disease level and the distance that separates areas with two different systems. In this scenario, it was assumed that in the tolerant system, the maximum tolerated disease level is 200,000 diseased leaflets and the system with low disease tolerance has a maximum level of 2,000 leaflets.

For the spatial separation scenario, a calculation was made of the maximum infection pressure that can occur in the low tolerance area that is 10 km away from a high tolerance area. A comparison was made between the infection pressure from a source at 100 m distance located in the low-tolerance area and a source at 10 km distance located in the high tolerance area. For both sources, the maximum tolerated disease level in their area was assumed.

Results

Sensitivity analysis

With the standard parameterisation used for the sensitivity analysis, the model predicts an infection pressure ranging from about 4 infections per m downwind distance close to the source with 1000 diseased leaflets, to less then 0.03 per m at 10 km distance (figure 2).

The infection gradient is steepest close to the source and becomes flatter with downwind distance. Variation of parameter values shows that the model is most sensitive to disease level in the source (table 3), with an effect factor of 100 (see also figure 3). The next important parameter, distance, has an effect of only a factor 10.8.
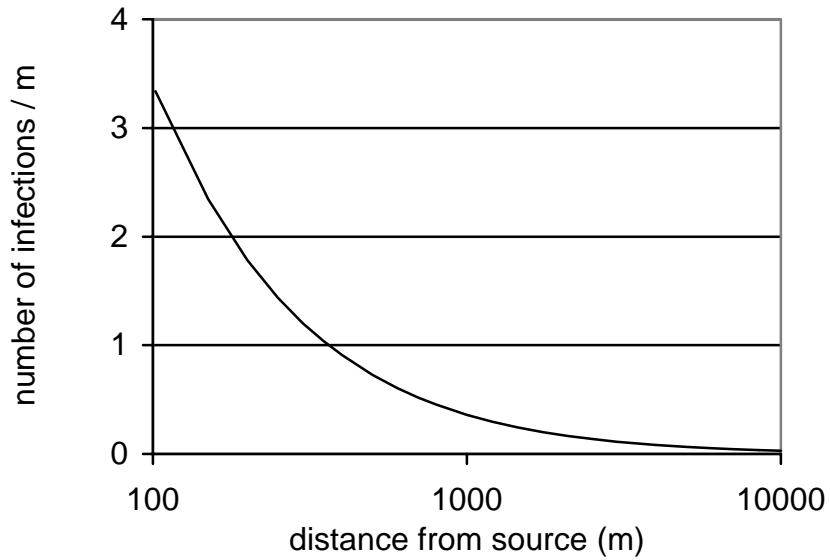
Figure 2: Potential infection pressure downwind from a source with 1000 diseased leaflets.
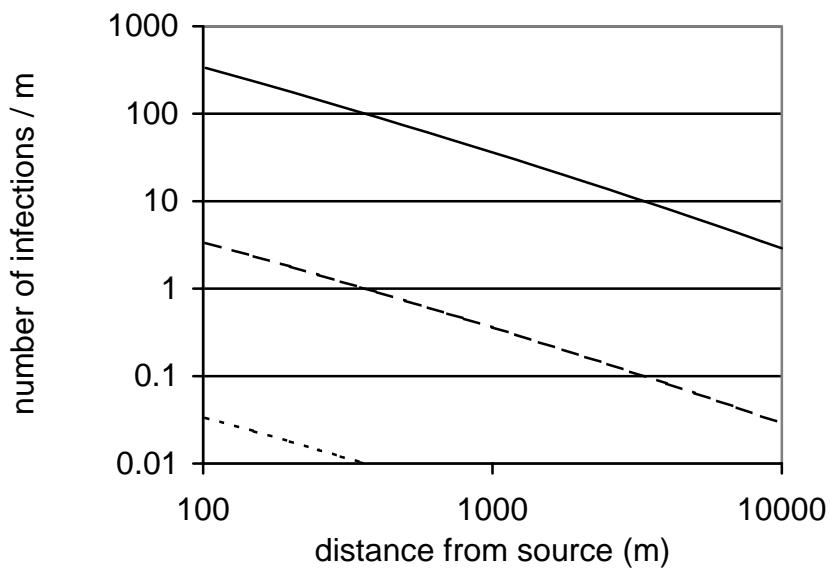
Figure 3: Effect of disease level (*L*, #) on potential infection pressure downwind from an inoculum source. Solid line: *L* = 10 diseased leaflets, dashed line: *L* = 1,000 diseased leaflets, dotted line: *L* = 100,000 diseased leaflets.

The parameters R_0, *IP* and f_e have a moderate effect on infection pressure, with an effect factor ranging from 2.6 for *IP* (see also figure 4) to 4.1 for f_e.

Wind speed and deposition velocity have a minor effect (factor 1.5 and 1.6, respectively). The effect of the other parameters, like escape distance (figure 5), is negligible (effect factor of 1.1 or less).
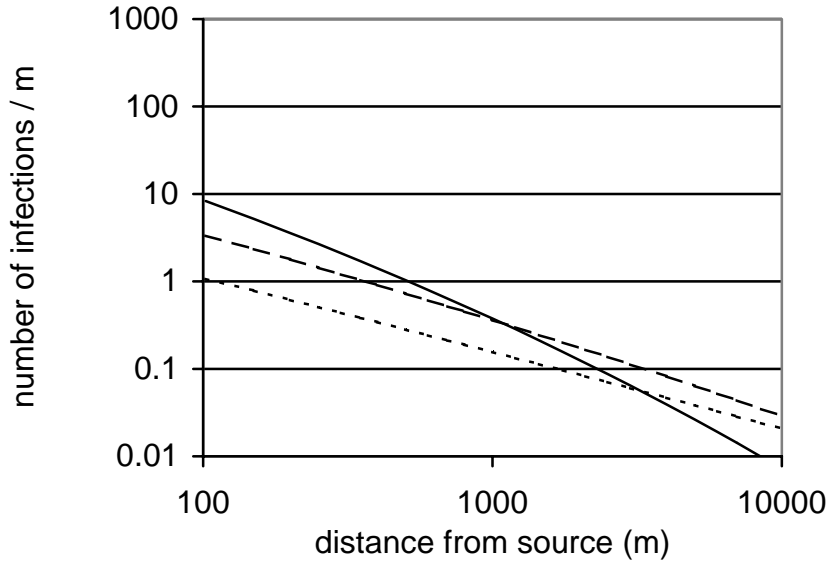
Figure 4: Effect of wind speed (u, m s^{-1}) on potential infection pressure downwind from an inoculum source. Solid line: $u = 1$ m s^{-1}, dashed line: $u = 3$ m s^{-1}, dotted line: $u = 10$ m s$^-$
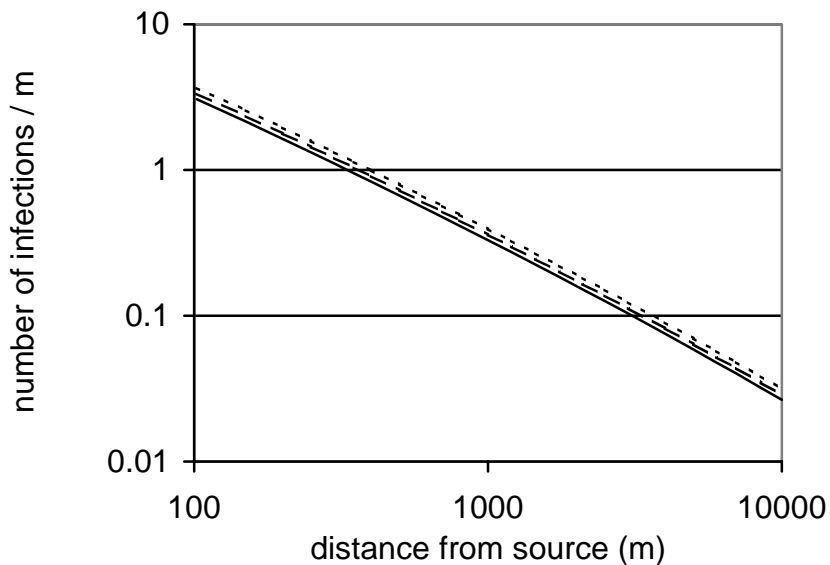
Figure 5: Effect of escape distance (x_{esc}, m) on potential infection pressure downwind from an inoculum source. Solid line: $x_{esc} = 20$ m, dashed line: $x_{esc} = 50$ m, dotted line: $x_{esc} = 100$ m.

Table 3: Sensitivity of infection pressure (number of infections per m downwind distance) to parameters in dispersal model.

Parameter	Minimum	Maximum	$\sqrt{\text{max/min}}$
L	0.0036	36	100
x	0.029	3.4	10.8
f_e	0.051	0.88	4.1
R_0	0.11	1.1	3.2
IP	0.11	0.73	2.6
ν_d	0.17	0.42	1.6
u	0.16	0.37	1.5
stability class	0.28	0.36	1.1
x_{esc}	0.33	0.39	1.1
z_0	0.34	0.36	1
z_{ref}	0.35	0.37	1
d	0.36	0.36	1
H	0.36	0.36	1

Table 4: Infection pressure (number of infections per m downwind distance) under different control strategies and fungicide efficacies (ε, -).

	$\varepsilon = 0\%$	$\varepsilon = 70\%$	$\varepsilon = 90\%$	$\varepsilon = 99\%$
standard run	381	114	38	3.8
source eradication	3.8	1.1	0.4	0.04
spatial separation of cropping systems	3.2	1.0	0.3	0.03
ban on the growing of susceptible cultivars	20	6.1	2.0	0.20
use of a resistant cultivar at receptor crop	82	25	8.2	0.8

Scenario studies

In the standard scenario, potential infection pressure is 3.8 infections per m (380 per 100 m) on a well protected crop on which the fungicide efficacy is 99%. Such a high level of potential infection pressure suggests that in addition to fungicides, control strategies are necessary to keep infection pressure low.

There is much variation in the effect of control strategies (table 4). Eradication of sources and separation of cropping systems are the most effective control strategies. They lead to a factor 100 reduction in infection pressure. Under these strategies, fungicide requirements become much lower. The potential infection pressure on

unsprayed crops in these scenarios is similar to that on well-sprayed crops in the standard scenario.

A ban on the cultivation of susceptible cultivars is more effective than the use of a resistant cultivar on the receptor crop by an individual farmer. To get the same potential infection pressure as in the standard scenario, with susceptible cultivars and 99% fungicide efficacy, the fungicide efficacy may be reduced to between 70% and 90% when the growing of susceptible cultivars is banned. In the case of use of a resistant cultivar by individual farmers, the efficacy must still be over 90%. The reason for the fact that a ban on growing of susceptible cultivars is more effective than the use of more resistant cultivars by individual farmers is that a ban reduces the spore production at the source as well as the infection efficiency on the receptor crop, whereas the use of a more resistant cultivars by individual farmers has no effect on the spore production at the source if this is still a susceptible crop.

Discussion and conclusions

The aim of this study was to identify the importance of various factors influencing potential infection pressure downwind from sources of inoculum of *Phytophthora infestans* and to determine how potential infection pressure may effectively be decreased in order to reduce fungicide requirements.

It was found that the infection pressure model is most sensitive to the disease level of the inoculum source. The large variation in disease level explains why the model is so sensitive to this parameter. Potential infection pressure is proportional with disease level at the source. A large variation in disease level thus leads to a proportionally large variation in potential infection pressure.

Source eradication and spatial separation of cropping systems were found to be the most effective control strategies. They lead to a strong reduction in both infection pressure and fungicide requirements. Source eradication targets the most sensitive parameter, disease level. The fairly steep gradients of infection pressure explain why distance is also an important parameter. Eradication of sources and spatial separation of cropping systems target these two parameters and therefore are effective control strategies. Although the model is less sensitive to distance than it is to disease level, eradication of sources, which targets disease level, is not much more effective than spatial separation of cropping systems, which targets distance. This is because eradication is only possible when sources can be found with enough certainty. The source eradication threshold used in this study reflects Dutch regulations, which set the

maximum allowed disease level to 2000 diseased leaflets. This choice is based on the practical experience that the disease is hard to find below this level (H. Hendriks, pers. communication). When the maximum allowed disease level had been lower in the source eradication strategy, this strategy would have come out as more effective.

The effectiveness of a ban on the growing of susceptible cultivars may be more effective in reducing fungicide requirements than is found in this study. This study only looked at instantaneous infection pressure, not at changes in infection pressure. When only resistant cultivars are used, disease will build up more slowly. A longer period of low disease levels at the start of the growing season can help reduce fungicide requirements during this period.

This slower build up may also be an additional reason for farmers to use more resistant cultivars individually. If their crop gets infected, the epidemic will not reach unacceptable levels as quickly. Using resistant cultivars is also a more robust strategy. It gives additional protection during prolonged wet periods when it may be impossible to spray, or when undiscovered sources pose an unknown threat to a crop.

In this study, several processes were not taken into account: washout, splash dispersal and survival of spores. This limits accuracy of model. Studies of Mizubuti *et al.* (2000) showed that solar radiation especially has a strong effect on spore survival. Kiraly (2000) found that rain could clear out the atmosphere in 50 minutes. Washout might thus cause an increased spore deposition and create suitable (wet) conditions for infection.

A disease gradient was found that led to a factor 10 reduction in infection pressure between 100 m and 1 km downwind. This gradient is consistent with disease gradients estimated from field observations by Zwankhuizen *et al.* (1998). Zwankhuizen *et al.* fitted an exponential model to observed disease levels in fields downwind from the probable source and found exponential slope parameters of between −0.0006 and −0.0074 m^{-1}, leading to between a factor 2 and 1500 decrease in infection pressure between 100 m and 1 km downwind. Our value of a factor 10 lies within this range.

The model could not be validated. This is related to the problem of doing experiments at the regional scale, which is why a modelling approach was chosen for this study. Results presented here should mostly be interpreted in relative terms, comparing strategies with each other, rather than in absolute terms, looking at the absolute infection pressure.

The results from this study make clear that infection of potato crops with late blight cannot be fully avoided. Practical experience indicates that sources can only be detected at levels of 2000 diseased leaflets or higher. This study indicates that undetected sources with levels around or below 2000 diseased leaflets can cause some infections in neighbouring crops. This means that in practise, a certain level of disease

cannot be fully avoided.

Which disease levels are tolerable remains a subject for discussion and research. It may very well be that for many farmers, the tolerance level lies below the detection level of about 2000 diseased leaflets. This would explain the, somewhat counter-intuitive, practical aim of spray advice systems. The aim of spray advice systems (Wim Nugteren, Opticrop B.V. personal communication) is to keep fields free of disease. This may seem somewhat counter-intuitive, considering that infection risks cannot be fully avoided. When the tolerance level is below the detection level, however, this aim makes sense. Disease free then means that the disease level should stay below the detection level.

The large effect of distance and disease levels also suggests that making infection pressure maps based on observed sources may help to reduce fungicide requirements. De Jong's (1988) calculations of the risk posed by a fungus used in biocontrol of a forest weed to nearby orchard indicated that the concentration of spores coming from the biocontrol site fell down to below background concentrations at 5 km downwind. A similar argument could be made here. In this study spore concentrations decrease by a factor 100 between 100 m and 10 km. This means that the potential infection pressure of a big source with 200,000 diseased leaflets at 10 km upwind is similar to that of a neighbouring small source (2000 diseased leaflets) at 100 m upwind. It should be noted however, that infection from a nearby source will occur more frequently, because plumes stay fairly narrow and thus are more likely to miss crops further away.

The overriding importance of disease level indicates that the most heavily infected sources need the most attention in a disease detection system. When looking at the potential infection pressure between two sources with different disease levels (figure 6), this becomes clear immediately. The potential infection pressure as much as 5.5 km downwind from a source with 100,000 infected leaflets is equal to the potential infection pressure only 50 m downwind from a source with 1000 diseased leaflets. The break-even point is at 110 m, only 1.2 % of the distance between the two sources. This suggests that in practise, infection pressure is dominated by the larger sources and that sources with lower disease levels can be ignored. This makes the task of source detection a bit easier, because large sources are easier to find. Unfortunately, confidence in the currently used source detection method in The Netherlands, via voluntary reports, is low due to the experience that important sources are not always reported timely. The implementation of new detection methods that are currently under development (Clark, 1990; Schutz *et al.*, 1999; Wojtowicz and Piekarcyk, 2001) might solve this problem.

At the same time, the overriding importance of disease level in the biggest sources makes it clear that control of the disease cannot be effective unless all farmers adhere
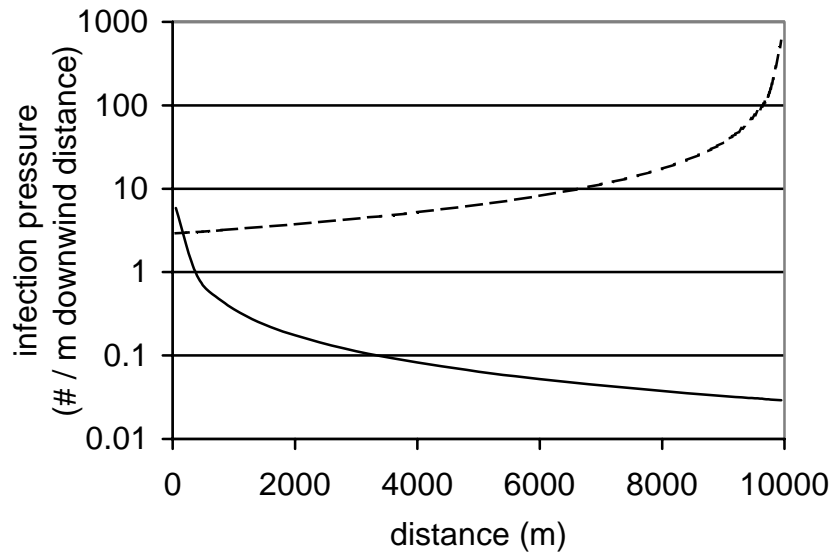
Figure 6: Potential infection pressure between two sources with a factor 100 difference in disease level (*L*, #) located 10 km away from each other. Solid line: *L* = 1,000 diseased leaflets, dashed line: *L* = 100,000 diseased leaflets.

to the source eradication regulations. Good farming practice by individual farmers cannot prevent their fields from getting infected. If all farmers do follow eradication policies, however, infection pressure can be reduced significantly and with it the use fungicides against potato late blight.

CHAPTER 6

General discussion

Potato late blight is a regional problem. This study concludes that at present, the possibilities for individual farmers to protect their crop from infection are limited and that the potato late blight problem can more effectively be tackled at the inoculum source than at the receptor crop.

Methodological advances

The results in this study were achieved through development, parameterisation, testing and use of two simple and conceptually credible models. One model was developed to describe disease development in a crop and another one to describe dispersal of spores from a source and deposition onto a receptor crop.

A new, mechanistic description of lesion growth and, derived from this, the sporulation curve of lesions was developed and incorporated in a simple mathematical expression for the relative growth rate (r, d^{-1}) of the local epidemic. This formula can be calculated from commonly measured disease components, such as lesion growth rate, infection efficiency and sporulation intensity. It can be used to evaluate the relative importance of factors like resistance, aggressiveness and weather on variability in disease components and rate of epidemic progress. It may also be used as part of a programme for screening of resistance or aggressiveness based on climate cabinet observations, thus allowing year-round experimentation. A problem that remains is that experience indicates that climate cabinet measurements of disease components are not always representative for the field situation. Development of a translation method could help overcome this problem. A field test, preferably in an experiment where component parameters and the relative epidemic growth rate are measured simultaneously can help to improve the formula and widen its usefulness and scope.

An empirical model for dispersal, the Gaussian plume model, was tested for its capability of describing spore dispersal near a source and further downwind. With this model, spore dispersal kernels can be calculated for distances of 50 m to 10 km downwind from inoculum sources. At the very start of the growing season, interregional spread, over distances more than 10 km may be important. A model to calculate risks of interregional spread could be developed following the methodology of Aylor (1986).

The local epidemic model and the spore dispersal model were coupled to allow for an evaluation of possible control strategies for reducing the fungicide requirements against late blight. The coupling of the local epidemic model to the spore dispersal model, using the regional net reproduction, is still sketchy. For a better coupling, existing dispersal kernels for dispersal close to the source (Paysour and Fry, 1983; Waggoner, 1952) must be extended up to, and preferably beyond, 50 m and be related

to the kernel presented here. Coupling of the local epidemic model to the spore dispersal model could further be improved through investigations on the relative amounts and effectiveness of spores dispersed by splash and by wind. The model presented here is based on calculation of potential risks, not taking into account the variable effects of factors like weather conditions and aggressiveness. Incorporating these factors in the model could allow a calculation of actual risks, instead of the potential risk calculated here.

The study on the accuracy of the source depletion method (chapter 4) quantifies the uncertainty (at most a factor 4) in the deposition rates calculated with this method. Using a different, more complex model, may decrease uncertainties. The advantage of implementing a different model should be weighed against the disadvantages of increased complexity and time taken away from reducing other uncertainties. Results of the sensitivity analysis with the infection pressure model (chapter 5) indicates that there are other uncertainties that probably require more attention, especially the detection of inoculum sources.

Inoculum sources

This study indicates that heavily diseased sources dominate infection pressure. Eradication of these sources is one of the most effective control measures to reduce infection pressure and fungicide requirements. This control measure is only effective if all heavily infected sources are found and eradicated. Practical experience indicates that currently used detection methods (visual observation) are limited in their detection efficiency. The detection efficiency depends on the accuracy of and time spent on sampling.

Improved sampling methodologies can lead to better control of late blight. The knowledge obtained in this study provides a basis to set criteria for new detection methodologies. A reduction in fungicide use can only be obtained if all the heavily diseased sources are detected. Information about the disease level of sources is an important aspect of source detection. If sources with low disease levels are not detected, this should not be a problem. Trustworthy information on location and disease level of inoculum sources could greatly reduce fungicide requirements by giving location specific spray recommendations or by identifying sources that must be eradicated.

Detection methods able to survey large areas, e.g. based on aerial photography (Clark, 1990; Wojtowicz and Piekarcyk, 2001) can be used to find the most heavily diseased sources in the region. Biosensors, which have been shown to be able to detect low disease levels (Schutz *et al.*, 1999), may be used to detect disease at the smaller than field scale. This would allow farmers, who are forced to eradicate the inoculum

sources in their field, to only eradicate patches that are really infected and find these patches at lower disease levels, before they cause major problems. Timely and site-specific eradication allows a farmer to harvest later and obtain a higher yield.

Spatial aspects

Not all potato cropping systems (seed tuber production, ware potato production, starch potato production, organically grown potatoes) are equally disease tolerant. In some systems, higher levels of disease are accepted than in other systems. Separation of cropping systems with different levels of disease tolerance could help to reduce fungicide requirements. This study suggests that separation of cropping systems can be as effective as eradication of sources. This measure may be difficult to implement in practise, since cropping systems are not spatially separated at present.

Spatial separation of cropping systems requires that specific areas are dedicated to cropping systems with different disease tolerance. The implementation of this measure could be beneficial to both farmers with a low disease tolerance and farmers with a high disease tolerance, however. Growth of potatoes of low disease tolerance cropping systems, e.g. seed tuber production could take place in areas with strict phytosanitary regulations, like covering of waste piles and killing of heavily diseased haulm. This would enable the growing of potatoes in these low disease tolerance systems in an area with reduced infection risk. In areas designated for cropping systems with higher disease tolerance, e.g., on organic farms, regulations on the killing of haulm may be loosened. Farmers can then kill the haulm later and thus achieve a higher yield.

Fungicide requirements

The modelling study presented here provides tools that can help to reduce infection risks and give farmers a more specific spray advice. This study indicates that risk of infection with late blight cannot be fully avoided, even with a high input of fungicides. But when adequate control measures are taken at the regional scale, infection risks caused by inoculum from distant sources may be substantially reduced, thus allowing a reduction in fungicide use. Adequate detection of sources and dissemination of this knowledge to farmers can help them to make better spraying decisions. When the model of infection risks is combined with field data about location and severity of sources in a decision support system, farmers can be given more specific spray advice. Thus, with the right control measures taken at the regional level and gathering and transfer of knowledge through decision support systems, infection risks and thus fungicide requirements may substantially be decreased.

References

Anonymous, 2002. 77th list of varieties of field crops. Wageningen, 300 pp.

Aylor, D.E. and Ferrandino, F.J., 1989. Dispersion of spores released from an elevated line source within a wheat canopy. Boundary Layer Meteorology 46: 251-274.

Aylor, D.E. and Irwin, M.E., 1999. Biophysical scaling and the passive dispersal of fungus spores: Relationship to integrated pest management strategies. Agricultural and Forest Meteorology 97: 275-292.

Aylor, D.E. and Taylor, G.S., 1983. Escape of *Peronospora tabacina* spores from a field of diseased tobacco plants. Phytopathology 73: 525-529.

Aylor, D.E., 1986. A framework for examining inter-regional aerial transport of fungal spores. Agricultural and Forest Meteorology 38: 263-288.

Aylor, D.E., 1990. The role of intermittent wind in the dispersal of fungal pathogens. Annual Review of Phytopathology 28: 73-92.

Aylor, D.E., 1996. Quantifying the probability of apple scab fungus infection to improve disease management. Frontiers of Plant Science 49: 5-8.

Aylor, D.E., 1998. The aerobiology of apple scab. Plant Disease 82: 838-849.

Aylor, D.E., Fry, W.E., Mayton, H. and Andrade Piedra, J.L., 2001. Quantifying the rate of release and escape of *Phytophthora infestans* sporangia from a potato canopy. Phytopathology 91: 1189-1196.

Aylor, D.E., Taylor, G.S. and Raynor, G.S., 1982. Long-range transport of tobacco blue mold spores. Agricultural Meteorology 27: 3-4.

Barad, M.L., 1958. Project prairie grass: A field program in diffusion. Vol. 1, Geophysics Research Directorate, Air Force Cambridge Research Center.

Brewster, C.C. and Allen, J.C., 1997a. Spatiotemporal model for studying insect dynamics in large scale cropping systems. Environmental Entomology 26: 473-482.

Brewster, C.C., Allen, J.C., Schuster, D.J. and Stansly, P.A., 1997b. Simulating the dynamics of *Bemisia argentifolii* (Homoptera: Aleyrodidae) in an organic cropping system with a spatiotemporal model. Environmental Entomology 26: 603-616.

Bruhn, J.A. and Fry, W.E., 1981. Analysis of potato late blight epidemiology by simulation modeling. Phytopathology 71:612-616.

Butler, H.J., Hogarth, W.L. and McTainsh, G.H., 2001. Effects of spatial variations in source areas upon dust concentration profiles during three wind erosion events in Australia. Earth Surface Processes and Landforms 26: 1039-1048.

Clark, E.E., 1990. Aerial photography in the control of crop disease. Chemistry-and-Industry-London 8: 250-253.

Colon, L.T., Budding, D.J., Keizer, L.C.P. and Pieters, M.M.J., 1995a. Components of resistance to late blight (*Phytophthora infestans*) in eight South American *Solanum* species. Eur. J. Plant Pathol. 101: 441-456.

Colon, L.T., Turkensteen, L.J., Prummel, W., Budding, D.J. and Hoogendoorn, J., 1995b. Durable resistance to late blight (*Phytophthora infestans*) in old potato cultivars. Eur. J. Plant Pathol. 101: 387-397.

Dacom and Agrevo, 1992. Waarnemen in aardappelen (in Dutch).

Dacom and PD, 1999. Waarnemen en registreren van P*hytophthora infestans* in aardappel seizoen 1998. Plantenziektenkundige Dienst, Wageningen, 10 pp. (in Dutch).

Day, J.P. and Shattock, R.C., 1997. Aggressiveness and other factors relating to displacement of populations of *Phytophthora infestans* in England and Wales. Eur. J. Plant Pathol. 103: 379-391.

De Jong, M.D., 1988. Risk to fruit trees and native trees due to control of black cherry (*Prunus serotina*) by silverleaf fungus (*Chondrostereum purpureum*). PhD thesis, Landbouwuniversiteit, Wageningen, 138 pp.

De Jong, M.D., Aylor, D.E. and Bourdot, G.W., 1998. A methodology for risk analysis of plurivorous fungi in biological weed control: *Sclerotinia sclerotiorum* as a model. BioControl 43: 397-419.

De Jong, M.D., G.W. Bourdot, G.A. Hurrell, D.J. Saville, H.J. Erbrink and J.C. Zadoks, 2002. Risk analysis for biological weed control: Simulating dispersal of *Sclerotinia sclerotiorum* (Lib.) de Bary ascospores from a pasture after biological control of *Cirsium arvense* (L.) Scop. Aerobiologia 18: 211-222.

De Jong, M.D., Scheepens, P.C. and Zadoks, J.C., 1990a. Risk analysis for biological control: A Dutch case study in biocontrol of *Prunus serotina* by the fungus *Chondrostereum purpureum*. Plant Disease 74: 189-194.

De Jong, M.D., Scheepens, P.C. and Zadoks, J.C., 1990b. Risk analysis applied to biological control of a forest weed, using the Gaussian plume model. Grana 29: 139-145.

De Jong, M.D., Wagenmakers, P.S. and Goudriaan, J., 1991. Modelling the escape of *Chondrostereum purpureum* spores from a larch forest with biological control of *Prunus serotina*. Netherlands Journal of Plant Pathology 97: 55-61.

Di-Giovanni, F., Beckett, P.M. and Flenley, J.R., 1989. Modelling of dispersion and deposition of tree pollen within a forest canopy. Grana 28: 129-139.

Dorrance, A.E. and Inglis, D.A., 1997. Assessment of greenhouse and laboratory screening methods for evaluating potato foliage for resistance to late blight. Plant Dis. 81: 1206-1213.

Draxler, R.D. and Elliott, W.P., 1977. Long-range travel of airborne material subjected

to dry deposition. Atmospheric Environment 11: 35-40.

Ekkes, J.J., Besseling, P.A.M. and Horeman, G.H., 2002. Evaluatie Meerjarenplan Gewasbescherming: einddocument. Ede, Expertisecentrum LNV, 77 pp.

Erbrink, J.J. and Van Jaarsveld, J.A., 1992. Het nationale model vergeleken met andere modellen en metingen. Lucht 9: 86-91.

Evans, M. and Swartz, T., 2000. Approximating integrals via Monte Carlo and deterministic methods. Oxford University Press, Oxford, 288 pp.

Eversmeyer, M.G. and Kramer, C.L., 1992. Local dispersal and deposition of fungal spores from a wheat canopy. Grana 31: 53-59.

Ferrandino, F.J. and Aylor, D.E., 1984. Settling speed of clusters of spores. Phytopathology 74: 969-972.

Flier, W.G., and Turkensteen, L.J., 1999. Foliar aggressiveness of *Phytophthora infestans* in three potato growing regions in the Netherlands. Eur. J. Plant Pathol. 105: 381-388.

Giddings, G., 2000. Modelling the spread of pollen from *Lolium perenne*. The implications for the release of wind-pollinated transgenics. Theor. Appl. Genet. 100: 971-974.

Gotelli, N.J., 1998. A primer of ecology. Sinauer Associates, Sunderland, MA, 236 pp.

Gregory, P.H., 1973. The microbiology of the atmosphere. 2nd ed., Leonard Hill Ltd, London, 377 pp.

Hanna, S.R., Chang, J.C. and Strimaitis, D.G., 1993. Hazardous gas model evaluation with field observations. Atmospheric Environment, Part A, 27: 2265-2285.

Hinrichsen, K., 1984. Comparison of four analytical dispersion models for near-surface releases above a grass surface. Atmospheric Environment 20: 29-40.

Hirst, J.M., 1953. Change in atmospheric spore content: Diurnal periodicity and the effects of weather. Transactions of the British Mycological Society 36: 375-393.

Horst, T.W., 1977. A surface depletion model for deposition from a Gaussian Plume. Atmospheric Environment 11: 41-46.

Kiraly, Z., 2000. A field evaluation of the effect of rain on wheat rust epidemics. Proceedings of the 10th Cereal Rusts and Powdery Mildews Conference, Budapest, Hungary, 28 August-1 September 2000.

KNMI, 1972. Klimatologische gegevens van Nederlandse stations. Frequentietabellen van de stabiliteit van de atmosfeer, No. 150-8. (in Dutch)

KNMI, 1979. Luchtverontreiniging en weer. Staatsuitgeverij, Den Haag. (in Dutch)

Lapwood, D.H., 1961. Potato haulm resistance to *Phytophthora infestans*. II. Lesion production and sporulation. Ann. Appl. Biol. 49: 316-330.

Legg, B.J., Long, I.F. and Zemroch, P.J., 1981. Aerodynamic properties of field bean and potato crops. Agricultural Meteorology 23: 21-43.

Lyons, T.J. and Scott, W.D., 1990. Principles of air pollution meteorology. CRC Press, Boca Raton, Fl., 224 pp.

McCartney, H.A. and Fitt, B.D.L., 1985. Construction of dispersal models. In: Ed. C.A. Gilligan, Mathematical modelling of crop disease. Academic Press Inc., London, 255 pp.

McCartney, H.A., Bainbridge, A. and Stedman, O.J., 1985. Spore deposition velocities measured over a barley crop. Phytopathologische Zeitschrift 114: 224-233.

Michaelides, S.C., 1985. A simulation model of the fungus *Phytophthora infestans* (Mont) De Bary [potato]. Ecological Modelling 28: 121-137.

Mizubuti, E.S.G., Aylor, D.E. and Fry, W.E., 2000. Survival of *Phytophthora infestans* sporangia exposed to solar radiation. Phytopathology 90: 78-84.

Mohan, M. and Siddiqui, T.A., 1998. Analysis of various schemes for the estimation of atmospheric stability classification. Atmospheric Environment 32: 3775-3781.

Pasquill, F., 1974. Atmospheric diffusion. 2nd ed., Wiley, New York, 429 pp.

Pasquill, F. and Smith, F.B., 1983. Atmospheric diffusion. 3rd ed., Wiley, New York, 430 pp.

Paysour, R.E. and Fry, W.E., 1983. Interplot interference: A model for planning field experiments with aerially disseminated pathogens. Phytopathology 73: 1014-1020.

Rao, S.T., Keenan, M., Sistala, G. and Samson, P., 1979. Dispersion of air pollutants near highways. U.S. Environment Protection Agency, New York.

Ross, G.J.S., 1990. Nonlinear estimation. Springer Verlag, New York.

Schutz, S., Weissbecker, B., Koch, U.T. and Hummel, H.E., 1999. Detection of volatiles released by diseased potato tubers using a biosensor on the basis of intact insect antennae. Biosensors and Bioelectronics 14: 221-228.

Sedefrian, L. and Bennett, E., 1980. A comparison of turbulence classification schemes. Atmospheric Environment 14: 741-750.

Singh, B.P. and Birhman, R.K., 1994. Laboratory estimation of field resistance of potato to late blight. J. Phytopathol. 140: 71-76.

Spijkerboer, H.P., Beniers, J.E., Jaspers, D., Schouten, H.J., Goudriaan, J., Rabbinge, R. and Van der Werf, W., 2002. Ability of the Gaussian plume model to predict and describe spore dispersal over a potato crop. Ecological Modelling 155: 1-18.

Stull, R.B., 1988. Introduction to boundary layer meteorology. 1 ed. Kluwer Academic Publishers, Dordrecht.

Van der Hoven, I., 1968. Deposition of particles and gases. In: Ed. D.H. Slade, Meteorology and atomic energy. U.S. Atomic energy commission, Oak Ridge, Tennessee, 445 pp.

Van der Zaag, D.E., 1956. Overwintering en epidemiologie van *Phytophthora infestans*, tevens enige nieuwe bestrijdingsmogelijkheden. PhD thesis, Landbouw-

hogeschool Wageningen.

Van Oijen, M., 1989. On the use of mathematical models from human epidemiology in breeding for resistance to polycyclic fungal leaf diseases of crops. In: Eds K.M. Louwes, Toussaint, H.A.J.M. and Dellaert, L.M.W., Parental line breeding and selection in potato breeding. Wageningen, Pudoc, pp. 26-37.

Van Oijen, M., 1991. Identification of the major characteristics of potato cultivars which affect yield loss caused by late blight. PhD thesis, Landbouwuniversiteit Wageningen, The Netherlands, 116 pp.

Van Oijen, M., 1992. Selection and use of a mathematical model to evaluate components of resistance to *Phytophthora infestans* in potato. Netherlands Journal of Plant Pathology 98: 192-202.

Venkatram, A., 1979. A note on the measurement and modeling of pollutant concentrations associated with point sources. Boundary-Layer Meteorol. 17: 523-536.

Vreugdenhil, C.B., 1989. Computational hydraulics: An introduction. Springer Verlag, Berlin.

Waggoner, P.E., 1952. Distribution of potato late blight around inoculum sources. Phytopathology 42: 323-328.

Wojtowicz, A. and Piekarczyk, J., 2001. Monitoring of *Phytophthora infestans* development with a luminancemeter. Journal of Plant Protection Research 41: 256-265.

Yang, Y., Wilson, L.T., Makela, M.E. and Marchetti, M.A., 1998. Accuracy of numerical methods for solving the advection-diffusion equation as applied to spore and insect dispersal. Ecological Modelling 109: 1-24.

Zadoks, J.C. and Schein, R.D., 1979. Epidemiology and plant disease management. Oxford University Press, New York, 427 pp.

Zwankhuizen, M.J., Govers, F. and Zadoks, J.C., 1998. Development of potato late blight epidemics: Disease foci, disease gradients, and infection sources. Phyto-pathology 88: 754-763.

Summary

Aerial dispersal of *Phytophthora infestans* spores from distant sources to crops is an essential part of the epidemiology of potato late blight. This makes late blight a regional problem. Control measures taken at the regional scale can reduce infection pressure from distant sources and may thus lead to a reduction in fungicide requirements. In this thesis, an interdisciplinary analysis of the regional late blight problem is carried out through model development, experimental parameterisation and analysis and scenario studies that investigate possibilities for effective control of the disease at the regional level.

A new equation was derived to estimate the relative exponential growth rate r (d^{-1}) of a plant disease epidemic from commonly used component parameters for pathogen aggressiveness and host resistance, such as the latency period, infection efficiency, sporulation intensity and lesion growth rate. The equation is based on well-established ecological theory in combination with a new, mechanistic, model for lesion growth and sporangium production on leaves with a finite size. The use of the equation is demonstrated with field measurements of resistance components against late blight for five potato cultivars. The index appeared sensitive to changes in all component parameters, except a shape factor for the leaves. Uncertainty in estimated index value was mostly due to uncertainty in the values of only three parameters: infection efficiency, sporulation intensity, and to a lesser extent, lesion growth rate. Infection efficiency and lesion growth rate together explained most of the variation in cultivar resistance.

To describe the dispersal of spores at distances up to 10 km downwind from an source of inoculum, the Gaussian plume model was used. To describe loss of spores near the source, the fraction of spores that escape the canopy must be determined. A field experiment was set up to calibrate the Gaussian plume model, as applied to the dispersal of spores. The model was calibrated with a weighted least squares method. A comparison of estimated concentrations with the measurements confirmed that spore clouds originating from a point source take the form of a Gaussian plume: the coefficient of correlation between measured spore concentrations and fitted concentrations was 0.8. The fraction of spores that escaped the canopy and was available for long distance dispersal amounted to 64% ± 17%.

To calculate the effect of deposition on loss of spores from the spore plume at distances between 50 m and 10 km from the source, the source depletion method was used. The source depletion method is a practical method to describe the dynamic

process of deposition in the static Gaussian plume model. A more accurate way of describing loss would be with the surface depletion method. However, the surface depletion method cannot be used in conjunction with the Gaussian plume model. The accuracy of the source depletion method was determined by comparing it with the more realistic surface depletion method in a modelling study. It was found that under worst case conditions, the source depletion method may lead to an error of at most a factor 4 in calculated deposition of *Phytophthora infestans* spores.

The infection pressure on receptor crops caused by inoculum from a distant source was calculated with a newly developed model. The sensitivity analysis showed that disease level at the source had by far the greatest impact on infection pressure, followed by distance from the source. Scenario studies were carried out with the model to evaluate the effectiveness of four control strategies. The scenario studies indicated that eradication of sources with high disease levels and spatial separation of cropping systems with different disease tolerances are more effective than use of more resistant cultivars for the receptor crop or a ban on the growing of susceptible cultivars.

Eradication of sources is only effective if all heavily infected sources are found and eradicated. Practical experience indicates that the currently used detection method of visual observation is limited in its detection efficiency. New sampling methodologies, which are currently under development may improve the detection efficiency. The knowledge obtained in this study suggests that if sources with low disease levels are not detected with the system, this should not be a problem: the potential infection pressure of a big source with 200,000 diseased leaflets at 10 km upwind is similar to that of a neighbouring small source (2000 diseased leaflets) at 100 m upwind.

Separation of cropping systems may be difficult to implement. The implementation of this measure, however, could be beneficial to both farmers with a low disease tolerance and farmers with a high disease tolerance. The benefit for farmers who grow crops with low disease tolerance (e.g., seed tubers) is that they can grow their crop in areas where infection pressure is lower. The benefit for farmers who grow crops with a higher disease tolerance (e.g., organic crops) is that in areas designated for these crops, the threshold at which haulm must be killed might be elevated above the present level (2000 diseased leaflets). This allows farmers to kill the haulm later than they would have to under current regulations. As a result of this, they can obtain a higher yield.

With the right control measures taken at the regional level and gathering and transfer of knowledge through decision support systems, infection risks and thus fungicide applications against potato late blight may substantially be decreased.

Samenvatting

Luchtverspreiding van de sporen van *Phytophthora infestans* vanuit verre bronnen naar een vanggewas is een belangrijk onderdeel van de epidemiologie van de aardappelziekte. Dit maakt aardappelziekte een regionaal probleem. Beheersingsmaatregelen die genomen worden op regionaal niveau kunnen de infectiedruk vanuit verre sporenbronnen verminderen en zo de fungicidenbehoefte verlagen. In dit proefschrift wordt een interdisciplinaire analyse van het *Phytophthora* probleem uitgevoerd, door middel van modellering, parameterisering en scenario studies waarin de effectiviteit van mogelijke maatregelen voor ziektebeheersing wordt geëvalueerd.

Een nieuwe formule is ontwikkeld om de relatieve groeisnelheid (r, d^{-1}) van een epidemie te berekenen op basis van standaard parameters, zoals de infectie-efficiëntie en de lesiegroeisnelheid. De formule is gebaseerd op algemene ecologische theorie, waaraan een nieuw, mechanistisch, model is toegevoegd voor sporulatie van lesies die groeien op blaadjes met een beperkt oppervlak. Deze relatieve groeisnelheid kan bijvoorbeeld gebruikt worden als een index voor rasgevoeligheid voor *Phytophthora* en bleek gevoelig voor alle parameters, behalve een factor die de vorm van blaadjes beschrijft. De onzekerheid in de geschatte waarde van de index werd voornamelijk bepaald door drie parameters: infectie-efficiëntie, sporulatie-intensiteit en, in mindere mate, lesiegroeisnelheid. De infectie-efficiëntie en de lesiegroeisnelheid verklaarden samen het grootste deel van de verschillen in resistentie tussen rassen.

Om de verspreiding van sporen over afstanden tot 10 km windafwaarts van een sporenbron te beschrijven, werd het Gaussische pluimmodel gebruikt. Om het verlies van sporen nabij de bron te beschrijven moet de ontsnappingsfractie bepaald worden. Een veldexperiment werd opgezet om het Gaussische pluimmodel, toegepast voor sporenverspreiding, te kalibreren. Een vergelijking van geschatte sporenconcentraties en gemeten concentraties liet zien, dat een wolk sporen die vrijkomt uit een puntbron inderdaad beschreven kan worden als een Gaussische pluim. De correlatiecoëfficiënt tussen geschatte en gemeten sporenconcentraties was 0.8. De fractie van sporen die uit het gewas ontsnapte en beschikbaar was voor verspreiding over grotere afstanden was 64% ± 17%.

Om het effect van depositie op het verlies van sporen uit de pluim te berekenen, werd de bron-depletiemethode gebruikt. De bron-depletiemethode is een praktische methode om de consequenties van depositie op te nemen in het Gaussische pluimmodel. Een nauwkeuriger methode om dit verlies te beschrijven is de

oppervlakte-depletiemethode. Deze dynamische methode kan echter niet gebruikt worden samen met het statische Gaussische pluimmodel. De nauwkeurigheid van de bron-depletiemethode werd bepaald door in een modelstudie de resultaten van deze methode te vergelijken met de resultaten van de oppervlakte-depletiemethode. Hieruit bleek dat de brondepletiemethode in het ergste geval een fout geeft van een factor 4 in de berekende depositie van *Phytophthora* sporen.

De infectiedruk op aardappelgewassen, veroorzaakt door sporen afkomstig uit verre bronnen (haarden) werd berekend met een nieuw ontwikkeld model. Een gevoeligheidsanalyse van dit model toonde aan dat het ziekteniveau van de bron het grootste effect had op de infectiedruk, gevolgd door afstand tot de bron. Scenariostudies werden uitgevoerd met het model om de effectiviteit van vier beheersmaatregelen te bepalen. De scenario studies gaven aan, dat het bestrijden van haarden met een hoog ziekteniveau en ruimtelijke scheiding van teeltsystemen met verschillende ziektetolerantie effectiever zijn dan het gebruik van een resistenter ras in het bedreigde gewas of een verbod op het telen van vatbare rassen.

Bestrijden van haarden is alleen effectief als alle zwaar besmette bronnen aangepakt worden. Uit de praktijk blijkt dat de huidige methode voor het detecteren van ziektebronnen beperkt is in haar detectie-efficiëntie. Nieuwe waarnemings-methodieken, die nu in ontwikkeling zijn, zouden de detectie-efficiëntie kunnen verbeteren. De kennis die vergaard is in dit onderzoek wijst uit, dat het niet zo erg zou zijn als kleine haarden niet opgespoord zouden worden: de potentiële infectiedruk van een haard met 200.000 zieke blaadjes op een afstand van 10 km is gelijk aan die van een kleine haard met 2000 zieke blaadjes op slechts 100 m afstand.

Het scheiden van teeltsystemen kan in de praktijk moeilijk te verwezenlijken zijn. De invoering van deze maatregel kan echter voordelen hebben voor zowel boeren die gewassen telen met een lage ziektetolerantie (b.v. pootgoed), als voor boeren die gewassen verbouwen met een hoge ziektetolerantie (b.v. biologische aardappelen). Het voordeel voor boeren die gewassen verbouwen met een lage ziektetolerantie is, dat zij hun gewassen kunnen telen in een gebied met lage ziektedruk. Het voordeel voor boeren die gewassen verbouwen met hoge ziektetolerantie is, dat in gebieden die zijn aangewezen voor deze gewassen het ziekteniveau waarop het loof gedood moet worden verhoogd kan worden ten opzichte van het huidige niveau (ongeveer 2000 zieke blaadjes). Dit stelt de boeren in staat om het loof later te doden en zo een hogere opbrengst te realiseren.

Door op regionaal niveau de juiste maatregelen te nemen en door informatie te verzamelen en te verspreiden via adviessystemen, kunnen infectierisico's verminderd worden waardoor het fungicidengebruik tegen *Phytophthora* substantieel omlaag zou kunnen.

Curriculum vitae

Hendrik Pieter Spijkerboer (roepnaam Diedert) werd geboren op 5 maart 1970 te Harderwijk. Na het behalen van het Atheneum-diploma aan het Christelijk Lyceum te Apeldoorn en enkele maanden studie Geologie aan de Rijksuniversiteit Utrecht begon hij in januari 1990 aan de studie Bodem, Water en Atmosfeer aan de Landbouwuniversiteit Wageningen. In augustus 1995 behaalde hij de ingenieursbul. Hij deed een jaar onderzoek naar de toepassingsmogelijkheden van wavelet-transformaties voor analyse van hoogfrequente meetsignalen bij de vakgroep Meteorologie van de Landbouwuniversiteit. In juli 1996 begon hij aan een door technologiestichting STW gefinancierd promotieonderzoek bij de toenmalige vakgroep Theoretische Productie-ecologie van de Landbouwuniversiteit en het Centrum voor Plantenveredeling en Reproductieonderzoek. Sinds 1 juli 2001 is hij als freelance onderzoeker werkzaam voor de Leerstoelgroepen Plantaardige Productiesystemen en Gewas- en Onkruidecologie van Wageningen Universiteit. De resultaten van het promotieonderzoek en van een deel van zijn freelance werkzaamheden zijn verwerkt in dit proefschrift.

Funding